Frontiers of Physics
https://doi.org/10.1007/s11467-019-0912-5
Front. Phys.
14(6), 63301 (2019)

VIEWPOINT

A collection of 505 papers on false or unconfirmed ferroelectric properties in single crystals, ceramics and polymers

Zbigniew Tylczyński

Faculty of Physics, Adam Mickiewicz University, Uniwersytetu Poznańskiego 2, Poznań, Poland
E-mail: zbigtyl@amu.edu.pl
Received April 11, 2019; accepted June 14, 2019

This collection presents 505 papers on ferroelectricity in single crystals, ceramics and polymers in which pointed or elliptical hysteresis loops would testify to their ferroelectric properties. In some papers, the authors ensure that ferroelectricity can occur even in materials that do not have a polar axis of symmetry.

Keywords ferroelectricity, hysteresis loop, single crystals, multiferroic, polymers

Proper ferroelectric hysteresis loop

Hundreds of papers whose drawbacks have been briefly outlined below have unfortunately been published in peer-reviewed journals, especially in the journals devoted to materials investigations, stirring confusions in scientific literature. The idea of this paper is to draw the attention of the scientific society to the fact that some authors wrote that the ferroelectricity is possible in crystals without polar axis or misinterpreted experimental results presenting an elliptical or pointed P–E hysteresis loop as evidence of ferroelectric properties.

Ferroelectricity was first discovered by Valasek in 1921 [1] in the well-known crystal, Rochelle salt – potassium sodium tartrate tetrahydrate. Since then, many organic and inorganic ferroelectric materials have been found. Ferroelectricity, that might be treated as an electric analogue of ferromagnetism, can exist only in crystals of 10 point groups of symmetry having a polar axis: 1, 2, m, mm2, 3, 3m, 4, 4mm, 6, 6mm [2]. According to the definition of ferroelectricity the polarization vector has to be reversed by an external electric field giving a characteristic hysteresis loop. Direct measurement of the ferroelectricity can be obtained with setups like a ferroelectric analyzer, and only a saturated P–E hysteresis loop informs about ferroelectric properties of crystals, see Fig. 1. Another proof that material reveals ferroelectric properties is the observation of pyroelectric current after poling sample in a static electric field, provided it changes sign when direction of this field is changed.

The elliptical or pointed shapes of P–E hysteresis loops in the papers mentioned in the tables below arise from the energy loss when the imperfect dielectric samples are subjected to an *ac* electric field. Scott, an authority in ferroelectricity, demonstrated in his work "*Ferroelectrics go bananas*" that even in a banana skin covered with electrodes a hysteresis loop appears in a strong alternating electric field but it would not be a ferroelectric hysteresis loop like that recorded for the well-known $Ba_2NaNb_5O_{15}$ (shortly BaNaNb) crystal [3, 4] – Fig. 2. Non-ferroelectric hysteresis loops can easily arise from experimental artifacts, e.g., in a nonferroelectric system consisting of two back-to-back metal-semiconductor contacts with a large concentration of traps near the electrodes [5] and in solid state electrolytic capacitors due to internal space charge polarization [6] or when a test sample was measured in a humid atmosphere [7] – Fig. 3. Thus there is a risk of misinterpreting non-intrinsic loops as evidence for ferroelectric behavior. The materials that show an elliptical or pointed P–E hysteresis loops cannot be considered as ferroelectrics.

The most common instrument used to study ferroelectricity is the simple Sawyer–Tower bridge. Diamant, Drenck and Pepinsky devised a new instrument which compensates for the conductivity and dielectric permittivity at saturation of the sample studied [8]. A simple method of checking whether a P–E loop is a ferroelectric one (and determining the saturation and remanence polarization and coercive field) is to record the current loop, i.e., the derivative of hysteresis loop [9]. Such loops are presented in Fig. 4. One can see that the current loop obtained from the pointed P–E loop does not show any indications of the typical peaks that occur for the saturated ferroelectric loop. Fukunaga and Noda have developed the double-wave method to refine ferroelectric P–E hysteresis loops from non-hysteresis components [10]. The use of one of these methods would remove doubts whether a given P–E hysteresis loop is ferroelectric or whether it results from the conductivity or imperfection of the tested

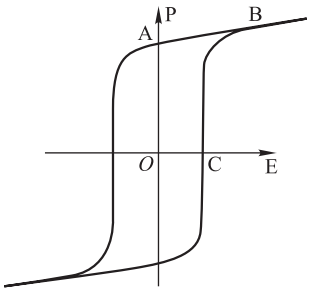

Fig. 1 Typical ferroelectric hysteresis loop [2].

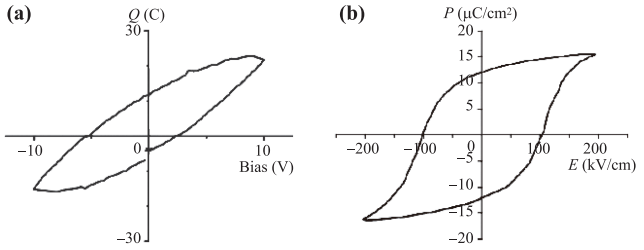

Fig. 2 P–E loops: Pointed shape on banana skin **(a)**, ferroelectric loop on $Ba_2NaNb_5O_{15}$ crystal **(b)** [3].

sample.

Peruse of dozens of scientific journals devoted to material investigation allowed identification of 505 papers in which P–E hysteresis loops were presented as ferroelectric ones. This collection only concerns bulk materials and has been divided into three parts. Part I is devoted to single crystals, Part II to polycrystalline ceramics and Part III to polymers. Each part consists of a table in which the names of false or unconfirmed "ferroelectric" substances, their symmetries and the shape of the observed P–E hysteresis loops and the corresponding references are presented. Ferroelectric properties of surfaces, liquid crystals or thin films as well as nanostructures are not shown.

The papers containing false or unconfirmed data about ferroelectric properties in 57 single crystals are summarized in Table 1. If crystals had ferroelectric properties at room temperature, the ferroelectric domain walls would exist in this phase. The presence of such walls would give a characteristic dispersion dependence of the dielectric loss. In the papers listed in Table 1 no such data are given. Some authors have presented a small maximum of the dielectric constant as the evidence of transition from ferroelectric phase to paraelectric one but a dielectric anomaly may be caused by many factors, not necessarily by the phase transition. The authors of the papers from 1 to 30 (marked in red) have drastically broken the principles of symmetry because they reported the existence of ferroelectricity in crystals without the polar axis. The authors of the papers collected in Table 1 did not specify the direction in which they measured the P–E dependence as well as the intensity and frequency of the electric field. Typical pointed and elliptical P–E loops obtained in methylamine borogermanate [I.45] and in L-prolinium tartrate [I.51] crystals are presented in Fig. 5.

Some authors have shown a series of elliptical or pointed P–E loops, and on this basis they have concluded that ferroelectricity exists in these materials. A typical series of elliptical and pointed P–E loops obtained at different intensities of the applied electric field in $Bi_{1-x}Dy_xFe_{0.98}Cu_{0.02}O_3$ ceramic [II.185] and in copper–(o-phthalate) polymer [III.16] are presented in Fig. 6. One can see that the remnant polarization grows from 20 to 230 $\mu C/cm^2$ (unbelievably high value) for $Bi_{1-x}Dy_xFe_{0.98}Cu_{0.02}O_3$ ceramic and from 0.02 to 0.5 $\mu C/cm^2$ for copper-(o-phthalate) polymer when the electric field increases 10 times. Such changes in polarization due to the increasing electrical field only show the increase in dielectric loss and do not prove the existence of spontaneous polarization.

The false or unconfirmed ferroelectric properties in polycrystalline ceramics and in polymers are collected in Table 2 and Table 3. All measurements were made on powdered samples in the form of pellets. Some of the investigated substances crystallize in the centrosymmetric systems – their symmetries are marked in red in Table 2 (1–14, 46–120, 284–289) and in Table 3 (1–4, 133) – i.e., they cannot exhibit ferroelectric properties. The authors of these papers have broken the principles of symmetry of the condensed phase physics. Over the past several years,

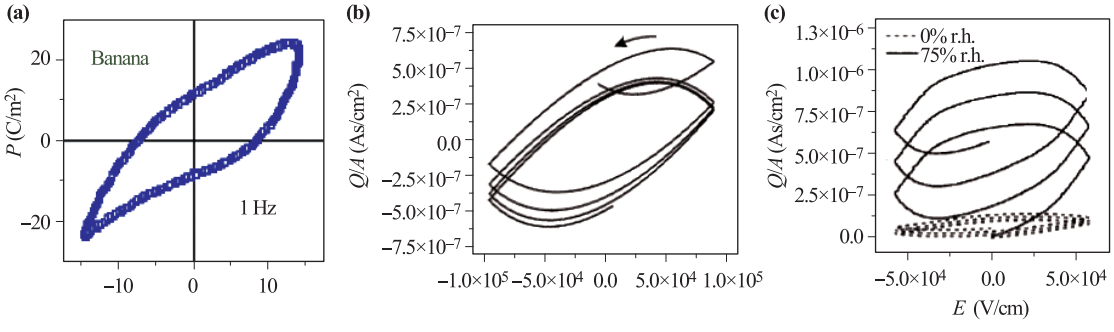

Fig. 3 P–E loops: Elliptical shape on banana **(a)** [4]; due to internal space charge polarization **(b)** [6]; measured for different relative humidities **(c)** [7].

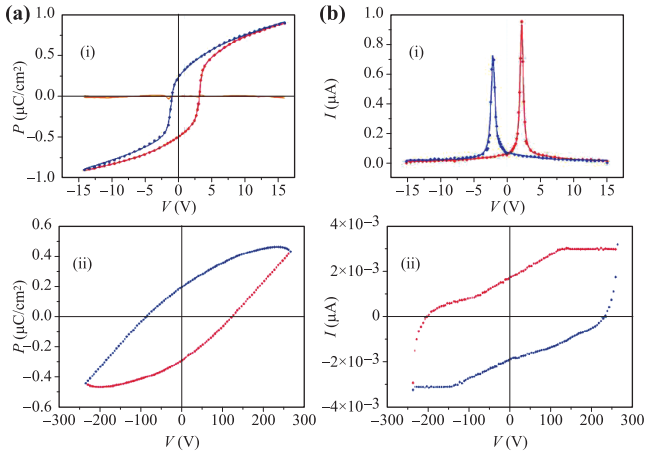

Fig. 4 Ferroelectric (i) and pointed (ii) loops. P–E loop **(a)** and its derivative – current loop **(b)** [9].

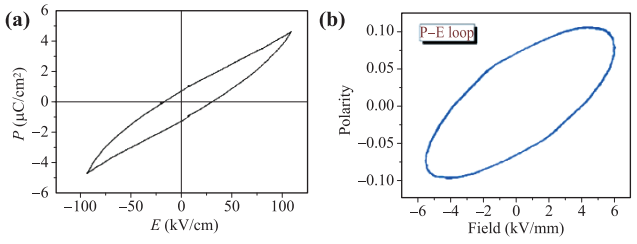

Fig. 5 Typical pointed and elliptical P–E loops obtained in methylamine borogermanate [I.45] **(a)** and in L-prolinium tartrate crystals [I.51] **(b)**.

hundreds of papers have been published in the scientific literatures devoted to materials having ferromagnetic as well as ferroelectric properties, the so-called multiferroics. This ceramic group was separated in Table 2.

Recapitulation

An overview of a number of published papers on ferroelectric materials reveal commonly encountered errors:

- not taking into account that ferroelectric properties can only exist in materials having a polar axis of symmetry;
- presentation of an elliptical or pointed P–E hysteresis loop as evidence of ferroelectric properties;
- enhancement the value of remnant polarization due to the increasing electrical field only show the increase in dielectric loss and not prove the existence of spontaneous polarization;
- interpretation of a small maximum of the dielectric constant as evidence of transition from ferroelectric to paraelectric phase of single crystal studied.

This critical analysis could help reviewers and authors to avoid making erroneous claims of ferroelectric properties based on incorrect interpretation of experimental data.

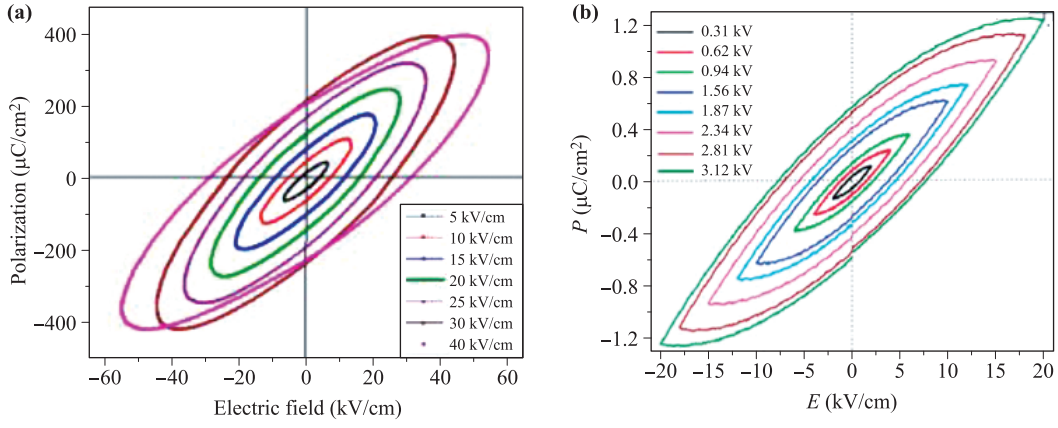

Fig. 6 Hysteresis loops at different intensities of the applied electric field in $Bi_{1-x}Dy_xFe_{0.98}Cu_{0.02}O_3$ ceramic [II.185] – elliptical shape in **(a)** and in copper-(o-phthalate) polymer [III.16] – pointed shape in **(b)**.

Part I

Table 1 False or unconfirmed ferroelectric properties in single crystals.

No.	Substance	Symmetry	Shape of P–E loop	Anomaly of dielectric permittivity	Ref.
1	urea oxalic acid *in fact it is bis-urea oxalic acid*	$P2_1/c$	without loop without loop	small max of ε' at 363 K small max of ε' at 373 K	[I.1] [I.2, I.3]
2	succinic acid	$P2_1/c$	without loop		[I.4]
3	urea succinic acid	$P2_1/c$	without loop elliptical loop		[I.5, I.6] [I.7]

Table 1 (Continued)

No.	Substance	Symmetry	Shape of P–E loop	Anomaly of dielectric permittivity	Ref.
4	bis(methylammonium) tetrachlorozincate	$P2_1/c$	without loop		[I.8]
5	dichloridoglycine zinc dihydrate	$C2/c$	elliptical loop without loop	max of ε' at 368 K value of ε' below 1 !	[I.9] [I.10]
6	glycine picrate *such crystal does not exist*	$P2_1/a$	elliptical loop		[I.11]
7	glycine manganese chloride dihydrate	$P2_1/n$	narrow pointed loop		[I.12]
8	α-glycine doped with formic acid	$P2_1/n$	pointed loops	unrealistic polarization: 300 $\mu C/cm^2$ and applied field: 200 kV/mm	[I.13]
9	$[N(CH_3)_3H]_2CuCl_4$	$P2_1/c$	without loop	max of ε' at 293 K	[I.14]
10	$LuFe_2O_4$	$R\bar{3}m$	narrow pointed loops	max of ε' at 280 K	[I.15]
11	ammonium tetroxalate dihydrate	$P\bar{1}$	without loop	small max of ε' at 373 K	[I.16]
12	$[N(CH_3)_3H]_2ZnCl_4$	$Pnma$	without loop	max of ε' at 280 K	[I.17]
13	disodium hydrogen orthophosphate	$Pbca$	without loop	max of ε' at 74 °C	[I.18]
14	para-ethyl anilinium nitrate	$P2_12_12_1$	series of pointed loops		[I.19]
15	rubidium hydrogen tartrate	$P2_12_12_1$	without loop		[I.20]
16	$[Mn_3(HCOO)_6](C_2H_5OH)$	$P\bar{1}$ (?) below T_c	narrow pointed loops	max of ε' at 165 K	[I.21]
17	$Rb_{0.82}Mn[Fe(CN)_6]_{0.94}\cdot H_2O$	$I\bar{4}m2$ at low-temp. phase	narrow pointed loop at 77 K		[I.22]
18	ethylenediamine ditartrate dihydrate	$P4_22_12$	elliptical loop		[I.23]
19	ethylenediaminium tetrachlorozincate	$P2_12_12_1$	series of pointed loops		[I.24]
20	L-Alanine	$P2_12_12_1$	elliptical loop		[I.25]
21	terbium hydrogen tartrate trihydrate	$P4_12_12$	elliptical loop	max of ε' at 95 °C	[I.26]
22	sodium acid phthalate	$P2_12_12_1$ *in fact B2ab*	elliptical loop		[I.27]
23	ammonium tetroxalate dihydrate	$P\bar{1}$	without loop	max of ε' at 373 K	[I.28]
24	2-furoic acid	$P\bar{1}$	without loop	small max of ε' at 318 K	[I.29]
25	$[C_7H_{16}N_2][ZnCl_4]$ 3-aminoquinuclidinediium tetrachlorozincate	$P2_1/c$	without loop	small maximum of ε' at 338 K	[I.30]
26	$(C_2H_5NO_2)_{1-x}(MnCl_2)_x$, $x = 0.005$, 0.02 $(C_2H_5NO_2)_{1-x}(MnCl_2)_x$, $x = 0.04$ $(C_2H_5NO_2)_{1-x}(MnCl_2)_x$, $x = 0.05$	$P\bar{1}$ $P2_1/c$ $P2_1/m$	without loop without loop without loop	small max of ε' at 200 K	[I.31]
27	tetramethyammonium cadmium bromide	$P6_3/m$	without loop	max of ε' at 433 K	[I.32]
28	lead nitrate	$Pa3$	without loop	max of ε' at 40 °C	[I.33]
29	magnesium hydrogen phosphate	$Pbca$	without loop		[I.34]
30	urea oxalic acid	$P2_1/c$	without loop	max of ε' at 373 K	[I.35]
31	sodium acid phthalate	B2ab	unrealistic applied field: 300 kV/cm		[I.36]
32	β-$CH_3NH_3PbI_3$	I4cm	series of pointed loops		[I.37]
33	lithium potassium sulphate	P3c	narrow pointed loops below $T_C = -24$ °C		[I.38]
34	sodium para-nitrophenolate dihydrate doped Fe^{3+}	Ima2	elliptical loop	small max of ε' at 28 °C	[I.39] [I.40]
35	potassium hydrogen phthalate doped: L-histidine, Ba^{2+}	$Pca2_1$	without loops	max of ε' at 373 K	[I.41] [I.42]
36	tri-glycine barium nitrate *such crystal does not exist*	orthorhombic	pointed loop		[I.43]
37	$(NH_4)_2ZnBr_2Cl_2$ $(NH_4)_2CaBr_2Cl_2$	orthorhombic tetragonal	elliptical loop elliptical loops	max of ε' at 423 K max of ε' at 443 K	[I.44]
38	$Cu(OH)_2$	$Cmc2_1$	without loop	max of ε' at 330 K	[I.45]
39	β-$K_2B_2Ge_3O_{10}$	C2	series of pointed loops powder sample		[I.46]
40	$(CH_3NH_3)_2[Ge(B_4O_9)]$	C2	pointed loops		[I.47]
41	$Ba_3[Ge_2B_7O_{16}(OH)_2](OH)(H_2O)$	Cc	series of elliptical loop		[I.48]

Table 1 (Continued)

No.	Substance	Symmetry	Shape of P–E loop	Anomaly of dielectric permittivity	Ref.
42	(diisopropylammonium)$_2$MnBr$_4$	Iba2	pointed loops		[I.49]
43	lithium sulphate monohydrate	$P2_1$	without loop	max of ε' at 74 °C	[I.50]
44	L-valine hydrobromide	$P2_1$	without loop	small max of ε' at 120 °C	[I.51]
45	L-histidinium dihydrogen arsenate orthoarsenic acid	$P2_1$	elliptical loops	small max of ε' at 307 K	[I.52]
46	L-prolinium tartrate	$P2_1$	elliptical loop	small max of ε' at 45 °C	[I.53] [I.54]
47	4-aminopyridinium hydrogen maleate	$P2_1$	elliptical loop		[I.55]
48	$C_{54}H_{86}Cl_4N_6Ni_3O_{34}$	$P2_1$	pointed loop		[I.56]
49	bis(imidazolium) L-tartrate	$P2_1$	unsaturated loops		[I.57]
50	glycine phosphite glycine phosphite - doped Ce^{3+}, Nd^{3+}, La^{3+} glycine phosphite - doped Zn^{2+}, Mg^{2+}, Cd^{2+}	$P2_1$ at ferro-phase	elliptical loop elliptical loops elliptical loops		[I.58] [I.58] [I.59]
51	N, N-dimethylurea picrate	monoclinic	without loop	small max of ε' at 323 K	[I.60]
52	L-alanine 2-furoic acid *in fact 2-furoic acid*	P1	without loop	small max of ε' at 318 K	[I.61]
53	lithium nitrate monohydrate oxalate *such crystal does not exist*	P1	elliptical loop	small max of ε' at 33 °C	[I.62]
54	$PbPt(IO_3)_6(H_2O)$	R3	elliptical loop		[I.63]
55	5, 5′-dimethyl-2, 2′-bipyridine: bromanilic acid *co-crystal*	$P\bar{1}$ or P1 below 253 K	pointed loop	max of ε' at 253 K	[I.64]
56	L-cystine hydrochloride	C2	pointed loop		[I.65]
57	L-arginine 4-nitrophenolate 4-nitrophenol dehydrate	$P2_1$	pointed loop		[I.66]
58	diammonium dibromodichlorinate Ca-doped diammonium dibromodichlorinate Zn-doped	tetragonal orthorhombic	pointed loop pointed loop	max of ε' at 433 K max of ε' at 423 K	[I.67]

Part II

Table 2 False or unconfirmed ferroelectric properties in polycrystalline ceramics.

No.	Substance	Symmetry	Shape of P–E loop	Ref.
1	hydroxyapatite $Ca_{10}(PO_4)_6(OH)_2 + x$Ce ($x = 0.2, 0.3, 0.4, 0.5$)	$P6_3/m$	elliptical loops	[II.1]
2	hydroxyapatite $Ca_{10}(PO_4)_6(OH)_2 + x$Sr ($x = 0.2, 0.3, 0.4, 0.5$)	$P6_3/m$	elliptical loops	[II.2]
3	hydroxyapatite $Ca_{10}(PO_4)_6(OH)_2 - x$La ($x = 0.1, 0.2, 0.3, 0.4, 0.5$)	$P6_3/m$	elliptical loops	[II.3]
4	$BaBi^{3+}_{0.5}(Bi^{5+}_{0.2}Nb^{5+}_{0.3})O_3$	$R\bar{3}$	series of elliptical loops	[II.4]
5	$Bi_3Pb_2Nb_2O_{11}Cl$	$P4/mmm$ at RT	without loop max of ε' at 683 K	[II.5]
6	$MnTeMoO_6$	$P2_12_12_1$	narrow pointed loop	[II.6]
7	$C_nH_{2n+1}NH_3{-}Sr_2Nb_3O_{10}$ ($n = 1 \div 6$)	$P2_12_12_1$	elliptical loops	[II.7]
8	$NaNbO_3$ $Na_{0.9}Li_{0.1}NbO_3$	$Pbma$ $Pbma$	series of pointed loops series of pointed loops	[II.8]
9	$Ni_4Nb_2O_9$	$Pbnm$	narrow pointed loops	[II.9]
10	$BaSn_{1-x}Te_xO_3$ ($x = 0, 0.05, 0.10, 0.15$)	$Fm3m$	narrow pointed loops	[II.10]
11	$Na_2Pb_2Sm_2W_2Ti_4$ Nb_4O_{30}	$C222$	narrow pointed loop	[II.11]
12	$Na_2Pb_2Nd_2W_2Ti_4V_4O_{30}$	$C222$	elliptical loop	[II.12]
13	$Na(Ta_{1-x}Nb_x)O_3$ ($x = 0.2, 0.4, 0.6, 0.8$)	$Pbcm$	pointed loops	[II.13]
14	$FeTiTaO_6$	$P4_2/mnm$	elliptical loop	[II.14]
15	$Na_2Pb_2La_2W_2Ti_4Nb_4O_{30}$	orthorhombic	pointed loop	[II.15]
16	$CaBi_2Nb_2O_9 + x$MnCO$_3$ ($x = 0, 0.125, 0.25, 0.375, 0.5$)	orthorhombic	pointed loop	[II.16]
17	$Pr_2Ti_2O_7$	$P2_1$	pointed loops	[II.17]
18	$Ba_5SmFe_{1.5}Nb_{8.5}O_{30}$	P4bm	series of pointed loops	[II.18]
19	$Bi_8Fe_4Ti_3O_{24}$ ($x = 0.1, 0.2, 0.3, 0.4$)	F2mm	pointed loops	[II.19]

Table 2 (Continued)

No.	Substance	Symmetry	Shape of P–E loop	Ref.
20	$Na_2Pb_2Eu_2W_2Ti_4X_4O_{30}$ (X = Nb, Ta)	Cmm2	pointed loops	[II.20]
21	$Bi_4Ti_3O_{12}$	orthorhombic	narrow pointed loop	[II.21]
22	$(1-x)BaZr_{0.025}Ti_{0.975}O_3$–$(x)BiFeO_3$ (x = 0.1, 0.2, 0.3, 0.4)	orthorhombic	pointed loops	[II.22]
23	$Cu_2[Mo(CN)_8]\cdot 8H_2O$ *nearly amorphous structure*	$C_{\infty v}$ after application of electric field	narrow pointed loop below 150 K	[II.23]
24	$(60-x)$ SiO_2–15CaO–$10Al_2O_3$–$5TiO_2$–$(10+x)Na_2O$ (x = 0, 5%, 10%, 15%)	amorphous	narrow pointed loops	[II.24]
25	$RbBiNb_2O_7$	$P2_1am$	elliptical loop	[II.25]
26	$AgMn_{0.04}Nb_{0.96}O_3$ $AgW_{0.04}Nb_{0.96}O_3$ $AgNbO_3$	orthorhombic	pointed loop pointed loop pointed loop	[II.26]
27	$BaCu_{1/3}Nb_{2/3}O_3$	P4mm	elliptical loop	[II.27]
28	$Ba(Cd_{1/3}Nb_{2/3})O_3$	perovskite structure	series of elliptical loops	[II.28]
29	$Sr_4Pr_2Ti_4Nb_6O_{30}$	tetragonal	pointed loop	[II.29]
30	$0.97Bi_{0.5}(Na_{0.80-x}Li_xK_{0.20})_{0.5}TiO_3$–$0.03CaZrO_3$ (x = 0, 0.02, 0.04, 0.06, 0.08, 0.10)	rhombohedral	elliptical loops	[II.30]
31	$CaBi_2Nb_2O_9$ + $x MnCO_3$ (x = 0, 0.25%, 0.375%, 0.50%)	$A2_1am$	pointed loops	[II.31]
32	$Bi_2VO_{5.5}$	mm2	narrow pointed loop	[II.32]
33	$La_{0.05}Li_{0.85}NbO_3$	R3c	pointed loop	[II.33]
34	$Bi_{0.5}Na_{0.5}TiO_3$–$Ba_{0.94}Sr_{0.06}(Sn_{0.08}Ti_{0.92})O_3$ (x = 0.00, 0.02, 0.04, 0.06, 0.08)	rhombohedral	pointed loops	[II.34]
35	PLZT 9/65/35 + $x Bi_2O_3/CuO$ (x = 0, 0.25%, 0.5%, 1.0%)	perovskite structure	elliptical loops	[II.35]
36	$Ba_4SrSmTi_3V_7O_{30}$ $Ba_4SrDyTi_3V_7O_{30}$	orthorhombic orthorhombic	narrow pointed loop narrow pointed loop	[II.36]
37	$Ba_3Sr_2DyTi_3V_7O_{30}$	orthorhombic	narrow pointed loop	[II.37]
38	$Na_{1/2}Y_{1/2}TiO_3$	orthorhombic	pointed loop	[II.38]
39	$KCa_2Nb_5O_{15}$	orthorhombic	narrow pointed loop	[II.39]
40	$Bi_4Ti_3O_{12}$ using urea, glycine and dextrose as fuel	B2cb	narrow pointed loops	[II.40]
41	$(1-x)CaBi_2Nb_2O_9$–$xNa_{0.5}Bi_{2.5}Nb_2O_9$ (x=0, 0.2, 0.4, 0.6, 0.8, 1.0)	$A2_1am$	pointed loops	[II.41]
42	$Ca_3Ti_2O_7$ $Ca_{2.85}Na_{0.15}Ti_2O_7$	$Ccm2_1$	narrow pointed loops	[II.42]
43	$Bi(Fe_{0.9}La_{0.1})O_3$	orthorhombic	elliptical loop	[II.43]
44	$Bi_2LaTiVO_9$	orthorhombic	elliptical loop	[II.44]
45	$(55-x)SiO_2$:xFe_2O_3:$1Al_2O_3$:6.3CaO:$0.2Sb_2O_3$:$13B_2O_3$:4.5BaO: $20Na_2O$ (x = 0, 5 mol%, 10 mol%, 15 mol%, 20 mol%, 25 mol%)	glass	narrow pointed loops	[II.45]
	Multiferroic ceramics			
46	$GdFe_{1-x}Cr_xO_3$ (x = 0.1, 0.3, 0.5, 0.7, 0.9)	Pbnm	pointed loops	[II.46]
47	$Bi_{0.9}Gd_{0.1}Fe_{1-x}Ti_xO_3$ (x = 0.05)	Pnma	pointed loop	[II.47]
48	$Bi_2Fe_{4(1-x)}Co_{4-x}O_9$ (x = 0, 0.005, 0.01, 0.015, 0.02)	Pbam	pointed loops	[II.48]
49	$SmFeO_3$ – doped Er^{3+}	Pnma	pointed loops	[II.49]
50	$BiFeO_3$ $Bi_{0.825}Pb_{0.175}FeO_3$ $Bi_{0.725}La_{0.1}Pb_{0.175}FeO_3$	R3c P4/mmm P4/mmm	pointed loop pointed loop pointed loop	[II.50]
51	$Bi_{0.8}Er_{0.2}FeO_3$ $Bi_{0.8}Er_{0.2}Fe_{0.9}Co_{0.1}O_3$ $Bi_{0.8}Er_{0.2}Fe_{0.9}Mn_{0.1}O_3$	Ibmm Ibmm Ibmm	narrow pointed loop narrow pointed loop elliptical loop	[II.51]
52	$Ba_{1-x}Gd_xCo_xFe_{12-x}O_{19}$ (x = 0, 0.1, 0.2, 0.3, 0.4, 0.5, 0.6)	$P6_3/mmc$	elliptical loops	[II.52]
53	$Bi_{1-x}La_xFeO_3$ (x = 0, 0.05, 0.10, 0.15, 0.20)	C222	elliptical loop at 800 °C	[II.53]
54	$Bi_{0.8}La_{0.2}Fe_{0.9}Mn_{0.1}O_3$	C222	elliptical loops	[II.54]
55	$Y_{0.1}Co_{1.9}MnO_4$	Fd3m	pointed loop	[II.55]
56	$Sr_3Co_2Fe_{24}O_{41}$	$P6_3/mmc$	series of pointed loops	[II.56]
57	$Bi_2Fe_4O_9$	Pbam	series of pointed loops	[II.57]
58	$Bi_2Fe_{4(1-x)}Ti_{4x}O_9$ (x = 0, 0.04, 0.08, 0.15, 0.2)	Pbam	series of pointed loops	[II.58]

Table 2 (Continued)

No.	Substance	Symmetry	Shape of P–E loop	Ref.
59	$0.5Ba(Zr_{0.2}Ti_{0.8})O_3$–$0.5(Ba_{0.7}Ca_{0.3})TiO_3$–$CoFe_2O_4$ $0.5Ba(Zr_{0.2}Ti_{0.8})O_3$–$0.5(Ba_{0.7}Ca_{0.3})TiO_3$–$Co(Fe_{1.5}Al_{0.5})O_4$	P4/mmm P4/mmm	narrow elliptical loops narrow elliptical loops	[II.59]
60	$0.5(BiFeO_3)$–$0.1(PrFeO_3)$–$0.1(DyFeO_3)$–$0.3(BaTiO_3)$ $0.45(BiFeO_3)$–$0.075(PrFeO_3)$–$0.025(DyFeO_3)$–$0.45(BaTiO_3)$ $0.45(BiFeO_3)$–$0.1(PrFeO_3)$–$0.45(BaTiO_3)$ $0.4(BiFeO_3)$–$0.1(PrFeO_3)$–$0.1(DyFeO_3)$–$0.4(BaTiO_3)$	R3c R3c Pm3m Pm3m	pointed loop pointed loop pointed loop pointed loop	[II.60]
61	$Bi_{1-x}Tb_xFeO_3$ ($x = 0.05$, 0.10) $Bi_{1-x}Tb_xFeO_3$ ($x = 0.15$)	R3c Pnma	narrow pointed loops narrow pointed loop	[II.61]
62	$Bi_2Fe_{4(1-x)}Cr_{4x}O_9$ ($x = 0$, 0.02, 0.04, 0.08)	Pbam	elliptical loops	[II.62]
63	$YFe_{1-x}Mn_xO_3$ ($x = 0.1$, 0.2, 0.4)	Pnma	narrow pointed loops at 153 and 123 K	[II.63]
64	$DyMnO_3$	Pbnm	pointed loops	[II.64]
65	$Eu_{1-x}Y_xMnO_3$ ($x = 0.2$, 0.3, 0.5)	Pbnm	narrow pointed loops	[II.65]
66	$Bi_2(Fe_{1-x}Al_x)_4O_9$ ($x = 0$, 0.05, 0.10, 0.15, 0.20, 0.25)	Pbnm	series of pointed loops	[II.66]
67	$La_{1-x}Dy_xFe_{1-y}O_3$ ($x/y = 0.1$)	Pbmn	pointed loops	[II.67]
68	$Ho_{0.9}Ca_{0.1}Mn_{0.9}Co._1O_3$	Pbnm	pointed loops	[II.68]
69	$Bi_{0.8}Gd_{0.2}FeO_3$	Pnam	pointed loop	[II.69]
70	$Bi_{0.9}Sm_{0.1}FeO_3$ $Bi_{0.9}Sm_{0.1}Fe_{1-y}Co_yO_3$ ($y = 0.02$, 0.04, 0.06, 0.08)	R3c Pnma	series of elliptical loops series of elliptical loops	[II.70]
71	$BaTi_{0.95-x}Hf_{0.05}Co_xO_3$ ($x = 0.05$, 0.1) $BaTi_{0.8}Hf_{0.05}Co_xO_3$	P4mm $P6_3/mmc$	elliptical loops elliptical loop	[II.71]
72	$Bi_{1-x}(Sr_{1/2}Pb_{1/2})_xFeO_3$ ($x = 0.1$, 0.18) $Bi_{1-x}(Sr_{1/2}Pb_{1/2})_xFeO_3$ ($x = 0.2$, 0.30)	R3c Pm3m	elliptical loops	[II.72]
73	$Fe_{1.95}Gd_{0.05}O_3$+NiO	Fd3m	narrow pointed loops	[II.73]
74	$Co_{1.25}Fe_{1.75}O_4$	Fd3m	pointed loops	[II.74]
75	$(x)YFeO_3$–(1-x)$Y_3Fe_5O_{12}$ ($x = 0.0$, 0.25, 0.50, 0.75, 1.0)	Ia3d	series of elliptical loops	[II.75]
76	Sr_2TiMnO_6	I4/m	series of pointed loops	[II.76]
77	$Ba_4YMn_{3-x}O_{11.5-\delta}$ ($x = 0.05$, 0.1, 0.2)	$R\bar{3}m$	elliptical loops	[II.77]
78	Nd_2CoMnO_6	$P2_1/n$	narrow elliptical loop	[II.78]
79	La_2NiMnO_6	Pbnm	series of pointed loops	[II.79]
80	$LaFeO_3$, $La_{0.8}Gd_{0.2}Fe_{0.97}Nb_{0.03}O_3$	Pbnm Pbnm	pointed loop pointed loop	[II.80, II.81]
81	$Bi_{1-x}Gd_xMn_2O_5$ ($x = 0.00$, 0.04, 0.08, 0.12)	Pbam	series of elliptical loops	[II.82]
82	$Sm_{1-x}Ca_xFeO_3$ ($x = 0$, 0.25, 0.5, 0.75, 1.0)	Pbnm	pointed loops	[II.83]
83	$Bi_2Fe_{4(1-x)}Co_{4x}O_9$ ($x = 0$, 0.005, 0.01, 0.015, 0.02)	Pbam	pointed loops	[II.84]
84	$YCr_{1-x}Ti_xO_3$ ($x = 0.0$, 0.01, 0.03, 0.05, 0.10)	Pnma	series of pointed loops	[II.85]
85	$Ni_{1-x}A_xTiO_3$ (A = Mn, Fe, Co; $x = 0$, 0.1) $Ni_{1-x}A_xTiO_3$ (A = Cu, Zn; $x = 0.05$)	$R\bar{3}m$	pointed loops	[II.86]
86	$CoFe_{2-x}Bi_xO_4$ ($x = 0$, 0.05, 0.1, 0.5, 1.0)	Fd3m	elliptical loops	[II.87]
87	$La_{0.9}Tb_{0.1}FeO_3$ $LaFeO_3$	Pbnm Pbnm	series of pointed loops series of pointed loops	[II.88]
88	$BaTi_{1-x}Fe_xO_3$ ($x = 0$, 0.1, 0.2, 0.3); $BaTi_{1-x}Fe_xO_3$ ($x = 0.4$, 0.5)	P4mm coexistence $6_3/mmc$ and P4mm	narrow pointed loops elliptical loops	[II.89]
89	$0.5Ba(Zr_{0.2}Ti_{0.8})O_3$–$0.5(Ba_{0.7}Ca_{0.3})TiO_3$–$CoFe_2O_4$	coexistence 4/mmm and spinel	pointed loop	[II.90]
90	$0.9Na_{0.5}Bi_{0.5}TiO_3$+$0.1BaFe_{12}O_{19}$	coexistence $6_3/mmm$ and Cc	pointed loops	[II.91]
91	$0.1Ni_{0.8}Zn_{0.2}Fe_2O_4$+$0.9Pb_{1-3x/2}La_xZr_{0.65}Ti_{0.35}O_3$ ($x = 0$, 0.01, 0.02, 0.03)	coexistence Fm3d and R3c	pointed loops	[II.92]
92	$xCo_{0.8}Ni_{0.2}Fe_2O_4$+$(1-x)Pb_{0.99625}La_{0.0025}Zr_{0.55}Ti_{0.45}O_3$ ($x = 0.05$, 0.10, 0.15)	coexistence Fm3d and P4mm	elliptical loops	[II.93]
93	$(1-x)Pb(Zr_{0.52}Ti_{0.48})O_3 - (x)CoFe_2O_4$ ($x = 0.20$, 0.35, 0.50)	coexistence Fm3d and P4mm	pointed loops	[II.94]
94	$Bi_{0.8}Ca_{0.2}Fe_{1-x}Nb_xO_3$ ($x = 0.00$, 0.05, 0.07, 0.10)	coexistence Pbnm and R3c	pointed loops	[II.95]

Table 2 (Continued)

No.	Substance	Symmetry	Shape of P–E loop	Ref.
95	$Ba_{0.85}Ca_{0.15}Zr_{0.1}Ti_{0.9}O_3$–$CoFe_2O_4$	coxistence Fm3d and P4mm	elliptical loops	[II.96]
96	$0.20(Co_{1-x}Zn_xFe_{2-y}Mn_yO_4)$–$0.80(Pb_{0.70}Ca_{0.30}TiO_3)$ ($x = 0.4$, $y = 0$); ($x = 0$, $y = 0.2$); ($x = 0.4$, $y = 0.2$)	coexistence Fm3d and P4mm	elliptical loops	[II.97]
97	$0.75BiFeO_3$–$0.25BaTiO_3$	coexistence Fm3d and R3c	series of elliptical loops	[II.98]
98	$(1-x)CoFe_2O_4+(x)BaTiO_3$ ($x = 0.25$, 0.5, 0.75, 1)	coexistence Fd3m and P4mm	elliptical loops	[II.99]
99	$(x)NiFe_2O_4$–$(1-x)BaTiO_3$ ($x = 0.1$, 0.2, 0.3, 0.4, 0.5, 0.6)	coexistence Fm3d and P4mm	narrow pointed loops	[II.100]
100	$(x)NiFe_2O_4$–$(1-x)BaTiO_3$ ($x = 0.1$, 0.2, 0.3, 0.4, 0.5, 0.6)	coexistence Fd3m and P4mm	narrow pointed loops	[II.101]
101	$(1-x)Pb(Zr_{0.52}Ti_{0.48})O_3$–$(x)CoFe_2O_4$ ($x = 0.10$, 0.20, 0.30, 0.40)	coexistence Fd3m and P4mm	pointed loops	[II.102]
102	$(1-x)BaTiO_3$–$(x)CoFe_{1.8}Zn_{0.2}O_4$ ($x = 0.10$, 0.20, 0.30, 0.40)	coexistence Fd3m and P4mm	elliptical loops	[II.103]
103	$(x)BaTiO_3$–$(1-x)Ni_{0.2}Cu_{0.2}Zn_{0.6}Fe_{1.96}O_4$ ($x = 0.1$, 0.5, 0.9)	coexistence Fd3m and P4mm	pointed loops	[II.104]
104	$(BaTiO_3)_{0.70}(Li_{0.3}Zn_{0.4}Fe_{2.3}O_4)_{0.30}$	coexistence Fd3m and P4mm	series of pointed loops	[II.105]
105	$(x)NiFe_2O_4$–$(1-x)Pb(Zr_{0.58}Ti_{0.42})O_3$ ($x = 0.2$, 0.3, 0.4, 0.5)	coexistence Fd3m and R3m	elliptical loops	[II.106]
106	$(1-x)BaTi_{0.9}Zr_{0.1}O_3$–$(x)Li_{0.5}Fe_{2.5}O_4$ ($x = 0$, 0.05, 0.1, 0.15)	coexistence cubic and tetragonal	elliptical loops	[II.107]
107	$(1-x)BiFeO_3$–$xNiFe_2O_3$ ($x = 0.01$, 0.02, 0.03) $(1-x)BiFeO_3$–$xNiFe_2O_4$ ($x = 0.01$, 0.02, 0.03)	cubic spinel cubic spinel	elliptical loops elliptical loops	[II.108]
108	$(1-x)Bi_{0.85}La_{0.15}FeO_3$–$(x)CoFe_2O_4$ ($x = 0.10$, 0.20, 0.30, 0.40, 0.50)	coexistence Pbnm and R3c	pointed loops	[II.109]
109	$(Bi_{0.86}Sm_{0.14})(Fe_{1-x}Ti_x)O_3$ ($x = 0$, 0.005, 0.010)	coexistence Pbam and R3c	series pointed loops	[II.110]
110	$CoFe_2O_4$, $CoFe_2O_4$–10%$BaTiO_3$; $CoFe_2O_4$–30%$BaTiO_3$	Fd3m coexistence cubic and tetragonal	elliptical loop narrow pointed loop	[II.111]
111	$(1-x)GaFeO_3$–$(x)Co_{0.5}Zn_{0.5}Fe_2O_4$ ($x = 0.0$, 0.1, 0.2)	coexistence Fd3m and $Pc2_1n$	poined loops	[II.112]
112	$0.1Ni_{0.8}Zn_{0.2}Fe_2O_4$–$0.9Pb_{1-3x/2}Sm_xZr_{0.65}Ti_{0.35}O_3$ ($x = 0$, 0.01, 0.02, 0.03)	coexistence cubic spinel and rhombohedral	pointed loops	[II.113]
113	$Ni_{0.5}Zn_{0.5}Fe_2O_4$–$Pb(Zr_{0.53}Ti_{0.47})O_3$	coexistence cubic spinel and tetragonal perovskite	elliptical loop	[II.114]
114	$Bi_{1-x}Sm_xFeO_3$ ($x = 0.00$, 0.05, 0.10, 0.15)	coexistence Pnma and R3c	pointed loops	[II.115]
115	$(1–x)Co_{0.8}Cu_{0.2}Fe_2O_4$–$(x)Ba_{0.6}Sr_{0.4}TiO_3$ ($x = 0$, 0.4, 0.45, 0.475, 0.5, 0.525, 0.55, 1)	coexistence cubic spinel and tetragonal	pointed loops	[II.116]
116	$(1-x)PZT$–$(x)NiFe_{1.9}Co_{0.02}O_{4-\delta}$ ($x = 0.1$, 0.2, 0.3)	coexistence cubic spinel and tetragonal	pointed loops	[II.117]
117	$xNi_{0.7}Zn_{0.3}Fe_2O_4$–$(1-x)BaTiO_3$ ($x = 0.1$, 0.3, 0.5, 0.7, 09)	coexistence cubic spinel and tetragonal	pointed loops	[II.118]
118	$BiFe_{1-x}Hf_{(3/4)x}O_3$ ($x = 0$, 0.05, 0.10, 0.15, 0.20)	cubic perovskite	pointed loops	[II.119]
119	$Sr_{1-x}Fe_xTi_{1.05-y}O_3$ ($x = 0.1$, 0.2; $y = 0$, 0.1, 0.2)	cubic perovskite	elliptical loops	[II.120]
120	$Bi_{1-x}La_xFeO_3$ ($x = 0.0$, 0.2, 0.4, 0.6, 0.8, 1.0)	coexistence R3m and Pbnm	pointed loops	[II.121]
121	$BaTi_{1-x}Fe_xO_3$ ($x = 0$, 0.01, 0.04, 0.07, 0.12)	coexistence tetragonal and hexagonal	series of narrow pointed loops	[II.122]
122	$Bi_{0.9}Eu_{0.1}FeO_3$ $Bi_{0.9}Gd_{0.1}FeO_3$ $Bi_{0.9}Eu_{0.05}Gd_{0.05}FeO_3$	perovskite structures	narrow pointed loops	[II.123]

Table 2 (Continued)

No.	Substance	Symmetry	Shape of P–E loop	Ref.
123	$0.7(Bi_{0.5}Na_{0.5})_{1-x}Ba_xTiO_3$–$0.3NiFe_2O_4$ (x = 0.02, 0.04, 0.06, 0.08, 0.1, 0.12)	coexistence perovskite and spinel structures	narrow pointed loops	[II.124]
124	$BaMgF_4$:xMn (x = 0%, 6%, 8%, 12%)	$Cmc2_1$	elliptical loops	[II.125]
125	$KBiFe_2O_5$	$P2_1cn$	series of pointed loops	[II.126]
126	$ErMnO_3$	$P6_3cm$	series of elliptical loops	[II.127]
127	$TmMnO_3$	$P6_3cm$	series of elliptical loops	[II.128]
128	$0.6BiFeO_3$–$0.4(Bi_{0.5}K_{0.5})TiO_3$	P4mm	elliptical loops	[II.129]
129	$Ba_{0.98}Bi_{0.02}Ti_{0.95}Fe_{0.05}O_3$	P4mm	pointed loop	[II.130]
130	$(1-x)(Bi_{0.5}Na_{0.5})TiO_{3-x}$–$CoFe_2O_4$ (x = 0.005, 0.01, 0.02)	rhombohedral	pointed loops	[II.131]
131	$Sr_{1-x}Mn_2Ni_xFe_4O_{11}$ (x = 0, 0.1, 0.2, 0.3)	hexagonal	pointed loops	[II.132]
132	$(1-x)BiFeO_3$–$(x)Ba(Cu_{1/3}Nb_{2/3})O_3$ (x = 0.025, 0.075, 0.10, 0.20)	coexistence tetragonal and rhombohedral	narrow pointed loops	[II.133]
133	$(1-x)BiFeO_3$–$(x)(Bi_{0.5}Na_{0.5})TiO_3$ (x = 0, 0.3, 0.4)	rhombohedral	series of pointed loops	[II.134]
134	$0.7Na_{0.5}Bi_{0.5}TiO_3$–$0.2Ba_{0.925}Nd_{0.05}TiO_3$–$0.1BiFeO_3$ $0.7Na_{0.5}Bi_{0.5}TiO_3$–$0.1Ba_{0.925}Nd_{0.05}TiO_3$–$0.2BiFeO_3$	rhombohedral	narrow pointed loops	[II.135]
135	$Bi_{0.80-x}Ba_{0.20}Ho_xFeO_3$ (x = 0.0, 0.05, 0.10, 0.15, 0.20)	coexistence R3c and P1	narrow pointed loops	[II.136]
136	$BiFe_{1-x}Ni_xO_3$ (x = 0, 0.01, 0.02, 0.03)	R3c	elliptical loops	[II.137]
137	$BiFeO_3$– *hydrothermal & hydroevaporated samples*	R3c	elliptical loops	[II.138]
138	$(Bi_{0.9}La_{0.1})FeO_3$–$Pb(Fe_{0.5}Nb_{0.5})O_3$	R3c	pointed loops	[II.139]
139	$Bi_{0.8}RE_{0.2}FeO_3$, RE = La, Nd, Dy	R3c	pointed loops	[II.140]
140	$Bi_{1-x}La_xFe_{1-y}Ni_yO_3$ (x = 0, 0.1; y = 0, 0.05)	R3c	elliptical loops	[II.141]
141	$AgAl_{0.02}Cr_{0.98}S_2$	R3m	pointed loops	[II.142]
142	$Bi_{1-x}Ba_xFeO_3$ (x = 0.1, 0.2, 0.3)	R3c	elliptical loops	[II.143]
143	$Bi_{1-x}Ba_xFeO_3$ (x = 0.1, 0.2)	R3c	elliptical loops	[II.144]
144	$(Bi_{1-x}Na_x)(Fe_{1-x}Nb_x)O_3$ (x = 0.1, 0.3, 0.5)	R3c	narrow pointed loops	[II.145]
145	$(1-x)BiFeO_3$–$(x)SrTiO_3$ (x = 0, 0.2, 0.3, 0.4, 0.6)	R3c	elliptical loops	[II.146]
146	$BiFeO_3$	R3c	series of pointed loops	[II.147–II.151]
147	$Bi_{1-x}Y_xFe_{1-y}Zr_yO_3$ (x = 0.05, 0.1, 0.15; y = 0.05)	R3c	narrow pointed loops	[II.152]
148	$Bi_{0.8}Dy_{0.2}Fe_{1-y}Ti_yO_3$ (y = 0.02)	R3c	pointed loop	[II.153]
149	$BiFe_xO_3$ (x = 0.8, 1.0, 1.2)	R3c	elliptical loops	[II.154]
150	$Bi_{1.05-x}Dy_xFeO_3$ (x = 0, 0.05. 0.1)	R3c	pointed loops	[II.155]
151	$Bi_{1-x}Nd_xFe_{0.96}Co_{0.04}O_3$ (x = 0.02, 0.05, 0.10, 0.15, 0.20)	R3c	elliptical loops	[II.156]
152	$Bi_{0.95}Eu_{0.05}FeO_3$ $Bi_{0.95}Ba_{0.05}FeO_3$ $Bi_{0.90}Eu_{0.05}Ba_{0.05}FeO_3$	R3c R3c R3c	narrow pointed loop narrow pointed loop narrow pointed loop	[II.157]
153	$Bi_{0.95}Gd_{0.05}FeO_3$ $Bi_{1-x}Gd_xFe_{0.98}Cu_{0.02}O_3$ (x = 1%, 2%, 3%, 4%, 5%)	R3c R3c	elliptical loop elliptical loop	[II.158]
154	$0.7BiFeO_3$–$0.3BaTiO_3$	R3c	elliptical loop	[II.159]
155	$Bi_{1-x}Eu_xFeO_3$ (x = 0, 0.01, 0.05, 0.10)	R3c	pointed loops	[II.160]
156	$0.5(BiLa_yFe_{1-y}O_3)$–$0.5(PbZrO_3)$ (x = 0.05, 0.10, 0.15, 0.20)	R3c	narrow pointed loops	[II.161]
157	$0.95BiFeO_3$–$0.05BaTiO_3$	R3c	pointed loop	[II.162]
158	$Bi_{1-x}La_xFeO_3$ (x = 0.0, 0.05, 0.10, 0.15, 0.20, 0.25)	R3c	elliptical loops	[II.163]
159	$Bi_{1-x}La_xFeO_3$ (x = 0.05, 0.10, 0.15)	R3c	elliptical loops	[II.164]
160	$(1–x)BiFeO_3$–$(x)BaTiO_3$ (x = 0, 0.10, 0.20, 0.25, 0.30)	R3c	pointed loops	[II.165]
161	$Bi_{1-x}Nd_xFe_{0.98}Co_{0.02}O_3$ (x = 0.01, 0.02, 0.03, 0.04, 0.05, 0.06)	R3c	elliptical loops	[II.166]
162	$0.70BiFeO_3$–$(x)A'(Zn_{1/2}Ti_{1/2})O_3$–$(0.30–x)SrTiO_3$ A′ = Bi, La; (x = 0.02, 0.04, 0.06)	R3c	elliptical loops	[II.167]
163	$(1-x)BiFeO_3$–$(x)SrTiO_3$ (x = 0, 0.1, 0.2, 0.3, 0.4)	R3c	series of elliptical loops	[II.168]
164	$Bi_{1-x}Sr_xFe_{0.80}Ti_{0.20}O_3$ (x = 0.05, 0.10, 0.15)	R3c	pointed loops	[II.169]

Table 2 (Continued)

No.	Substance	Symmetry	Shape of P–E loop	Ref.
165	$(x)PbNiO_3$–$(y)PbZrO_3$–$(x–y)PbTiO_3$ (x=0.5; y=0.15, 0.25, 0.35)	R3m	elliptical loops	[II.170]
166	$BiFe_{1-x}Zr_xO_3$ (x = 0.00, 0.05, 0.10, 0.20, 0.30)	R3c	pointed loops	[II.171]
167	$Bi_{0.95}Mn_{0.05}FeO_3$	R3c	pointed loops	[II.172]
168	$Bi_{1-x}Pb_xFeO_3$ (x = 0.03, 0.05, 0.07)	R3c	pointed loops	[II.173]
169	$Bi_{1-x}Ho_xFeO_3$ (x = 0, 0.05, 0.1)	R3c	pointed loops	[II.174]
170	$Bi_{0.9}La_{0.1}FeO_3$; $BiFe_{0.95}Ni_{0.05}O_3$; $Bi_{0.9}La_{0.1}Fe_{0.95}Ni_{0.05}O_3$	R3c	pointed loops	[II.175]
171	$Bi_{0.8}Ba_{0.2}Fe_{1-x}Ti_xO_3$ (x = 0, 0.1, 0.2)	R3c	pointed loops	[II.176]
172	$Bi_{1-x}Tb_xFe_{1-x}Mn_xO_3$ (x = 0, 0.10, 0.15, 0.20)	R3c	pointed loops	[II.177]
173	$Bi_{1-x}La_xFe_{1-y}Mn_yO_3$ (x = 0, 0.05, 0.10, 0.15, 0,20, 0.25; y = 0, 0.5)	R3c	elliptical loops	[II.178]
174	$BiFe_{0.985}Co_{0.005}Ta_{0.01}O_{3.01}$ $BiFe_{0.98}Co_{0.01}Ta_{0.01}O_{3.01}$	R3c R3c	pointed loop	[II.179]
175	$Bi_{1-x}Ba_xFeO_3$ (x = 0, 0.1, 0.2, 0.3)	R3c	narrow pointed loops	[II.180]
176	$Bi_{1-x}Zn_xFe_{1-y}Ni_yO_3$ (x = y = 0.025, 0.05, 0.075, 0.1)	R3c	pointed loops	[II.181]
177	$LiNbO_3$	R3c	pointed loop	[II.182]
178	$BiFe_{1-x}Ni_xO_3$ (x = 0, 0.05, 0.1, 0.15)	R3c	pointed loops	[II.183]
179	$Bi_{1-x}Ba_xFeO_3$ (x = 0.10, 0.15, 0.20, 0.25)	R3c	elliptical loops	[II.184]
180	$Bi_{1-x}Dy_xFe_{0.98}Cu_{0.02}O_3$ (x = 1%, 2%, 3%, 4%, 5%)	R3c	series of elliptical loops	[II.185]
181	$(1-x)PbFe_{0.5}Nb_{0.5}O_3$–$(x)BiFeO_3$ (x = 0.0, 0.1, 0.2, 0.3, 0.4)	R3c	narrow pointed loops	[II.186]
182	α-$Fe_{1.6}Ga_{0.4}O_3$	R3c	pointed loops	[II.187]
183	$Bi_{1-x}Pr_xFeO_3$ (x = 0, 0.05, 0.10, 0.15, 0.20, 0.25)	R3c	elliptical loops	[II.188]
184	$(1-x)BiFeO_3$–$(x)Ba_{0.8}Sr_{0.2}TiO_3$ (x = 0.1, 0.2, 0.3)	R3c	elliptical loops	[II.189]
185	$Bi_{1-x}Eu_xFeO_3$ (x = 0, 0.01, 0.05, 0.10)	R3c	pointed loops	[II.190]
186	$Ba_4YMn_{3-x}Fe_xO_{11.5-\delta}$ (x = 0.05, 0.1, 0.2)	R3m	elliptical loop	[II.191]
187	$Bi_{0.9}Ce_{0.1}FeO_3$ $BiFe_{0.9}Zr_{0.1}O_3$	R3c R3c	pointed loop pointed loop	[II.192]
188	$Bi_{1-x}Sm_xFe_{1-y}Ti_yO_3$ (x, y = 0.00, 0.03, 0.06)	R3c	series of elliptical loops	[II.193]
189	$(1-x)Na_{0.5}Bi_{0.5}TiO_3$–$(x)Co_{0.75}Zn_{0.25}Cr_{0.2}Fe_{1.8}O_4$ (x = 0.0, 0.25, 0.5, 0.75, 1.0)	R3c	series of pointed loops	[II.194]
190	$Bi_{0.95-x}La_{0.05}Y_xFe_{0.95}Ti_{0.05}O_3$ (x = 0, 0.04, 0.06, 0.08, 0.10)	R3c	narrow pointed loops	[II.195]
191	$BiFe_{1-x}Ni_xO_3$ (x = 0, 0.01, 0.03, 0.05, 0.07)	R3c	series of pointed loops	[II.196]
192	$Bi_5Ti_3CuO_{15}$ $Bi_5Ti_3MnO_{15}$ $Bi_5Ti_3NiO_{15}$ $Bi_5Ti_3VO_{15}$	R3c R3c R3c perovskite structure	series of elliptical loops series of pointed loops series of elliptical loops series of elliptical loops	[II.197]
193	$(1-x)BiFeO_3$–$(x)BaTi_{0.95}(Yb_{0.5}Nb_{0.5})_{0.05}O_3$ (x = 0.1, 0.2, 0.3)	P4mm	elliptical loops	[II.198]
194	$PbTi_{1-x}Fe_xO_3$ (x = 0.03, 0.5)	P4mm	series of elliptical loops	[II.199]
195	$(Ba_{1-x}Gd)(Ti_{1-x}Fe_x)O_3$ (x = 0.1, 0.2, 0.3, 0.4, 0.5)	P4mm	elliptical loops	[II.200]
196	$Bi_{1-x}Pb_xFeO_3$ (x = 0, 0.05, 0.10, 0.15, 0.20, 0.25, 0.30)	R3c	elliptical loops	[II.201]
197	$Bi_{1-x}Sm_xFe_{1-y}Ti_yO_3$ (x, y = 0.00, 0.03, 0.06)	R3c	series of narrow pointed loops	[II.202]
198	$Bi_{1-x}Gd_xFeO_3$ (x = 0.05, 0.10) $Bi_{1-x}Gd_xFeO_3$ (x = 0.05) $Bi_{1-x}Gd_xFeO_3$ (x = 0.1, 0.15, 0.2)	R3c R3c $Pn2_1a$	narrow elliptical loops elliptical loops elliptical loops	[II.203] [II.204]
199	$SmFeO_3$	$Pna2_1$	pointed loop	[II.205]
200	$AgNbO_3$+$xTiO_2$ (x = 0.01, 0.02, 0.03, 0.04)	$Pmc2_1$	pointed loops	[II.206]
201	$BaMg_{1-x}Mn_xF_4$ (x = 0, 0.03, 0.05, 0.07)	$Cmc2_1$	elliptical loops	[II.207]
202	$SmBi_4Fe_{0.5}Co_{0.5}Ti_3O_{15}$	$A2_1am$	pointed loops	[II.208]
203	$Bi_5Ti_3FeO_{15}$ $Bi_{4.25}La_{0.75}Ti_3FeO_{15}$	$A2_1am$	pointed loop pointed loop	[II.209]
204	$Bi_{5-x}La_xTi_3Fe_{0.5}Co_{0.5}O_{15}$ (x = 0, 0.25, 0.5, 0.75, 1.0)	F2mm	elliptical loops	[II.210]
205	$Bi_{1-x}Nd_xFe_{1-y}Co_yO_3$ (x = 0, 0.10; y = 0, 0.10)	P1	pointed loops	[II.211]

Table 2 (Continued)

No.	Substance	Symmetry	Shape of P–E loop	Ref.
206	$(Bi_{0.9}La_{0.1})FeO_s$ $0.8(Bi_{0.9}La_{0.1})FeO_s$–$0.2Ba(Fe_{0.5}Nb_{0.5})O_3$ $0.5(Bi_{0.9}La_{0.1})FeO_s$–$0.5Ba(Fe_{0.5}Nb_{0.5})O_3$	coexistence rhombohedral and monoclinic	pointed loop pointed loop	[II.212]
207	$(1-x)Ba_{0.99}Ca_{0.01}Zr_{0.02}Ti_{0.98}O_3$–$(x)BiFeO_3$ (x = 0.00, 0.05, 0.10, 0.15)	coexistence tetragonal and rhombohedral	pointed loop	[II.213]
208	$KBiFe_2O_5$	orthorhombic	series of narrow pointed loops	[II.214]
209	$(Bi_{0.5}K_{0.5})(Fe_{0.5}Ta_{0.5})O_3$	hexagonal	pointed loop	[II.215]
210	$Ba_{1-x}Sr_xTiO_3$–$La_{0.67}Sr_{0.33}MnO_3$ (x = 0.20, 0.25, 0.30)	rhombohedral	narrow pointed loops	[II.216]
211	$(x)BaZr_{0.52}Ti_{0.48}O_3$–$(1-x)BiFeO_3$ (x = 0.2, 0.3) (x = 0.5)	 rhombohedral tetragonal	 narrow pointed loops narrow pointed loop	[II.217]
212	$Ba_5Li_2Ti_2Nb_5O_{30}$	tetragonal	elliptical loop	[II.218]
213	$Bi_{0.75}Ba_{0.25}Fe_{1-x}Ni_xO_3$ (x = 0, 0.025)	tetragonal	pointed loops	[II.219]
214	$(0.45Bi_{0.9}La_{0.1}FeO_3$–$0.55Co_{0.5}Ni_{0.5}Fe_2O_4)$–$(x)BaTiO_3$ (x = 0, 0.1, 0.15, 0.20)	coexistence tetragonal and orthorhombic	narrow pointed loops	[II.220]
215	$(0.75-x)BiFeO_3$–$0.25BaTiO_3$–$(x)Bi_{0.5}(Na_{0.8}K_{0.2})_{0.5}TiO_3$ + 1 mol% MnO_2 (x = 0, 0.02, 0.04, 0.06, 0.08)	orthorhombic perovskite	pointed loops	[II.221]
216	$(Bi_{1-x}Na_x)$ $(Fe_{1-x}Nb_x)O_3$ (x = 0.1, 0.2, 0.3)	rhombohedral	pointed loops	[II.222]
217	$Bi_{1-x}Ba_xFeO_3$ (x = 0.05, 0.1) $Bi_{1-x}Ba_xFe_{1-x}Nb_xO_3$ (x = 0.05, 0.1)	rhombohedral rhombohedral	elliptical loops elliptical loops	[II.223]
218	$(x)CoFe_2O_4$–$(1-x)BaTiO_3$ (x = 0.25, 0.5, 0.75, 1)	perovskite structure	elliptical loops	[II.224]
219	$(Sb_{1/2}Na_{1/2})(Fe_{2/3}W_{1/3})O_3$	orthorhombic	elliptical loop	[II.225]
220	$Dy_{2-x}Fe_xO_3$ (x = 0.7 ÷ 1.5)	orthorhombic	elliptical loops	[II.226]
221	$(La_{1/2}Li_{1/2})(Fe_{1/2}V_{1/2})O_3$	orthorhombic	elliptical loop	[II.227]
222	$(LaLi)_{1/2}(Fe_{2/3}Mo_{1/3})O_3$	orthorhombic	elliptical loop	[II.228]
223	$0.8BaTiO_3$–$0.2BaFe_{12}O_{19}$	tetragonal	elliptical loop	[II.229]
224	$Pb_2Fe_2O_5$	monoclinic	series of pointed loops	[II.230]
225	$BaFe_{12}O_{19}$	hexagonal	elliptical loop	[II.231]
226	$SrFe_{12}O_{19}$	hexagonal	elliptical loop	[II.232]
227	$Ba_{0.5}Sr_{0.5}Ti_{1-x}Fe_xO_3$ (x = 0.1, 0.4)	tetragonal	pointed loops	[II.233]
228	$Bi_4Ti_{3-x}Mg_xO_{12}$ (x = 0.2, 0.4, 0.6)	orthorhombic	pointed loops	[II.234]
229	Bi_3TiVO_9	orthorhombic	pointed loops	[II.235]
230	$Bi_2Fe_4O_9$ $Bi_{25}FeO_{39}$ $Bi_{46}Fe_2O_{72}$	rhombohedral rhombohedral rhombohedral	pointed loops pointed loops pointed loops	[II.236]
231	$Bi_4Ti_{3-x}(Nb_{0.5}Fe_{0.5})_xO_{12}$ (x = 0.5, 0.8, 1.0, 1.5, 2.0)	orthorhombic	pointed loops	[II.237]
232	$YCrO_3$	orthorhombic	series of pointed loops	[II.238]
233	$(100-x)Na_{0.5}Bi_{0.5}TiO_3$–$(x)MnFe_2O_4$ (x = 50, 70, 90)	rhombohedral	series of pointed loops	[II.239]
234	$Y_{1.8}Fe_{0.2}O_3$	tetragonal	series of pointed loops	[II.240]
235	$(Pb_{1-x}Bi_{0.5x}La_{0.5x})(Fe_xTi_{1-x})O_3$ (x = 0.1, 0.3, 0.5, 0.7)	coexistence rhombohedral and tetragonal	narrow pointed loops	[II.241]
236	$LaFeO_3$ $La_{1-x}Zn_xFeO_3$ (x = 0.10, 0.30)	perovskite structures	series of pointed loops	[II.242]
237	$Bi_{1-x}Ba_xFeO_3$ (x = 0.10, 0.15)	perovskite structure	narrow of pointed loops	[II.243]
238	$(1-x)Ba_{0.9}Sr_{0.1}Zr_{0.1}Ti_{0.9}O_3$–$(x)CoFe_2O_4$ (x = 0.0, 0.05, 0.10, 0.20, 0.30)	P4mm	elliptical loops	[II.244]
239	$Ba_5CaTi_{2-x}Cu_xNb_8O_{30}$ (x = 0.00, 0.02, 0.04, 0.06, 0.08)	P4bm	elliptical loops	[II.245]
240	$0.70Bi_{0.90}Ca_{0.10}FeO_3$–$0.30PbTiO_3$	coexistence R3c and P4mm	pointed loops	[II.246]
241	$Bi_{0.8}Ba_{0.2}Fe_{0.8}Mn_{0.2}O_3$	R3c	pointed loop	[II.247]
242	$Bi_{1-x}Pb_xFeO_3$ (x = 0, 0.05, 0.10, 0.15, 0.20, 0.25, 0.30)	R3c	elliptical loops	[II.248]

Table 2 (Continued)

No.	Substance	Symmetry	Shape of P–E loop	Ref.
243	$Bi_4(Ti_1Fe_2)O_{12-\delta}$	B1a1	elliptical loops	[II.249]
244	$(Bi_{3.15}Nd_{0.85})(Ti_2Fe_{0.5}Co_{0.5})O_{12-\delta}$	orthorhombic	series of poined loops	[II.250]
245	$Bi_8Fe_6Ti_3O_{27}$	orthorhombic	narrow pointed loop	[II.251]
246	$(Ba_{1-x}Gd)(Ti_{1-x}Fe_x)O_3$ (x = 0.2, 0.3, 0.4, 0.5)	tetragonal	elliptical loops	[II.252]
247	$Bi(Cd_{0.45}Ti_{0.45}Fe_{0.10})O_3$	orthorhombic	series of elliptical loops	[II.253]
248	$M_{3-x}(NH_4)_xCrO_8$ (M = Na, K, Rb, Cs) $(NH_4)_3CrO_8$	$Pmc2_1$ $Pmc2_1$	without loop small max of ε' at 250 K	[II.254] [II.255]
249	$Bi(Fe_{1-x}Ti_x)O_3$ (x = 0.005, 0.01, 0.015)	R3c	pointed loops	[II.256]
250	$Bi_{3.25}La_{0.75}Ti_3O_{12}$–$(La_{0.7}Sr_{0.3})MnO_3$	$A2_1am$	pointed loops	[II.257]
251	$Bi_{5-x}La_xFe_{0.5}Co_{0.5}Ti_3O_{15}$ (x = 0, 0.25, 0.5, 0.75, 1.0)	F2mm	pointed loops	[II.258]
252	$Ba_2YFeNb_4O_{15}$	P4bm	narrow pointed loop	[II.259]
253	$YMn_{0.8}Fe_{0.2}O_3$	$P6_3cm$	narrow pointed loop	[II.260]
254	$BiFeO_3$	R3c	elliptical loops	[II.261]
255	$Bi_{1-x}La_xFeO_3$ (x = 0.0, 0.05, 0.10, 0.15, 0.20, 0.25)	R3c	elliptical loops	[II.262]
256	$0.75BiFeO_3$–$0.25BaTiO_3$ (La, K = 0.5 mol%, 1 mol%, 3 mol%, 5 mol%)	rhombohedral	pointed loops	[II.263]
257	$Bi_{1-x}Er_xFeO_3$ (x = 0.00, 0.05, 0.10, 0.15, 0.20)	R3c	pointed loops	[II.264]
258	$Bi_{0.9}Pr_{0.1}FeO_3$ $Bi_{0.9}Pr_{0.1}Fe_{0.9}Ti_{0.1}O_3$	R3c	elliptical loops	[II.265]
259	$Bi_{0.95}Eu_{0.05}Fe_{1-x}Ti_xO_3$ (x = 0, 0.05, 0.10, 0.15)	R3c	pointed loops	[II.266]
260	$(1-x)BiFeO_3$–$(x)Ba_{0.7}Ca_{0.3}TiO_3$ (x = 0, 20, 0.225, 0.25, 0.275, 0.30)	perovskite structure	pointed loops	[II.267]
261	$Bi_4NdTi_3Fe_{0.7}Ni_{0.3}O_{15}$	perovskite structure	elliptical loop	[II.268]
262	$Bi_{0.8}Ba_{0.2}FeO_3$ $Bi_{0.8}Ba_{0.2}Fe_{0.95}Cr_{0.05}O_3$ $Bi_{0.8}Ba_{0.2}Fe_{0.9}Cr_{0.1}O_3$	rhombohedral	pointed loops	[II.269]
263	$0.7Bi_{1-x}Eu_xFeO_3$–$0.3Bi_{0.5}Na_{0.5}TiO_3$ (x = 0, 0.025, 0.05, 0.1)	rhombohedral	pointed loops	[II.270]
264	$BiFeO_3$ $Bi_{0.90}Y_{0.10}FeO_3$ $Bi_{0.95}Y_{0.05}FeO_3$	R3c	series of pointed loops	[II.271]
265	$Bi_{0.9}Pr_{0.1}FeO_3$ $BiFe_{0.9}Ti_{0.1}O_3$ $Bi_{0.9}Pr_{0.1}Fe_{0.9}Ti_{0.1}O_3$ $Bi_{0.9}Pr_{0.1}Fe_{0.95}Ti_{0.05}O_3$	rhombohedral	pointed loops	[II.272]
266	$BiFeO_3$ $Bi_{0.95}Ce_{0.05}FeO_3$, $Bi_{0.90}Ce_{0.10}FeO_3$ $Bi_{0.95}Ce_{0.05}Fe_{0.95}Mn_{0.05}O_3$, $Bi_{0.90}Ce_{0.10}Fe_{0.95}Mn_{0.05}O_3$	rhombohedral rhombohedral rhombohedral	series of elliptical loops	[II.273]
267	$Bi_{0.95-x}Eu_{0.05}Sr_xFeO_3$ (x = 0, 0.05, 0.10)	rhombohedral	pointed loops	[II.274]
268	$(BiLi)_{1/2}(Fe_{2/3}W_{1/3})O_3$	orthorhombic	elliptical loop	[II.275]
269	$Al_xGa_{1-x}FeO_3$ (x = 0.05, 0.10, 0.20)	$Pc2_1n$	pointed loops	[II.276]
270	$Bi_{0.86}Sm_{0.14}FeO_3$ $Bi_{0.86}Sm_{0.14}Fe_{0.99}FeO_3$ $Bi_{0.86}Sm_{0.14}Fe_{0.9}FeO_3$	R3c	pointed loops	[II.277]
271	$Bi_6Fe_{2-x}Ni_xTi_3O_{18}$ (x = 0, 0.2, 0.4, 0.6, 0.8, 1)	B2cb	pointed loops	[II.278]
272	$Bi_6Fe_{2-x}Co_{x/2}Ni_{x/2}Ti_3O_{18}$ (x = 0, 0.2, 0.4, 0.6, 0.8, 1)	B2cb	series of pointed loops	[II.279]
273	$Bi_7Fe_2CrTi_3O_{21}$	$A2_1am$	series of pointed loops	[II.280]
274	$(x)PbZr_{0.52}Ti_{0.48}O_3$+$(1-x)CoFe_2O_4$ (x = 0.8, 0.9) $(x)PbZr_{0.52}Ti_{0.48}O_3$+$(1-x)Ni_{0.7}Zn_{0.3}Fe_2O_4$ (x = 0.8, 0.9)	tetragonal tetragonal	pointed loops pointed loops	[II.281]
275	$BiAl_xFe_{1-x}O_3$ (x = 0.0, 0.025, 0.05, 0.075, 0.1)	R3c	pointed loops	[II.282]
276	$Bi(Co_{0.40}Ti_{0.40}Fe_{0.20})O_3$	ferrite structure	series of pointed loops	[II.283]
277	$Bi_{1-x}Gd_xFeO_3$ (x = 0, 0.1, 0.2, 0.3)	R3c and $Pn2_1a$	series of pointed loops	[II.284]
278	$Bi_{1-x}Ba_xFeO_3$ (x = 0.0, 0.1, 0.2)	R3c	narrow pointed loops	[II.285]
279	$Bi_{1-x}Gd_xFe_{1-y}Co_yO_3$ (x = 0.00, 0.05; y = 0.00, 0.05, 0.10)	R3c	elliptical loops	[II.286]
280	$Bi_{0.95}Dy_{0.05}Fe_{0.95}T_{0.05}O_3$ (T = Cr, Mn, Ni)	R3c	pointed loops	[II.287]
281	$(1-x)Ba(Zr_{0.2}Ti_{0.8})O_3$–$(x)Ba_{0.7}Ca_{0.3}FeTaO_5$ (x = 0.2, 0.25, 0.4)	P4mm	series of pointed loops	[II.288]
282	$(Bi_{0.5}Na_{0.5})(Nb_{0.5}Fe_{0.5})O_3$–PVDF (50%/50%)	tetragonal structure	Pointed loop	[II.289]
283	$Ba_{0.2}Cu_{0.8-x}La_xFe_2O_4$ (x = 0.2, 0.4, 0.6)	cubic spinel structure	narrow elliptical loops	[II.290]

Table 2 (Continued)

No.	Substance	Symmetry	Shape of P–E loop	Ref.
284	$Bi_{1-x}Ho_xFeO_3$ ($x = 0.00, 0.05, 0.10$) ($x = 0.15, 0.18, 0.20$)	R3c Pnma	pointed loops pointed loops	[II.291]
285	$Bi_{0.8}Gd_{0.2}Fe_{0.95}Ti_{0.05}O_3$	Pnma	elliptical loop	[II.292]
286	$Bi_{1-x}(Ca_{1/2}Pb_{1/2})_xFeO_3$ ($x = 0.1$) $Bi_{1-x}(Ca_{1/2}Pb_{1/2})_xFeO_3$ ($x = 0.2, 0.3$)	R3c Pm3m	elliptical loop narrow pointed loops	[II.293]
287	$(Ni_{0.45}Co_{0.2}Zn_{0.35}F_2O_4)_{1-x}$(Na-acetylacetonate)$_x$ ($x = 0, 0.2, 0.4, 0.6, 0.8, 1$)	cubic spinel structure	elliptical loops	[II.294]
288	$(PLZT)_{0.3}(BiFeO_3)_{0.7}$	cubic spinel structure	pointed loop	[II.295]
289	$BaAl_{2-2x}(Zn_{0.5}Si_{0.5})_{2x}O_4$ ($x = 0, 0.2, 0.4, 0.6, 0.8, 1.0$)	$P6_3$	series of narrow pointed loops	[II.296]
290	$Bi_{0.80}Pr_{0.20}FeO_3$ $Bi_{0.80}Y_{0.20}FeO_3$	R3c R3c	pointed loop pointed loop	[II.297]
291	$BiFeO_3$ (air and Ar annealed)	rhombohedral	elliptical loops	[II.298]
292	$BiFe_{0.75}Ti_{0.25}O_3$	rhombohedral	narrow pointed loop	[II.299]
293	$BiFe_{0.5}Ti_{0.5}O_3$ $0.5BiFe_{0.5}Ti_{0.5}O_3$–$0.5PbTiO_3$	orthorhombic tetragonal	pointed loops pointed loops	[II.300]
294	$Bi_3Nb_{1+2x}Fe_xCo_xTi_{1-4x}O_9$ ($x = 0.0625$)	$A2_1am$	pointed loop	[II.301]
295	$(1-x)BiFeO_3$–$(x)PbTiO_3$ ($x = 0.3, 0.4, 0.5, 0.6$)	coexistence monoclinic Cc and tetragonal P4mm	pointed loops	[II.302]
296	$Bi_{0.95}Dy_{0.05}Fe_{0.95}Mn_{0.05}O_3$, $Bi_{0.95}Dy_{0.05}Fe_{0.95}Cr_{0.05}O_3$ $Bi_{0.95}Dy_{0.05}Fe_{0.95}Mn_{0.05}$–$Ni_{0.05}O_3$	R3c	pointed loops	[II.303]

Part III

Table 3 False or unconfirmed ferroelectric properties in polymers.

No.	Substance	Symmetry	Shape of P–E loop	Ref.
1	$\{[Cu^I_4Cu^{II}(Et_2dtc)_2Cl_3][Cu^{II}(Et_2dtc)_2]_2(FeCl_4)\}_n$ Et_2dtc = diethyldithiocarbamate	Pnam	pointed loops	[III.1]
2	$Rb_{0.82}Mn[Fe(CN)_6]_{0.94}\cdot H_2O$ rubidium manganese hexacyanoferrate	F222	pointed loop	[III.2]
3	CoFe Prussian blue analogue/polyvinylidene fluoride	Fm3m	series of elliptical loops	[III.3]
4	tetrathiafulvalene-pillar[5]quinine.dioxane	$P\bar{1}$ (?)	elliptical loop	[III.4]
5	N-dehydroabietyl-4-bromobenzamide	$P2_1$	series of pointed loops	[III.5]
6	$[Ni(en)_2pip][B_5O_6(OH)_4]_2$ en = etylenediamine; pip = piperazine	P2	series of pointed loops	[III.6]
7	(1Z, 4Z)-2, 4-bis(trifluoromethyl)-5a, 6, 7, 8, 9, 9a-hexahydro-3H-benzo[b][1, 4]diazepine	C2	pointed loop	[III.7]
8	$[Me_2NH_2][Cd_2Na_3(2,4\text{-}PYDC)_4]\cdot 2H_2O$ $[Me_2NH_2][CdNa(OH\text{-}m\text{-}BDC)_2(H_2O)_2]\cdot 2H_2O$ 2, 4-PYDC = 2, 4-pyridinedicarboxylic acid OH-m-BDC = 5-hydroxyi-sophthalic acid	Fdd2 $Pca2_1$	series of elliptical loops series of pointed loops	[III.8]
9	$[H_2dbco]_2\cdot[Cl_3]\cdot[CuCl_3(H_2O)_2]\cdot H_2O$ dbco = 1, 4-Diaza-bicyclo[2, 2, 2]octane	$Pna2_1$	elliptical loop	[III.9]
10	$\{[Cd(BDAC)]2\cdot H_2O\}_n$ BDAC = 1_H-[2, 2_]biimidazoly-1-yl-acetic acid	Ccc2	pointed loop	[III.10]
11	$\{[Cu(4, 4'\text{-}H_2bpz)Br]\cdot 0.5H_2O\}_n$ 4, 4′-H_2bpz = 3, 3′, 5, 5′-tetramethyl-4, 4′-bipyrazole	Ima2	pointed loop	[III.11]
12	$[Zn_2(mtz)\text{-}(nic)_2(OH)]_n\cdot 0.5nH_2O$ $[Zn(phtz)(nic)]_{2n}$ mtz = 5-methyltetrazole phtz = 5-phenyltetrazole nic = nicotinic acid	Ccc2 Pc	series of pointed loops series of pointed loops	[III.12]
13	[Ag8(L)4](NO3)8·4H_2O L = bis(3, 5-bis((1H-imidazol-1-yl)methyl)-2, 4, 6-trimethylphenyl) methane	Fdd2	pointed loop	[III.13]
14	$[Co(pmtz)(\mu_{1,3}\text{-}N_3)(H_2O)]_n$ pmtz = 5-(pyrimidyl)tetrazolate	Aba2	series of pointed loops	[III.14]

Table 3 (Continued)

No.	Substance	Symmetry	Shape of P–E loop	Ref.
15	$[Cd(trtr)_2]_n$ trtr = 3-(1, 2, 4-triazole-4-yl)-1*H*-1, 2, 4-triazole	Fdd2	series of pointed loops	[III.15]
16	$[Cu(C_8H_4O_4)(C_3H_4N_2)_2]_n$ copper–(o-phthalate)	$Pna2_1$	series of pointed loops	[III.16]
17	$[Cd(L–N_3)_2(H_2O)_2]_n$ L = trans-2, 3-dihydro-2-(4′-pyridyl)-3-(3″-cyanophenyl) benzo[e]indole	Aba2	series of narrow pointed loops	[III.17]
18	$Cd(imazethapyr)_2$	Fdd2	pointed loops	[III.18]
19	$[Cu_3(4, 4'\text{-bipyridine})_5]_2[H_2SiW_{11}O_{39}]\cdot 5H_2O$	$Pca2_1$	narrow pointed loop	[III.19]
20	[m-R-benzylidene-1-aminopyridinium][PbI_3] R = F, Cl, Br, NO_2, CN	$P6_3$	series of pointed loops	[III.20] [III.21]
21	[m-NO_2-Bz-1-APy][PbI3] [m-F-Bz-1-APy][PbI3] [m-Cl-Bz-1-APy][PbI3] [m-Br-Bz-1-APy][PbI3] Bz-1-APy = benzylidene-1-aminopyridinium	$P6_3$ $P6_3$ $P6_3$ $P6_3$	series of pointed loops series of pointed loops series of pointed loops series of pointed loops	[III.22]
22	$\{[Zn(TBPR)\cdot 0.25(HClO_4](0.25HClO)\}_n$ TBPR = (S)-N-2-tetrazoylbenzylproline	P4	pointed loop max of ε' at 250 K	[III.23]
23	olefin-copper N, N′, N″-(2, 4, 6-trimethyl-benzene-1, 3, 5-triyl)tris(methylene)tris(N-allylpropen-amine)-[Cu_4Br_7]	$P4_1$	pointed loop	[III.24]
24	2-pyridyl carboxylic acid – $ZnBr_2$	R3	narrow pointed loop	[III.25]
25	$(CH_3NH_3)_{12}\{Cu^{II}_{24}[(S, S)\text{-hismox}]_{12}(OH_2)_3\}\cdot 178H_2O$	R3	pointed loop at 223 K	[III.26]
26	$[Sr(\mu\text{-BDC})(DMF)]_\infty$ DMF = N, N-dimethylformamide BDC = benzene-1, 4-dicarboxylate	$P3_1$	series of pointed loops	[III.27]
27	$[FeL_3](BF_4)_2$ L = (S)-1-phenyl-N-(1-butyl-imidazole-2-methylene)-ethylamine	R3	pointed loop	[III.28]
28	[Dy(FTA)3L] FTA = 2-furyl-trifluoro-acetonate L = (S, S)-2, 2'-Bis(4-benzyl-2-oxazoline)	$P3_2$	series of pointed loops	[III.29]
29	$(DAMP)_3(Cu_4Br_4)_2(H_2O)_3$ DAMP = (*S*)-1, 4-diallyl-2-methylpiperazine	P3	series of pointed loops	[III.30]
30	$[Mn_3(\text{pyridine-2, 4, 6-tricarboxylicacid})_2(H_2O)_9]_n$	Cc	narrow pointed loop	[III.31]
31	metal-polycarboxylates: $(Me_2NH_2)[Cd(OH\text{-m-HBDC})(OH\text{-m-BDC})]\cdot DMF\cdot CH_3OH\cdot H_2O$ $(Me_2NH_2)[CdLi(SDBA)_2]\cdot DMF\cdot CH_3OH$ $(Me_2NH_2)[Cd_3(H_2O)_3(\mu_3\text{-OH})(SDBA)_3]$ OH-m-BDC = 5-hydroxy-1, 3-benzenedicarboxylate DMF = N, N-dimethylformamide SDBA = 4, 4'-sulfonyldibenzoic acid	Cc Cc P3	series of pointed loops series of pointed loops series of pointed loops	[III.32]
32	*N*-(4-cyanobenzyl)-(*S*)-proline - $CdCl_2$	Cc	series of elliptical loops	[III.33]
33	$Zn_2(etza)_4$ etza = ethyl 1H-tetrazole-5-acetate	$P2_1$	series of pointed loops	[III.34]
34	$[Zn_2Co(tib)_3(H_2O)_5][Zn_6(tib)_2(1, 2, 4\text{-BTC})_6]\cdot 12.7H_2O$ tib = 1, 3, 5-tris(1-imidazolyl)benzene BTC = 1, 3, 5-benzenetricarboxylic acid	$P6_3$	pointed loop	[III.35]
35	$[Zn(S\text{-nip})_2]_n$ $\{[Co(S\text{-nip})_2]\cdot(H_2O)_{0.5}\}_n$ S-nip = (S)-2-(1, 8-naphthalimido)-3-(4-imidazole)propanoate	$P2_1$ $P2_1$	series of pointed loops series of pointed loops	[III.36]
36	$(TBC\text{-}N_4)_2Zn(N_3)_4(X_2O)$ TBC-N_4 = 4-tetrazoylbenzylcinchonidine X = H, D	$P2_1$	pointed loops	[III.37] [III.38]
37	$[Mn((R, R)\text{-Salcy})Fe(bpca)(CN)_3\cdot H_2O]_n$ Salcy = N, N′-(1, 2-cyclohexanediylethylene)bis(salicylideneiminato) bpca = bis(2-pyridylcarbonyl)amidate	$P2_1$	series of pointed loops	[III.39]
38	$[Cd_3(BPT)_2(H_2O)_9]\cdot 2H_2O$ BPT = biphenyl-3, 4′, 5-tricarboxylate	C2	without loop theoretical calculation	[III.40]
39	$[Cu(L_R)Cl_2]_n\cdot 2H_2O$ L_R = (+)-4, 5-pinenepyridyl-2-pyrazine	$P2_1$	pointed loop	[III.41]
40	$[Re_2(L_R)(CO)_6Cl_2]\cdot 4CH_2Cl_2$ L_R = 2, 5-bis(4, 5-pinene-2-pyridyl)pyrazine	$P2_1$	pointed loop	[III.42]

Table 3 (Continued)

No.	Substance	Symmetry	Shape of P–E loop	Ref.
41	Tb(dibenzoylmethanato)$_3$((R, R)-1, 2-diphenylethylenediamine)	$P2_1$	series of pointed loops	[III.43]
42	$[Zn_4(L_2)(H_2O)_3(DMA)]\cdot 2H_2O$ L = tetrakis[4-(carboxyphenyl)oxamethyl]methane	Cc	series of pointed loops	[III.44]
43	$(MeTp)_2Fe_2(CN)_6Ni[(1R, 2R)\text{-chxn}]_2$ MeTp = methyltris(pyrazolyl)borate chxn = 1, 2-diaminocyclohexane	$P2_1$	series of elliptical loops	[III.45]
44	$(Lig)_2Tb(H_2O)_2(ClO_4)$ Lig = L-ethyl lactate	C2	pointed loop	[III.46]
45	$[Cd_3(BPT)_2(H_2O)_9]\cdot 2H_2O$ BPT = biphenyl-3, 4′, 5-tricarboxylate	C2	pointed loop	[III.47]
46	steroid: $4C_{36}H_{55}N_3O_{44}C_3H_8O$	P1	series of pointed loops	[III.48]
47	1-benzyl-2-phenyl-1H-benzimidazole-ClO_4 1-benzyl-2-phenyl-1H-benzimidazole-NO_3 1-benzyl-2-phenyl-1H-benzimidazole-Cl	P1 P1 P1	elliptical loops elliptical loops elliptical loops	[III.49]
48	poly[aqua[m$_4$-2-(carboxylatobenzoyl)benzonato]-cadmium(II)]	Aba2	pointed loop	[III.50]
49	$[Ni(en)_3][InSbSn]$ en = ethylenediamine	R3c	pointed loop	[III.51]
50	$[Zn_2(X)(CH_3CH_2OH)]\cdot 3H_2O$ X = tetrakis[4-(carboxyphenyl)oxamethyl]methane acid	Cc	pointed loops	[III.52]
51	$\{[Co(L)_2][Co(bpa)(H_2O)_4][Co(H_2O)_6]_2\cdot 7H_2O\}_n$ $\{[Mn_2(HL)(L)(H_2O)_4]_2[Mn(bpe)_2(H_2O)_4][Mn(H_2O)_6]_2\cdot xH_2O\}_n$ $\{[Mn_2(HL)(L)(H_2O)_4]_2[Mn(bpa)_2(H_2O)_4][Mn(H_2O)_6]_2\cdot xH_2O\}_n$ L = methylenediisophthalic acid bpa = 1, 2-bis(4-pyridyl)ethane; bpe = 1, 2-bis(4-pyridyl)ethylene;	Cc C2 C2	pointed loop pointed loop pointed loop	[III.53]
52	$[Zn(HQA)Br_2\text{-}(H_2O)_3]_n$ $[Zn(HQA)Br_2\text{-}(D_2O)_3]_n$ HQA = 6-methoxyl-(8S,9R)-cinchonan-9-ol-3-carboxylic acid	$P2_1$ $P2_1$	pointed loop pointed loop	[III.54]
53	$[Cd(papa)(Hpapa)]ClO_4\cdot H_2O$ papa = 3-pyridyl-3-aminopropionate	Cc	pointed loops	[III.55]
54	1-pyridyl-2-ethoxycarbonyl-3-amino-1H-naphtho-[2, 1-b]pyran-2'-methylacetic acid	$P2_1$	pointed loops	[III.56]
55	$[Eu(Lig)_2\text{-}(H_2O)_2][ClO_4]$ $[Eu(Lig)_2\text{-}(D_2O)_2][ClO_4]$ Lig = L-ethyl lactate	C2 C2	pointed loops pointed loops	[III.57]
56	$[H_3O][Co_2(dat)(sdba)_2]\cdot H_2sdba\cdot 5H_2O$ dat = 3, 5-diamino-1, 2, 4-triazole sdba = 4, 4'-sulfonyldibenzoic acid	$Pna2_1$	series of elliptical loops	[III.58]
57	$[Fe(tib)_{2/3}(H_2O)_4]SO_4\}_n$ tib = 1, 3, 5-tris(1-imidazolyl)benzene	R3c	series of pointed loops	[III.59]
58	$[Cd_3(S\text{-}L^2)_4](ClO_4)_2$ L^2 = 2-(1-(2-pyridine)-ethylimino)-5-bromo-6-methoxy-pheno)	$P2_1$	series of pointed loops	[III.60]
59	$Zn((-)\text{-}L_1)Cl_2$ $(-)\text{-}L_1$ = (-)-4, 5-pinene bipyridine,	$P2_1$	series of pointed loops	[III.61]
60	$\{[Mn(tib)_2(H_2O)_4]SO_4\}_n$ $\{[Co(tib)_2(H_2O)_4]SO_4\}_n$ tib = 1, 3, 5-tris(1-imidazolyl)benzene	R3c R3c	series of pointed loops series of pointed loops	[III.62]
61	1, 4-diazabicyclo [2, 2, 2]octane N, N′-dioxide di(perchlorate)	$P2_1$	series of pointed loops	[III.63]
62	$[Cu(L)(H_2O)]\cdot H_2O$ L = (S)-3-phenyl-2-(pyrazine-2-carboxamido) propanoic acid	$P4_3$	pointed loop	[III.64]
63	$ReL_{R,R}(CO)_3Cl$ $L_{R,R}$ = (-)-4, 5-pinene-2, 2′-bipyridine[(6R)-5, 6, 7, 8-tetrohedro-7, 7-dimethyl-3-(2-pyridinyl)-6, 8-methanoisoquinoline]	$P2_1$	series of pointed loops	[III.65]
64	$Cu(L1)(L2)H_2O]\cdot 3H_2O$ $Ni(L1)(SCN)(H_2O)_2]\cdot 2H_2O$ L1 = L-histidine; L2 = L-alanine	$P2_1$ $P2_1$	narrow pointed loop narrow pointed loop	[III.66]
65	$[Co(bimb)(L^1)_2]$ bimb = 1, 4-bis(imidazol-1–yl)-butane L^1 = 3, 5-dinitro-benzoic acid $[Co(bix)(L^2)]$ bix = 1, 4-bis(imidazol-1-yl-methylene)-benzene L^2 = o-phthalic acid	$P2_1$ Cc	narrow pointed loop narrow pointed loop	[III.67]

Table 3 (Continued)

No.	Substance	Symmetry	Shape of P–E loop	Ref.
66	$[Co(titb)(L)]\cdot 3H_2O$ titb = 1, 3, 5-tris(imidazol-1-ylmethyl)-2, 4, 6-trimethylbenze L = 4, 4′-(ethene-1, 2-diyl)dibenzoic acid	Cc	narrow pointed loop	[III.68]
67	$Pr(DMSO)_4(H_2O)_3Cr(CN)_6]$ DMSO = dimethylsulfoxide	$P2_1$	series of narrow pointed loops	[III.69]
68	$Ag_4(dob)_4(BF_4)_4$ dob = 1, 3-di(2-oxazolinyl)benzene	Cc	narrow pointed loop	[III.70]
69	$[Zn(BTA)_2(H_2O)]_n$ BTA = 2-(1*H*-benzotriazol-1-yl)acetic acid	Cc	series of pointed loops	[III.71]
70	$[Cd_3Na_4(3, 3'\text{-BPDA})_5(DME)_7]\cdot DME$ 3, 3′-BDPA = 1, 1′-biphenyl-3, 3′-dicarboxylic acid	$Pca2_1$	elliptical loop	[III.72]
71	$[Cd_6(L)_4(D\text{-Cam})_4(H_2O)_4]\cdot 2H_2O$; $[Cd_6(L)_4(L\text{-Cam})_4(H_2O)_4]\cdot 2H_2O$ L = 3, 5-di(imidazol-1-yl)benzoic acid D-H_2Cam = D-camphoric acid; L-H_2Cam = L-camphoric acid	C2	series of pointed loops	[III.73]
72	$[Cu_2I_2(L^1)_2$ L^1 = 2-[(*S*)-4-isopropyl-2-oxazolyl]quinoline $\{[Cu(L^2)_2]_2(OH)\}(BF_4)_3\cdot H_2O$ L^2 = 2-[(*S*)-4-phenyl-2-oxazolyl]quinoline	P1 $P2_1$	elliptical loop elliptical loop	[III.74]
73	$Ag(L_R)\cdot NO_3]_n$ L_R = (−)-2, 5-bis(4, 5-pinene-2-pyridyl)pyrazine	C2	pointed loop	[III.75]
74	$[Cu_3(OH)(PhPyCNO)_3(NO_3)\ (CH_3OH)]\cdot(NO_3)$ PhPyCNO = phenyl 2-pyridyl ketoxime	$P2_1$	series of pointed loops	[III.76]
75	$[Cd(anp)_2Br_2]H_2O$ anp = 2-amino-5-nitropyridine	Pnn2	elliptical loop	[III.77]
76	$\{[Ag_2(HPIDC)]\}_n$ HPIDC = 2-(pyridin-4-yl)-1H-imidazole-4, 5-dicarboxylaic acid	Cc	elliptical loop	[III.78]
77	$Zn_3(titmb)(BTC)_2(H_2O)$ titmb = 1, 3, 5-tris(1-imidazol-1-ylmethyl)-2, 4, 6-trimethylbenzene BTC = 1, 3, 5-benzene-tricarboxylic acid	$P2_1$	series of pointed loops	[III.79]
78	$Mn(H_2O)(SCMC)$ SCMC = S-carboxymethyl-l-cysteine	$P2_1$	narrow pointer loop	[III.80]
79	$\{(EMI)_2[Zn_3(1, 2, 4, 5\text{-BTC})_2]\cdot 2H_2O\}_n$ 1, 2, 4, 5-BTC = 1, 2, 4, 5-benzenetetracarboxylate EMI = 1-ethyl-3-methyl imidazolium	Fdd2	series of pointed loops	[III.81]
80	$Cu_5Cl_9(H_2Quinine)_2$	C2	narrow pointed loop	[III.82]
81	$Co(5\text{-ATZ})_4Cl_2$ $Cu(5\text{-ATZ})_4Cl_2$ 5-ATZ = 5-amino-1-H-tetrazole	P4nc P4nc	series of pointed loops series of pointed loops	[III.83]
82	$\{[Zn(TBPR)\subset 0.25(HClO_4)](0.25HClO_4)\}_n$ TBPR = (S)-N-2-tetrazoylbenzylproline	P4	pointed loop	[III.84]
83	$[Mn((R, R)\text{-Salcy})Fe(bpca)(CN)_3\cdot H_2O]_n$ bpca = bis(2-pyridylcarbonyl)amidate (R, R)-Salcy = (R, R)-N, N′-(1, 2-cylohexanediylethylene)-bis(salicylidene-iminato)	$P2_1$	series of pointed loops	[III.85]
84	$[Cd_2(L)_4(\mu_2\text{-Cl})(Cl)(H_2O)]_n$ $[Cd_2(L)_4(\mu_2\text{-Br})(Br)(H_2O)]_n$ L = 2-(1H-imidazol-1-ylmethyl)-1H-benzoimidazole	P4nc P4nc	pointed loop pointed loop	[III.86]
85	$[NH_3C_6H_4(CH_2)_2(CH)(NH_3)COOH]_2(SnCl_3)_2\cdot(H_2O)_3$	I2	narrow pointed loop	[III.87]
86	$[Zn(Mitz)Cl]_n$ Mitz = 3-tetrazolyl-6-methyl-5-(4-pyridyl)-2-pyridone	$Pna2_1$	series of pointed loops	[III.88]
87	$[Cu((R)\text{-hmp}^*)(dca)]_n$ hmp* = α-methyl-2-pyridinemethanol; dca = dicyanamide	$P2_1$	series of elliptical loops	[III.89]
88	$[(Cd)_4(L)_3(H_lL_1)_2(DMF)(H_2O)_2](DMF)_3(H_2O)_2\}_n$ H_1L_1 = l-(+)-lactic acid L = 2, 6, 2′, 6′-tetranitro-biphenyl-4, 4′-dicarboxylic acid DMF = *N*, *N*′-dimethylformamide	P1	very narrow pointed loop	[III.90]
89	$\{[Cu_2(L)(H_2O)_2]\cdot(4DMF)(4H_2O)\}_n$ L = 5, 5′-[(*S*)-(+)-2-methylpiperazine-1, 4-diyl]diisophthalic acid DMF = *N*, *N*′-dimethylformamide	R3	series of pointed loops	[III.91]
90	DAST = 4-N, N′dimethylamino-N-methyl-4-stil-bazolium tosylate	Cc	elliptical loop	[III.92]
91	$[Cu(Clma)_2]_n$ $[Mn(H_2O)(Clma)_2]_n$ Clma = (R)-2-Chloromandelic acid	$P2_1$ $P2_1$	narrow pointed loop narrow pointed loop	[III.93]

Table 3 (Continued)

No.	Substance	Symmetry	Shape of P–E loop	Ref.
92	$\{[Cd(pmida)H_2O]\cdot 1.8\ H_2O]\}_n$ pmida = *N*-(4-pyridylmethyl)iminodiacetate	$Pna2_1$	narrow pointed loop	[III.94]
93	$[Eu(tta)_3L](C_3H_6O)\cdot 0.5(H_2O)$ L = "dipineno"-(4, 5 : 4′′, 5′′)-fused 2, 2′ : 6′, 2′′-terpyridine tta = 2-thenoyltrifluoroacetonate	$P2_1$	series of pointed loops	[III.95]
94	homochiral uranyl-bis[(S)-lactate]	$P2_1$	narrow pointed loop	[III.96]
95	$[Ni(en)_3][InSbS_4]$ en = ethylenediamine	R3c	pointed loop	[III.97]
96	polyaniline	amophous	narrow poited loop	[III.98]
97	$[Cd(L–N_3)_2(H_2O)_2]_n$ L = *trans*-2,3-dihydro-2-(4'-pyridyl)-3-(3'-cyanophenyl)benz[*e*]indole $[Cd(TBP–N_3)_2(H_2O)_2]_n$ TBP = N-(4-cyanobenzyl)-(S)-proline	C_{2v} Cc	narrow pointed loops elliptical loop	[III.99]
98	Pb(TDC) TDC = thiophene-2, 5-dicarboxylic acid	$Pmc2_1$	series of pointed loops	[III.100]
99	$\{[Cd_5(L)_2(H_2O)_4(DMAc)_3]\cdot 10H_2O\cdot 7DMAc\}_n$ L = 3, 5-bis(1-methoxy-3, 5-benzene dicarboxylic acid; DMAc = *N*, *N*′-dimethylacetamide	$P2_1$	series of pointed loops	[III.101]
100	$[NH_4][Ag_3(C_9H_5NO_4S)_2(C_{13}H_{14}N_2)_2]\cdot 8H_2O$	Fdd2	series of pointed loops	[III.102]
101	$[Zn(DBA)(Hpyim)]_n\cdot nH_2O$ DBA = 4, 4′-methylenedibenzoic acid Hpyim = 2-(2-pyridyl)imidazole	Cc	series of pointed loops	[III.103]
102	$\{[CuCN][Cu(isonic)_2]\}_n$isonic = isonicotinic acid	Cc	series of elliptical loops	[III.104]
103	$[(UO_2)Cd(bipy)(mal)_2]\cdot H_2O$ mal = malonic acid, bipy =4, 4′-bipyridine	Cc	series of elliptical loops	[III.105]
104	$K_2(H_2O)_4Nd(H_2O)_7[Nd(H_2O)_3HAlW_{11}O_{39}]\cdot nH_2O$	$Pna2_1$	elliptical loop	[III.106]
105	$[Pd(L^2)Cl]$ L^2 = 2, 6-bis[(S)-4-phenyl-2-oxazolyl]pyridine	$P2_1$	pointed loop	[III.107]
106	$\{[Cd_{2.5}L(BTC)_{1.5}(H_2O)_{1.5}(DMF)](H_2O)_{2.35}\}_n$	C2	series of pointed loops	[III.108]
107	$[NH_4][Ag_3(C_9H_5NO_4S2(C_{13}H_{14}N_2)_2]\cdot 8H_2O$	mm2	series of pointed loops	[III.109]
108	$\{[Cu_2L_4(H_2O)_2]\cdot(ClO_4)_4\cdot(H_2O)_5\cdot(CH_3OH)\}_\infty$ L = $PhPO(NH^3Py)_2$; ^3Py = 3-pyridyl	R3	elliptical loop	[III.110]
109	$[Cu_3(OH)(PhPyCNO)_3(NO_3)\ (CH_3OH)]\cdot(NO_3)$	$P2_1$	series of pointed loops	[III.111]
110	$\{[Ag_2(HPIDC)]\}_n$ PIDC = 2-(pyridin-4-yl)-1H-imidazole-4,5-dicarboxylaic acid	Cc	pointed loop	[III.112]
111	$Zn_3(titmb)(BTC)_2(H_2O)$ titmb = 1, 3, 5-tris(1-imidazol-1-ylmethyl)-2, 4, 6-trimethylbenzene BTC = 1, 3, 5-benzene-tricarboxylic acid	Cc	series of pointed loops	[III.113]
112	$Mn(H_2O)(SCMC)$ SCMC = S-carboxymethyl-l-cysteine	$P2_1$	narrow pointed loop	[III.114]
113	$[Zn(phen)(H_2O)_2L]L$ L = m-nitro-benzoic acid phen = 1, 10-phenanthroline	$P2_1$	series of pointed loops	[III.115]
114	$[Zn(bpp)(FNA)]\cdot H_2O$ $Zn_2(bpp)_2(FNA)_2$ bpp = 1, 3-bi(4-pyridyl)propane FNA = 4-nitrobenzene-1, 2-dicarboxylic acid	$P4_3$ Cc	series of pointed loops series of pointed loops	[III.116]
115	$Cu_2(bpy)(H_2O)(Clma)_2$ Cu(bpp)(Clma) bpy = 4, 4′-dipyridine bpp = 1, 3-di(4-pyridyl)propane Clma = (*R*)-2-chloromandelic acid	$P2_1$ $P2_1$	series of pointed loops series of pointed loops	[III.117]
116	$[Cu(phen)Cl](\mu_2{-}Cl)(\mu_2{-}L)[Cu(phen)L$ phen = 1, 10-phenanthroline L = m-hydroxybenzoic acid	$Pna2_1$	series of pointed loops	[III.118]
117	$[Tb(H_2O)_3(C_4H_5O_6)(C_4H_4O_6)]$	$P4_1$	series of pointed loops	[III.119]
118	(4aR, 8aR)-2, 3-Di(thiophen-2-yl)-decahydroquinoxal	$P2_1$	series of pointed loops	[III.120]
119	[Cd(tib)(BDC)]·2H2O tib = 1, 3, 5-tris(1-imidazolyl)benzene – BDC = 1, 4-benzenedicarboxylic acid	$P4_1$	narrow pointed loop	[III.121]

Table 3 (Continued)

No.	Substance	Symmetry	Shape of P–E loop	Ref.
120	$[Ce_2(H_2O)_3(D\text{-tar})_3]\cdot 3H_2O$ $[Ce_2(H_2O)_3(L\text{-tar})_3]\cdot 3H_2O$ tar = tartaric acid	P1	series of narrow pointed loops	[III.122]
121	$\{[Cd_{2.5}L(BTC)_{1.5}(H_2O)_{1.5}(DMF)](H_2O)_{2.35}\}_n$ – L = (1, 1′, 1″-(2, 4, 6-trimethybenzene-1, 3, 5-triyl)-tris(methylene) tris(4-carboxypyridinium) tribromide – BTC = 1, 3, 5-Benzenetricarboxylic acid DMF = dimetyloformamid	C2	series of pointed loops	[III.123]
122	$Mn(H_2O)(C_6H_8O_4)$ $H_2(C_6H_8O_4)$ = adipic acid	$P2_1$	pointed loop	[III.124]
123	Cu_8Cl_{10}(H-quinine)$_2$	C2	narrow pointed loop	[III.125]
124	$[Eu(tta)_3L](C_3H_6O)\cdot 0.5(H_2O)$ L = "dipineno"-(4,5:4",5")-fused 2,2':6',2"-terpyridine tta = 2-thenoyltrifluoroacetonate	$P2_1$	series of pointed loops	[III.126]
125	uranyl-bis[(*S*)-lactate]	$P2_1$	narrow pointed loop	[III.127]
126	$[Ni(en)_3][InSbS_4]$ en = ethylenediamine	R3c	pointed loop	[III.128]
127	$[Tb(H_2O)_3(C_4H_5O_6)(C_4H_4O_6)]$	$P4_1$	series of pointed loops	[III.129]
128	$[Zn_4(HL)_2(L)_2\cdot(CH_3OH)_2]\cdot(NO_3)_2$ H_2L = 2-[(1-benzyl-2-hydroxy-ethylimino)-methyl]-6-methoxy-phenol	$P2_1$	series of narrow pointed loops	[III.130]
129	$[EG]\cdot[Cu(phen)_2\cdot SO_4]$ EG = ethylene glycol; phen = 1, 10-phenanthroline;	Cc	pointed loops	[III.131]
130	$[Ni(L)_2(H_2O)_6]\cdot 2H_2O$ $[Cu(L)_2(H_2O)_3]\cdot H_2O$ $[Zn(L)_2(H_2O)_2]\cdot H_2O$ $[Cd(L)_2(H_2O)_2]\cdot H_2O$ $[Cd(L)_2(H_2O)]_n$ L = (S)-naproxen anion	P1 C2 C2 C2 Cc	pointed loop pointed loop pointed loop narrow pointed loop pointed loop	[III.132]
131	$\{[Cd_2(mpba)_2(bpmp)_2]\cdot 2H_2O\}_n$ H_2mpba = (S)-4, 4′-(2-methylpiprazine-1, 4-diyl)bis(methylene) dibenzoic acid bpmp = 4-bis(4-pyridinylmethyl)piperazine	P1	series of narrow pointed loops	[III.133]
132	R-$[Zn_3(R\text{–}L)_2(CH_3COO)_4]$ L = 2-methoxy-6-[(1-phenyl-ethylimino)-methyl]-phenol R = 2-amino-3-phenyl-1- propanol	$P2_1$	series of pointed loops	[III.134]
133	$BaTiO_3$-poly(vinylidene fluoride) $BaTiO_3$-poly(vinylidene fluoride) modified by polyethylene glycol	P4/mm P4/mm	elliptical loop elliptical loop	[III.135]

References

1. J. Valasek, Piezoelectric and allied phenomena in Rochelle salt, *Phys. Rev.* 17(4), 475 (1921)
2. F. Jona and G. Shirane, Ferroelectric Crystals, Pergamon Press Ltd., Oxford, 1962
3. J. F. Scott, Ferroelectrics go bananas, *J. Phys.: Condens. Matter* 20(2), 021001 (2008)
4. A. Loidl, S. Krohns, J. Hemberger, and P. Lunkenheimer, Bananas go paraelectric, *J. Phys.: Condens. Matter* 20(19), 191001 (2008)
5. L. Pintilie and M. Alexe, Ferroelectric-like hysteresis loop in nonferroelectric system, *Appl. Phys. Lett.* 87(11), 112903 (2005)
6. H. Kliem and B. Martin, Pseudo-ferroelectric properties by pace charge polarization, *J. Phys.: Condens. Matter* 20(32), 321001 (2008)
7. B. Martin and H. Kliem, Electrode effects in solid electrolyte capacitors, *J. Appl. Phys.* 98(7), 074102 (2005)
8. H. Diamant, K. Drenck, and R. Pepinsky, Bridge for accurate measurement of ferroelectric hysteresis, *Rev. Sci. Instr.* 28(1), 30 (1957)
9. L. Corbellini, J. Plathier, C. Lacroix, C. Harnagea, D. Menard, and A. Pignolet, Hysteresis loops revisited: An efficient method to analyze ferroic materials, *J. Appl. Phys.* 120(12), 124101 (2016)
10. M. Fukunaga and Y. Noda, New technique for measuring ferroelectric and antiferroelectric hysteresis loops, *J. Phys. Soc. Jpn.* 77(6), 064706 (2008)

References for Part I

I.1. V. Chithambaram, S. Jerome Das, S. Krishnan, M. Basheer Ahamed, and R. Arivudai Nambi, Growth and characterization of urea-oxalic acid crystals by solution

growth technique, *Eur. Phys. J. Appl. Phys.* 64(2), 20201 (2013)

I.2. R. E. Vizhi, R. Dhivya, and D. R. Babu, Synthesis, grown, optical and mechanical studies of ferroelectric urea-oxalic acid single crystals, *J. Cryst. Growth* 452, 213 (2016)

I.3. R. Dhivya, R. E. Vizhi, and D. R. Babu, Investigation on nucleation kinetics, growth and characterization of urea oxalic acid – ferroelectric single crystal, *J. Cryst. Growth* 468, 84 (2017)

I.4. S. Krishnan, J. Raj, R. Robert, and A. Ramanand, Growth and characterization of succinic acid single crystals, *Cryst. Res. Technol.* 42(11), 1087 (2007)

I.5. S. Krishnan, C. J. Raj, and S. J. Das, Growth and characterization of novel ferroelectric urea-succinic acid single crystal, *J. Cryst. Growth* 310(14), 3313 (2008)

I.6. R. Dhivya, R. Ezhil Vizhi, and D. R. Babu, Nucleation kinetic of urea succinic acid – ferroelectric single crystal, *AIP Conf. Proc.* 1665, 100020 (2016)

I.7. B. K. Singh, N. Sinha, N. Singh, K. Kumar, M. K. Gupta, and B. Kumar, Structural, dielectric, optical and ferroelectric property of urea succinic acid crystals grown in aqueous solution containing maleic acid, *J. Phys. Chem. Solids* 71(12), 1774 (2010)

I.8. R. Priya, S. Krishnan, G. Bhagavannarayana, and S. Jerome Das, Growth and characterization of novel ferroelectric bis (methylammonium) tetrachlorozincate, *Physica B* 406(8), 1345 (2011)

I.9. S. Suresh, A. Ramanand, D. Jayaraman, S. M. Priya, and R. Vasanthakumari, Synthesis, structural and dielectric properties of ferroelectric dichloridoglycine zinc dihydrate single crystals, *J. Miner. Mater. Charact. Eng.* 10(04), 339 (2011)

I.10. B.Uma, Rajnikant, K. SakthiMurugesan, S.Krishnan, and B. MiltonBoaz, Growth, structural, optical, thermal and dielectric properties of a novel semi-organic nonlinear optical crystal: Dichloro-diglycine zinc II, *Progr. Nat. Sci.: Mater. Inter.* 24, 378 (2014)

I.11. M. Shakir, B. K. Singh, B. Kumar, and G. Bhagavannarayana, Ferroelectricity in glycine picrate: An astonishing observation in a centrosymmetric crystal, *Appl. Phys. Lett.* 95(25), 252902 (2009)

I.12. C. Balarew, V. Spasov, and S. Tepavitcharova, Pyro- and ferroelectric properties of nGly·MeCl$_2$·2H$_2$O (Me = Mn, Co; n = 1, 2), *Ferroelectrics* 158(1), 157 (1994)

I.13. P. Justin and K. Anitha, Influence of formic acid on optical and electrical properties of glycine crystal, *Mater. Res. Express* 4(11), 115101 (2017)

I.14. M. Ben Bechir, K. Karoui, M. Tabellout, K. Guidara, and A. Ben Rhaiem, Electric and dielectric studies of the [N(CH$_3$)$_3$H]$_2$CuCl$_4$ compound at low temperature, J. Alloys. Compounds 588, 551 (2014)

I.15. J. Y. Park, J. H. Park, Y. K. Jeong, and H. M. Jang, Dynamic magnetoelectric coupling in "electronic ferroelectric" LuFe$_2$O$_4$, *Appl. Phys. Lett.* 91(15), 152903 (2007)

I.16. E. Jerusha, R. I. Shyam Kumar, S. S. Kirupavathy, and R. Gopalakrishnan, Investigations on the growth and characterisation of an isomorphous ammonium tetroxalate dihydrate superacid crystal, *Optik (Stuttg.)* 127(9), 3896 (2016)

I.17. M. Ben Bechir, K. Karoui, A. Bulou, M. Tabellout, K. Guidara, and A. Ben Rhaiem, [N(CH$_3$)$_3$H]$_2$ZnCl$_4$: Ferroelectric properties and characterization of phase transitions by Raman spectroscopy, *J. Appl. Phys.* 116(21), 214104 (2014)

I.18. S. Yadava, B. K. Pandey, S. P. Dubey, and J. P. Seth, Ferroelectricity and phase transitions in disodium hydrogen orthophosphste, *Asian J. Chem.* 20, 2051 (2008)

I.19. H. M. Mande and P. S. Ghalsasi, Designing chiral, propolar structures for observing ferroelectricity: Molecular analogue of KNO$_3$, *Cryst. Growth Des.* 16(1), 3 (2016)

I.20. C. C. Desai and A. H. Patel, Some aspects of the electrical conductivity of ferroelectric rubidium hydrogen tartrate single crystals, *J. Mater. Sci. Lett.* 6(9), 1066 (1987)

I.21. H. Cui, Z. Wang, K. Takahashi, Y. Okano, H. Kobayashi, and A. Kobayashi, Ferroelectric porous molecular crystal, [Mn$_3$(HCOO)$_6$](C$_2$H$_5$OH), exhibiting ferrimagnetic transition, *J. Am. Chem. Soc.* 128(47), 15074 (2006)

I.22. H. Tokoro and S. Ohkoshi, Novel magnetic functionalities of Prussian blue analogs, *Dalton Trans.* 40(26), 6825 (2011)

I.23. V. Subhashini, S. Ponnusamy, and C. Muthamizhchelvan, Growth, optical, thermal, piezo and ferroelectric studies on ethylenediamine ditartrate dihydrate (EDADTDH) single crystals, *J. Cryst. Growth* 312(7), 1040 (2010)

I.24. S. Kalyanaraman, P. M. Shajinshinu, and S. Vijayalakshmi, Refractive index, band gap energy, dielectric constant and polarizability calculations of ferroelectric Ethylenediaminium Tetrachlorozincate crystal, *J. Phys. Chem. Solids* 86, 108 (2015)

I.25. M. Loganayaki and P. Murugakoothan, Studies on dielectric and ferroelectric behaviour of L-alanine single crystal, *Asian J. Chem.* 23, 5089 (2011)

I.26. B. Want and R. Samad, Dielectric, ferroelectric and optical behaviour of terbium hydrogen tartrate trihydrate crystals, *J. Mater. Sci.* 49(14), 4891 (2014)

I.27. G. Ray, S. Kumar, N. Sinha, and B. Kumar, Enhanced dielectric piezo-/ferro-/electric properties of dye doped sodium acid phthalate crystal, *Curr. Appl. Phys.* 17(5), 813 (2017)

I.28. E. Jerusha, R. I. S. Kumar, S. S. Kirupavathy, and R. Gopalakrishnan, Investigations on the growth and characterisation of an isomorphous ammonium tetroxalate dihydrate superacid crystal, *Optik (Stuttg.)* 127(9), 3896 (2016)

I.29. B. Uma, K. S. Murugesan, S. Krishnan, S. J. Das, and B. M. Boaz, Optical and dielectric studies on organic nonlinear optical 2-furoic acid single crystals, *Optik (Stuttg.)* 124(17), 2754 (2013)

I.30. I. B. Hadj Sadok, F. Hajlaoui, K. Karoui, N. Audebrand, T. Roisnel, and N. Zouari, Crystal structure, optical and electrical properties of metal-halide compound $[C_7H_{16}N_2][ZnCl_4]$, *J. Phys. Chem. Solids* 129, 71 (2019)

I.31. O. M. Mailoud, A. H. Elsayed, H. A. El Fetouh, and A. H. A. ELazm, Synthesis and characterization of paramagnetic isotropic glycine manganese chloride single crystal with various dopant concentrations, *Results Phys.* 12, 925 (2019)

I.32. N. Bhuvaneswari and K. Venkatachalam, Structural, vibrational and physical properties on tetramethyammonium cadmium bromide ferroelectric single crystals, *Asian J. Chem.* 30(2), 386 (2018)

I.33. S. Yadava, B. K. Pandey, S. P. Dubey, and R. N. Gupta, Dielectric behaviour of lead nitrate with its phase transition, *Asian J. Chem.* 20, 731 (2008)

I.34. C. C. Desai and K. N. Patel, Synthesis and characterization of ferroelectric magnesium hydrogen phosphate single crystals, *Cryst. Res. Technol.* 24(7), 681 (1989)

I.35. R. Dhivya, R. Ezhil Vizhi, and D. Rajan Babu, Investigation on nucleation kinetics, growth and characterization of urea oxalic acid – ferroelectric single crystal, *J. Cryst. Growth* 468, 84 (2017)

I.36. S. Krishnan, C. J. Raj, S. Dinakaran, R. Uthrakumar, R. Robert, and S. J. Das, Optical, thermal, dielectric and ferroelectric behaviour of sodium acid phthalate (SAP) single crystals, *J. Phys. Chem. Solids* 69(11), 2883 (2008)

I.37. C. C. Stoumpos, Ch. D. Malliakas, and M. G. Kanatzidis, Semiconducting tin and lead iodide perovskites with organic cations: Phase transitions, high mobilities, and near-infrared photoluminescent properties, *Inorg. Chem.* 52(15), 9019 (2013)

I.38. S. Fujimoto, N. Yasuda, H. Hibino, and P. S. Narayanan, Ferroelectricity in lithium potassium sulphate, *J. Phys. D Appl. Phys.* 17(2), L35 (1984)

I.39. J. Dalal and B. Kumar, Remarkable enhancement in dielectric, piezoelectric, ferroelectric and SHG properties by iron doping in sodium para-nitrophenolate dihydrate single crystals, *Mater. Lett.* 165, 99 (2016)

I.40. J. Dalal, N. Sinha, H. Yadav, and B. Kumar, Structural, electrical, ferroelectric and mechanical properties with Hirshfeld surface analysis of novel NLO semiorganic sodium p-nitrophenolate dihydrate piezoelectric single crystal, *RSC Advances* 5(71), 57735 (2015)

I.41. A. C. Sajikumar, S. Vinu, and C. Krishnan, Studies on structural, optical and thermal properties of L-histidine doped potassium hydrogen phthalate single crystal, *Inter. J. Engn. Res. Technol.* 4(01), 525 (2015)

I.42. A. C. Sajikumar, S. Vinu, and C. Krishnan, Growth and characterization of barium doped potassium hydrogen phthalate single crystal, *Int. J. Eng. Res. Appl.* 5, 50 (2015)

I.43. R. E. Vizhi and D. R. Babu, A study on structural, optical, mechanical and ferroelectric properties of triglycine barium nitrate single crystals, *Ferroelectr. Lett. Sect.* 40(1–3), 1 (2013)

I.44. V. Duraikkan, S. A. Bahadur, N. Nallamuthu, S. Athimoolam, and A. Manikandan, Investigation of phase transition in some ferroelectrics calcium and zinc doped diammonium dibromodichlorinate, *J. Inorg. Organomet. Polym. Mater.* 27(1), 363 (2017)

I.45. S. C. Abrahams, J. Ravez, A. Simon, A. Reller, and H. R. Oswald, $Cu(OH)_2$: A new ferroelectric, *J. Appl. Cryst.* 28(5), 594 (1995)

I.46. A. C. Y. Pan, H. D. Mai, and G. Y. Yang, A new zeotype borogermanate β-$K_2B_2Ge_3O_{10}$: Synthesis, structure, property and conformational polymorphism, *Microporous Mesoporous Mater.* 168, 183 (2013)

I.47. T. G. J. Cao, W. H. Fang, S. T. Zheng, and G. Y. Yang, $(CH_3NH_3)_2[Ge(B_4O_9)]$: An organically-templated chiral borogermanate with second-order nonlinear and ferroelectric properties, *Inorg. Chem. Commun.* 13(9), 1047 (2010)

I.48. J. H. Zhang, F. Kong, and J. G. Mao, $Ba_3[Ge_2B_7O_{16}(OH)_2](OH)(H_2O)$ and $Ba_3Ge_2B_6O_{16}$: Novel alkaline-earth borogermanates based on two types of polymeric borate units and GeO_4 tetrahedra, *Inorg. Chem.* 50(7), 3037 (2011)

I.49. C. Jiang, N. Zhong, C. Luo, H. Lin, Y. Zhang, H. Peng, and C. G. Duan, (Diisopropylammonium)$_2MnBr_4$: A multifunctional ferroelectric with efficient green-emission and excellent gas sensing properties, *Chem. Commun. (Camb.)* 53(44), 5954 (2017)

I.50. P. S. L. Mageshwari, R. Priya, S. Krishnan, V. Joseph, and S. J. Das, Optical, dielectric and ferroelectric behaviour on doped lithium sulphate crystals, *Optik (Stuttg.)* 125(10), 2289 (2014)

I.51. S. Moitra and T. Kar, Second harmonic generation of a new nonlinear optical material L-valine hydrobromide, *J. Cryst. Growth* 310(21), 4539 (2008)

I.52. N. Tyagi, N. Sinha, H. Yadav, and B. Kumar, Growth, morphology, structure and characterization of L-histidinium dihydrogen arsenate orthoarsenic acid single crystal, *Acta Crystallogr. B* 72(4), 593 (2016)

I.53. K. Thukral, N. Vijayan, B. Singh, I. Bdikin, D. Haranath, K. K. Maurya, J. Philip, H. Soumya, P. Sreekanth, and G. Bhagavannarayana, Growth, structural and mechanical analysis of a single crystal of L-prolinium tartrate: A promising material for nonlinear optical applications, *CrystEngComm* 16(39), 9245 (2014)

I.54. S. Kumar, N. Sinha, H. Yadav, and B. Kumar, Growth, structural, dielectric, ferroelectric, and mechanical properties of L-prolinium tartrate single crystal, *J. Mater. Sci.* 51(16), 7614 (2016)

I.55. U. Charoen-In and P. Manyum, Growth of ferroelectric crystals: 4-aminopyridinium hydrogen maleate single crystals and their characterization, *Ceram. Int.* 41, S76 (2015)

I.56. D. W. Fu, Y. M. Song, G. X. Wang, Q. Ye, R. G. Xiong, T. Akutagawa, T. Nakamura, P. W. H. Chan, and S. D. Huang, Dielectric anisotropy of a homochiral trinuclear nickel(II) complex, *J. Am. Chem. Soc.* 129(17), 5346 (2007)

I.57. Z. Sun, T. Chen, J. Luo, and M. Hong, Bis(imidazolium) L-tartrate: A hydrogen-bonded displacive-type molecular ferroelectric material, *Angew. Chem. Int. Ed.* 51(16), 3871 (2012)

I.58. K. Senthilkumar, S. M. Babu, B. Kumar, and G. Bhagavannarayana, Effect of rare earth ions on the properties of glycine phosphite single crystals, *J. Cryst. Growth* 362, 343 (2013)

I.59. K. Senthilkumar, S. M. Babu, B. Kumar, and G. Bhagavannarayana, Improvement in structural, dielectric, ferroelectric and mechanical properties in metal ions doped glycine phosphite single crystals, *Ferroelectrics* 437(1), 126 (2012)

I.60. A. Shanthi, C. Krishnan, and P. Selvarajan, Studies on growth and characterization of a novel nonlinear optical and ferroelectric material, N,N-dimethylurea picrate single crystal, *J. Cryst. Growth* 393, 7 (2014)

I.61. B. Uma, R. S. Selvaraj, S. Krishnan, and B. M. Boaz, Growth and characterization of a novel organic nonlinear optical material: L-alanine 2-furoic acid, *Optik (Stuttg.)* 125(2), 651 (2014)

I.62. J. Dalal and B. Kumar, Bulk crystal growth, optical, mechanical and ferroelectric properties of new semiorganic nonlinear optical and piezoelectric Lithium nitrate monohydrate oxalate single crystal, *Opt. Mater.* 51, 139 (2016)

I.63. C. F. Sun, C. L. Hu, and J. G. Mao, $PbPt(IO_3)_6(H_2O)$: A new polar material with two types of stereoactive lone-pairs and a very large SHG response, *Chem. Commun. (Camb.)* 48(35), 4220 (2012)

I.64. Y. Yamamura, E. Saito, H. Saitoh, N. Hoshino, and K. Saito, New organic ferroelectrics: Cocrystal of $5,5'$-dimethyl-$2,2'$-bipyridine and bromanilic acid, *Chem. Lett.* 41(1), 119 (2012)

I.65. M. Vij, H. K. Sonia, H. K. Verma, M. S. Jayalakshmy, B. Singh, S. Verma, and K. K. Maurya, Nonlinear optical single crystal of L-cystine hydrochloride: Insights into the crystalline perfection, thermal, mechanical and optical properties for device fabrication, *Physica B* 550, 250 (2018)

I.66. S. Sonia, N. Vijayan, M. Vij, P. Kumar, B. Singh, S. Das, R. Rajnikant, and H. Soumya, Assessment of the imperative features of an L-arginine 4-nitrophenolate 4-nitrophenol dihydrate single crystal for nonlinear optical applications., *Mater. Chem. Front.* 1(6), 1107 (2017)

I.67. V. Duraikkan, S. A. Bahadur, N. Nallamuthu, S. Athimoolam, and A. Manikandan, Investigation of phase transition in some ferroelectrics calcium and zinc doped diammonium dibromodichlorinate, *J. Inorg. Organomet. Polym.* 27(1), 363 (2017)

References for Part II

II.1. N. M. Khusayfan, Ferroelectric properties of Ce doped hydroxyapatite nanoceramics, *J. Alloys Compd.* 685, 350 (2016)

II.2. R. AL-Wafi, Ferroelectric properties of Sr doped hydroxyapatite bioceramics for biotechnological applications, *J. Alloys Compd.* 689, 169 (2016)

II.3. A. A. Hendi, Hydroxyapatite based nanocomposite ceramics, *J. Alloys Compd.* 712, 147 (2017)

II.4. R. V. K. Mangalam, P. Mandal, E. Suard, and A. Sundaresan, Ferroelectricity in ordered perovskite $BaBi^{3+}_{0.5}(Bi^{5+}_{0.2}Nb^{5+}_{0.3})O_3$with Bi^{3+}:$6s^2$ lone pair at the *B*-site, *Chem. Mater.* 19(17), 4114 (2007)

II.5. A. M. Kusainova, P. Lightfoot, W. Zhou, S. Y. Stefanovich, A. V. Mosunov, and V. A. Dolgikh, Ferroelectric properties and crystal structure of the layered intergrowth phase $Bi_3Pb_2Nb_2O_{11}Cl$, *Chem. Mater.* 13(12), 4731 (2001)

II.6. C. Jin, Ferroelectric behavior of nonlinear optical material $MnTeMoO_6$, *Optik (Stuttg.)* 130, 1021 (2017)

II.7. Z. Zhong, W. Ding, W. Hou, Y. Chen, X. Chen, Y. Zhu, and N. Min, Preparation, characterization, and ferroelectric properties of the alkylamine-intercalated layered perovskite-type oxides ($C_nH_{2n+1}NH_3$–$Sr_2Nb_3O_{10}$, $n = 1$–6), *Chem. Mater.* 13(2), 538 (2001)

II.8. V. Isaza-Zapata, A. Arias, C. Maya, W. Martínez, A. Agudelo, B. Álvarez, A. Gómez, and J. L. Izquierdo, Ferroelectric response of $Na_{0.9}Li_{0.1}NbO_3$ at room temperature, *J. Phys. Conf. Ser.* 850, 012009 (2017)

II.9. O. Khamman, J. Jainumpone, A. Watcharapasorn, and S. Ananta, Fabrication, phase formation and microstructure of $Ni_4Nb_2O_9$ ceramics fabricated by using the two-stage sintering technique, *J. Korean Phys. Soc.* 69(3), 365 (2016)

II.10. R. N. P. Kumar, R. N. P. Choudhary, and B. P. Singh, Structural, dielectric and electrical properties of Te modified barium stannates using impedance analysis, *J. Mater. Sci.* 42(19), 8306 (2007)

II.11. P. R. Das, R. N. P. Choudhary, and B. K. Samantray, Diffuse ferroelectric phase transition in $Na_2Pb_2Sm_2W_2Ti_4$ Nb_4O_{30} ceramics, *Mater. Chem. Phys.* 101(1), 228 (2007)

II.12. P. R. Das, B. N. Parida, R. Padhee, and R. N. P. Choudhary, Structural and dielectric properties of $Na_2Pb_2Nd_2W_2Ti_4V_4O_{30}$ ferroelectric ceramics, *Indian J. Phys.* 90(2), 155 (2016)

II.13. X. M. Chen, Y. T. Lu, D. Z. Jin, and X. Q. Liu, Dielectric and ferroelectric characterization of Na(Ta, Nb)O_3 solid solution ceramics, *J. Electroceram.* 15(1), 21 (2005)

II.14. Y.-D. Hou, Y. Shi, H.-Y. Ge, M.-K. Zhu, and H. Yan, Comparative studies of ferroelectric behavior in rutile type $FeTiTaO_6$ and $AlTiTaO_6$, *Mater. Res. Bull.* 47(2), 184 (2012)

II.15. L. Biswal, P. R. Das, B. Behera, and R. N. P. Choudhury, Structural, dielectric and conductivity studies of $Na_2Pb_2La_2W_2Ti_4Nb_4O_{30}$ ferroelectric ceramic, *J. Electroceram.* 29(3), 204 (2012)

II.16. X. Tian, S. Qu, Y. Zhou, B. Xu, and Z. Xu, Effects of Mn-addition on the microstructure and ferroelectric properties of high-temperature $CaBi_2Nb_2O_9$ ceramics, *J. Inorg. Organomet. Polym.* 23(4), 877 (2013)

II.17. S. J. Patwe, V. Katari, N. P. Salke, S. K. Deshpande, R. Rao, M. K. Gupta, R. Mittal, S. N. Achary, and A. K. Tyag, Structural and electrical properties of layered perovskite type $Pr_2Ti_2O_7$: Experimental and theoretical investigations, *J. Mater. Chem. C* 3(17), 4570 (2015)

II.18. X. L. Zhu, Y. Bai, X. Q. Liu, and X. M. Chen, Ferroelectric and dielectric properties in $Ba_5SmFe_{1.5}Nb_{8.5}O_{30}$ tungsten bronze ceramics, *Adv. Appl. Ceramics* 112(7), 412 (2013)

II.19. Z. Lei, T. Chen, W. Li, M. Liu, W. Ge, and Y. Lu, Cobalt-substituted seven-layer aurivillius $Bi_8Fe_4Ti_3O_{24}$ ceramics: Enhanced ferromagnetism and ferroelectricity, *Crystals (Basel)* 7(3), 76 (2017)

II.20. P. R. Das, L. Biswal, B. Behera, and R. N. P. Choudhary, Structural and electrical properties of $Na_2Pb_2Eu_2W_2Ti_4X_4O_{30}$ (X = Nb, Ta) ferroelectric ceramics, *Mater. Res. Bull.* 44(6), 1214 (2009)

II.21. O. Subohi, G. S. Kumar, M. M. Malik, and R. Kurchania, Synthesis of bismuth titanate with urea as fuel by solution combustion route and its dielectric and ferroelectric properties, *Optik (Stuttg.)* 125(2), 820 (2014)

II.22. P. A. Jha, P. K. Jha, A. K. Jha, and R. K. Dwivedi, Dielectric behavior of $(1–x)BaZr_{0.025}Ti_{0.975}O_3–(x)BiFeO_3$ solid solutions, *Mater. Res. Bull.* 48(1), 101 (2013)

II.23. K. Nakagawa, H. Tokoro, and S. Ohkoshi, Observation of ferroelectricity in paramagnetic copper octacyanomolybdate, *Inorg. Chem.* 47(23), 10810 (2008)

II.24. B. Kaur, K. Singh, O. P. Pandey, and S. Thakur, Influence of modifier on dielectric and ferroelectric properties of aluminosilicate glasses, *J. Non-Cryst. Solids* 465, 26 (2017)

II.25. B. W. Li, M. Osada, T. C. Ozawa, and T. Sasaki, $RbBiNb_2O_7$: A new lead-free high-T_c ferroelectric, *Chem. Mater.* 24(16), 3111 (2012)

II.26. R. Muduli, P. Kumar, R. K. Panda, and S. Panigrahi, Dielectric, ferroelectric and impedance spectroscopic studies of Mn and W modified $AgNbO_3$ ceramics, *Mater. Chem. Phys.* 180, 422 (2016)

II.27. W. Zhang, N. Kumada, Y. Yonesaki, T. Takei, N. Kinomura, T. Hayashi, M. Azuma, and M. Takano, Ferroelectric perovskite-type barium copper niobate: $BaCu_{1/3}Nb_{2/3}O_3$, *J. Solid State Chem.* 179(12), 4052 (2006)

II.28. M. Pastor and K. Biswas, Synthesis and electrical characterization of $Ba(Cd_{1/3}Nb_{2/3})O_3$ ferroelectric compound, *Mater. Chem. Phys.* 139(2–3), 634 (2013)

II.29. C. Hu, L. Fang, X. Peng, C. Li, B. Wu, and L. Liu, Dielectric and ferroelectric properties of tungsten bronze ferroelectrics in $SrO–Pr_2O_3–TiO_2–Nb_2O_5$ system, *Mater. Chem. Phys.* 121(1–2), 114 (2010)

II.30. N. V. Quyet, L. H. Bac, and D. D. Dung, Enhancement of the electrical-field-induced strain in lead-free $Bi_{0.5}(Na,K)_{0.5}TiO_3$-based piezoelectric ceramics: Role of the phase transition, *J. Korean Phys. Soc.* 66(8), 1317 (2015)

II.31. X. Tian, S. Qu, Y. Zhou, B. Xu, and Z. Xu, Effects of Mn-addition on the microstructure and ferroelectric properties of high-temperature $CaBi_2Nb_2O_9$ ceramics, *J. Inorg. Organomet. Polym.* 23(4), 877 (2013)

II.32. S. K. Ramasesha, A. K. Singh, and K. B. R. Varma, Effect of pressure on dielectric and ferroelectric properties of bismuth vanadate, *Mater. Chem. Phys.* 48(2), 136 (1997)

II.33. C. A. Diaz-Moreno, Y. Ding, J. Portelles, J. Heiras, A. H. Macias, A. Syeed, A. Paez, C. Li, J. López, and R. Wicker, Optical properties of ferroelectric lanthanum lithium niobite, *Ceram.* 44, 4727 (2018)

II.34. Q. Yin, Z. Sun, S. Shi, J. Yang, C. Tian, and M. Bao, Structure and electrical properties of lead-free piezoelectric ceramics $Bi_{0.5}Na_{0.5}TiO_3$-$Ba_{0.94}Sr_{0.06}(Sn_{0.08}Ti_{0.92})O_3$, *Asian J. Chem.* 26(6), 1698 (2014)

II.35. S. Somwan, A. Ngamjarurojana, and A. Limpichaipanit, Dielectric, ferroelectric and induced strain behavior of PLZT 9/65/35 ceramics modified by Bi_2O_3 and CuO codoping, *Ceram. Int.* 42(9), 10690 (2016)

II.36. P. S. Sahoo, A. Panigrahi, S. K. Patri, and R. N. P. Choudhary, Structural, dielectric, electrical and piezoelectric properties of $Ba_4SrRTi_3V_7O_{30}$ (R = Sm, Dy) ceramics, *Cent. Eur. J. Phys.* 6, 843 (2008)

II.37. P. S. Sahoo and A. Panigrahi, Dielectric properties of $Ba_3Sr_2DyTi_3V_7O_{30}$ ceramics, *Cent. Eur. J. Phys.* 8(4), 639 (2010)

II.38. S. K. Barik, R. N. P. Choudhary, and P. K. Mahapatra, Structural and dielectric studies of lead-free ceramics: $Na_{1/2}Y_{1/2}TiO_3$, *Cent. Eur. J. Phys.* 6(4), 849 (2008)

II.39. B. Behera, P. Nayak, and R. N. P. Choudhary, Structural and electrical properties of $KCa_2Nb_5O_{15}$ ceramics, *Cent. Eur. J. Phys.* 6, 289 (2008)

II.40. O. Subohi, G. S. Kumar, M. M. Malik, and R. Kurchania, Study of influence of fuel on dielectric and ferroelectric properties of bismuth titanate ceramics synthesized using solution based combustion technique, *Mater. Res. Express* 2(3), 036302 (2015)

II.41. X. Tian, S. Qu, B. Wang, and Z. Xu, Microstructure and electrical properties of ultra high temperature $(1–x)CaBi_2Nb_2O_9–xNa_{0.5}Bi_{2.5}Nb_2O_9$ ceramics, *Mater. Res. Innov.* 19(3), 171 (2015)

II.42. C. Huang, W. Wong-Ng, W. F. Liu, X. N. Zhang, Y. Jiang, P. Wu, B. Y. Tong, H. Zhao, and S. Y. Wang, Major improvement of ferroelectric and optical properties in Na-doped Ruddlesden–Popper layered hybrid improper ferroelectric compound, $Ca_3Ti_2O_7$, *J. Alloys Compd.* 770, 582 (2019)

II.43. N. Kumar, A. Shukla, N. Kumar, S. Sahoo, S. Hajra, and R. N. P. Choudhary, Structural, electrical and ferroelectric characteristics of $Bi(Fe_{0.9}La_{0.1})O_3$, *Ceram. Int.* 44(17), 21330 (2018)

II.44. P. Gupta, P. K. Mahapatra, and R. N. P. Choudhary, Structural and electrical characteristics of an aurivillius family compound $Bi_2LaTiVO_9$, *Cryst. Res. Technol.* 53(12), 1800045 (2018)

II.45. H. Wattanasarn, S. Sansupan, P. Srinuanlae, A. Namthaisong, S. Phewphong, W. Phontankham, T. Sumphao, J. Kongphimai, W. Chaiphaksa, and J. Kaewkhao, Effect of Fe_2O_3-dopped on ferroelectric properties of $(55-x)SiO_2$:xFe_2O_3:$1Al_2O_3$:$6.3CaO$:$0.2Sb_2O_3$:$13B_2O_3$:$4.5BaO$:$20Na_2O$, *Mater. Today* 5, 13934 (2018)

Multiferroics ceramics

II.46. Y. Qiao, Y. Zhou, S. Wang, L. Yuan, Y. Du, D. Lu, G. Che, and H. Che, Composition dependent magnetic and ferroelectric properties of hydrothermally synthesized $GdFe_{1-x}Cr_xO3$ ($0.1 \leq x \leq 0.9$) perovskites, *Dalton Trans.* 46(18), 5930 (2017)

II.47. S. Madolappa, A. V. Anupama, P. W. Jaschin, K. B. R. Varma, and B. Sahoo, Magnetic and ferroelectric characteristics of Gd^{3+} and Ti^{4+} co-doped $BiFeO_3$ ceramics, *Bull. Mater. Sci.* 39(2), 593 (2016)

II.48. S. R. Mohapatra, B. Sahu, M. Chandrasekhar, P. Kumar, S. D. Kaushik, S. Rath, and A. K. Singh, Effect of cobalt substitution on structural, impedance, ferroelectric and magnetic properties of multiferroic $Bi_2Fe_4O_9$ ceramics, *Ceram. Int.* 42(10), 12352 (2016)

II.49. X. Wang, J. Yu, J. C. Zhang, X. Yan, C. Song, Y. Long, K. Ruan, and X. Li, Structural evolution, magnetization enhancement, and ferroelectric properties of Er^{3+}- doped $SmFeO_3$, *Ceram. Int.* 43(18), 16903 (2017)

II.50. D. Varshney, P. Sharma, S. Satapathy, and P. K. Gupta, Structural, electrical and magnetic properties of $Bi_{0.825}Pb_{0.175}FeO_3$, and $Bi_{0.725}La_{0.1}Pb_{0.175}FeO_3$ multiferroics, *Mater. Res. Bull.* 49, 345 (2014)

II.51. Y. Han, W. Mao, C. Quan, X. Wang, J. Yang, T. Yang, X. Li, and W. Huang, Enhancement of magnetic and ferroelectric properties of $BiFeO_3$ by Er and transition element (Mn, Co) co-doping, *Mater. Sci. Eng. B* 188, 26 (2014)

II.52. T. Kaur, J. Sharma, S. Kumar, and A. K. Srivastava, Optical and multiferroic properties of Gd-Co substituted barium hexaferrite, *Cryst. Res. Technol.* 52(9), 1700098 (2017)

II.53. P. T. Lin, X. Li, L. Zhang, J. H. Yin, X. W. Cheng, Z. H. Wang, Y. C. Wu, and G. H. Wu, La-doped $BiFeO_3$: Synthesis and multiferroic property study, *Chin. Phys. B* 23(4), 047701 (2014)

II.54. B. Chatterjee, H. Kevin, G. D. Dwivedi, H. D. Yang, S. Chatterjee, and A. K. Ghosh, Enhancement of ferromagnetic and ferroelectric properties in Co-doped $BiFeO_3$, *Asian J. Chem.* 23(12), 5563 (2011)

II.55. L. Yi, Coexistence of magnetic and ferroelectric properties in $Y_{0.1}Co_{1.9}MnO_4$, *Chin. Phys. B* 19(7), 077201 (2010)

II.56. N. Raju, S. S. Kumar Reddy, J. Ramesh, C. G. Reddy, P. Y. Reddy, K. R. Reddy, V. G. Sathe, and V. R. Reddy, Magnetic, ferroelectric, and spin phonon coupling studies of $Sr_3Co_2Fe_{24}O_{41}$ multiferroic Z-type hexaferrite, *J. Appl. Phys.* 120(5), 054103 (2016)

II.57. Z. M. Tian, S. L. Yuan, X. L. Wang, X. F. Zheng, S. Y. Yin, C. H. Wang, and L. Liu, Size effect on magnetic and ferroelectric properties in $Bi_2Fe_4O_9$ multiferroic ceramics, *J. Appl. Phys.* 106(10), 103912 (2009)

II.58. Z. M. Tian, Y. Qiu, S. L. Yuan, M. S. Wu, S. X. Huo, and H. N. Duan, Enhanced multiferroic properties in Ti-doped $Bi_2Fe_4O_9$ ceramics, *J. Appl. Phys.* 108(6), 064110 (2010)

II.59. M. Naveed-Ul-Haq, V. V. Shvartsman, G. Constantinescu, H. Trivedi, S. Salamon, J. Landers, H. Wende, and D. C. Lupascu, Effect of Al^{3+} modification on cobalt ferrite and its impact on the magnetoelectric effect in BCZT–CFO multiferroic composites, *J. Mater. Sci.* 52(23), 13402 (2017)

II.60. J. S. Kim, C. I. Cheon, W.-S. Oh, and P. W. Jang, Crystal structure and multiferroic properties of the $BiFeO_3$–$PrFeO_3$–$DyFeO_3$–$BaTiO_3$ system, *phys. stat. sol. (b)* 241(7), 1629 (2004)

II.61. M. Muneeswaran, R. Dhanalakshmi, and N. V. Giridharan, Effect of Tb substitution on structural, optical, electrical and magnetic properties of $BiFeO_3$, *J. Mater. Sci. Mater. Electron.* 26(6), 3827 (2015)

II.62. Y. Qiu, Z. J. Zou, R. R. Sang, H. Wang, D. Xue, Z. M. Tian, G. S. Gong, and S. L. Yuan, Enhanced magnetic and ferroelectric properties in Cr doped $Bi_2Fe_4O_9$ ceramics, *J. Mater. Sci. Mater. Electron.* 26(3), 1732 (2015)

II.63. Y. Ma, Y. J. Wu, Y. Q. Lin, and X. M. Chen, Microstructures and multiferroic properties of $YFe_{1-x}Mn_xO^3$ ceramics prepared by spark plasma sintering, *J. Mater. Sci. Mater. Electron.* 21(8), 838 (2010)

II.64. S. Samantaray and B. K. Roul, Dielectric and magnetic properties of $DyMnO_3$ ceramics, *J. Mater. Sci. Mater. Electron.* 24(9), 3387 (2013)

II.65. J. A. Moreira, A. Almeida, W. S. Ferreira, M. R. Chaves, J. B. Oliveira, J. M. Machado da Silva, M. A. Sá, S. M. F. Vilela, and P. B. Tavares, Ferroelectricity in antiferromagnetic phases of $Eu_{1-x}Y_xMnO_3$, *Solid State Commun.* 151(5), 368 (2011)

II.66. S. Huang, L. R. Shi, Z. M. Tian, S. L. Yuan, C. M. Zhu, G. S. Gong, and Y. Qiu, Effect of Al^{3+} substitution on the structural, magnetic, and electric properties in multiferroic $Bi_2Fe_4O_9$ ceramics, *J. Solid State Chem.* 227, 79 (2015)

II.67. A. Mitra, A. S. Mahapatra, A. Mallick, A. Shaw, M. Ghosh, and P. K. Chakrabarti, Simultaneous enhancement of magnetic and ferroelectric properties of $LaFeO_3$ by co-doping with Dy^{3+} and Ti^{4+}, *J. Alloys Compd.* 726, 1195 (2017)

II.68. P. P. Rout, S. K. Pradhan, S. K. Das, S. Samantaray, and B. K. Roul, Enhancement of magnetic and ferroelectric behaviour in (Ca, Co) co-doped $HoMnO_3$ multiferroics, *J. Magn. Magn. Mater.* 345, 106 (2013)

II.69. Y. Tian, F. Xue, Q. Fu, D. Zhou, Y. Hu, L. Zhou, Z. Zheng, and Z. Xin, Impedance spectroscopy and ferromagnetic properties of $Bi_{0.8}Gd_{0.2}FeO_3$ multiferroics, *J. Magn. Magn. Mater.* 435, 154 (2017)

II.70. B. K. Vashisth, J. S. Bangruwa, A. Beniwal, S. P. Gairola, A. Kumar, N. Singh, and V. Verma, Modified ferroelectric/magnetic and leakage current density properties of Co and Sm co-doped bismuth ferrites, *J. Alloys Compd.* 698, 699 (2017)

II.71. S. K. Das, and B. K. Roul, Room temperature magnetism and ferroelectricity in $BaTi_{0.95-x}Hf_{0.05}Co_xO_3$ ceramics, *J. Magn. Magn. Mater.* 363, 77 (2014)

II.72. X. Yuan, L. Shi, J. Zhao, S. Zhou, Y. Li, C. Xie, and J. Sr Guo, Sr and Pb co-doping effect on the crystal structure, dielectric and magnetic properties of $BiFeO_3$ multiferroic compounds, *J. Alloys Compd.* 708, 93 (2017)

II.73. K. K. Bharathi, J. A. Chelvane, and G. Markandeyulu, Magnetoelectric properties of Gd and Nd-doped nickel ferrite, *J. Magn. Magn. Mater.* 321(22), 3677 (2009)

II.74. R. N. Bhowmik and A. K. Sinh, Improvement of room temperature electric polarization and ferrimagnetic properties of $Co_{1.25}Fe_{1.75}O_4$ ferrite by heat treatment, *J. Magn. Magn. Mater.* 421, 120 (2017)

II.75. S. R. Wadgane, S. E. Shirsath, A. S. Gaikwad, S. Satpute, A. B. Kadam, and R. H. Kadam, Ferro- and magneto-electric characteristics in $YFeO_3$–$Y_3Fe_5O_{12}$ nanocomposites, *J. Magn. Magn. Mater.* 457, 103 (2017)

II.76. J. Roa-Rojas, C. Salazar, D. Llamosa, A. A. León-Vanegas, D. A. L. Téllez, P. Pureur, F. T. Dias, and V. N. Vieira, Magnetoelectric response of new Sr_2TiMnO_6 manganite-like material, *J. Magn. Magn. Mater.* 320(14), e104 (2008)

II.77. S. S. Yadava, A. Khare, P. Gautam, A. Kumar, and K. D. Mandal, Dielectric, ferroelectric and magnetic study of iron doped hexagonal $Ba_4YMn_{3-x}O_{11.5-\delta}$(BYMO) and its dependence on temperature as well as frequency, *New J. Chem.* 41(11), 4611 (2017)

II.78. A. Rathi, H. Borkar, P. K. Rout, A. Gupta, H. K. Singh, A. Kumar, B. Gahtori, R. P. Pant, and G. A. Basheed, Antisite disorder-driven large electric polarization in multiferroic Nd_2CoMnO_6, *J. Phys. D Appl. Phys.* 50(46), 465001 (2017)

II.79. M. G. Masud, A. Ghosh, J. Sannigrahi, and B. K. Chaudhuri, Observation of relaxor ferroelectricity and multiferroic behaviour in nanoparticles of the ferromagnetic semiconductor La_2NiMnO_6, *J. Phys.: Condens. Matter* 24(29), 295902 (2012)

II.80. Z. Wang, R. Gao, X. Deng, G. Chen, W. Cai, and C. Fu, Dielectric and ferroelectric properties of $LaFeO_3$ particles derived from metal organic frameworks precursor, *Ceram. Int.* 45(2), 1825 (2019)

II.81. A. Mitra, A. S. Mahapatra, A. Mallick, A. Shaw, N. Bhakta, and P. K. Chakrabarti, Improved magneto-electric properties of $LaFeO_3$ in $La_{0.8}Gd_{0.2}Fe_{0.97}Nb_{0.03}O_3$, *Ceram. Int.* 44(4), 4442 (2018)

II.82. M. S. Alam, R. Hossain, and M. A. Basith, Enhanced multiferroism in Gd-doped $BiMn_2O_5$ ceramics, *Ceram. Int.* 44(2), 1594 (2018)

II.83. K. Praveena, P. Bharathi, H. L. Liu, and K. B. R. Varma, Structural, multiferroic properties and enhanced magnetoelectric coupling in $Sm_{1-x}Ca_xFeO_3$, *Ceram. Int.* 42(12), 13572 (2016)

II.84. S. R. Mohapatra, B. Sahu, M. Chandrasekhar, P. Kumar, S. D. Kaushik, S. Rath, and A. K. Singh, Effect of cobalt substitution on structural, impedance, ferroelectric and magnetic properties of multiferroic $Bi_2Fe_4O_9$ ceramics, *Ceram. Int.* 42(10), 12352 (2016)

II.85. A. Durán, J. M. Jiménez, M. Solórzano, and R. Falconi, Improvement of the ferroelectric properties of Ti-doped $YCrO_3$ceramic, *J. Phys. Chem. Solids* 123, 228 (2018)

II.86. R. Tursun, Y. C. Su, Q. S. Yu, J. Tan, T. Hu, Z. B. Luo, and J. Zhang, Effect of doping on the structural, magnetic, and ferroelectric properties of $Ni_{1-x}A_xTiO_3$ (A = Mn, Fe, Co, Cu, Zn; x = 0, 0.05, and 0.1), *J. Alloys Compd.* 773, 288 (2019)

II.87. K. L. Routray, D. Sanyal, and D. Behera, Gamma irradiation induced structural, electrical, magnetic and ferroelectric transformation in bismuth doped nanosized cobalt ferrite for various applications, *Mater. Res. Bull.* 110, 126 (2019)

II.88. A. S. Mahapatra and P. K. Chakrabarti, Enhanced magnetic and ferroelectric properties of $La_{0.9}Tb_{0.1}FeO_3$, *Mater. Sci. Eng.* 240, 140 (2019)

II.89. P. P. Khirade, S. D. Birajdar, A. V. Raut, and K. M. Jadhav, Multiferroic iron doped $BaTiO_3$ nanoceramics synthesized by sol-gel auto combustion: Influence of iron on physical properties, *Ceram. Int.* 42(10), 12441 (2016)

II.90. M. Naveed-Ul-Haq, V. V. Shvartsman, G. Constantinescu, H. Trivedi, S. Salamon, J. Landers, H. Wende, and D. C. Lupascu, Effect of Al^{3+} modification on cobalt ferrite and its impact on the magnetoelectric effect in BCZT–CFO multiferroic composites, *J. Mater. Sci.* 52(23), 13402 (2017)

II.91. R. Pattanayak, S. Kuila, S. Raut, S. P. Ghosh, S. Dhal, and S. Panigrahi, Observation of grain size effect on multiferroism and magnetoelectric coupling of $Na_{0.5}Bi_{0.5}TiO_3$–$BaFe_{12}O_{19}$ novel composite system, *J. Magn. Magn. Mater.* 444, 401 (2017)

II.92. R. Rani, J. K. Juneja, S. Singh, K. K. Raina, and C. Prakash, Study of $0.1Ni_{0.8}Zn_{0.2}Fe_2O_4$–$0.9Pb_{1-3x/2}La_xZr_{0.65}Ti_{0.35}O_3$ magnetoelectric composites, *J. Magn. Magn. Mater.* 325, 47 (2013)

II.93. S. Dipti, S. Singh, J. K. Juneja, K. K. Raina, R. K. Kotnala, and C. Prakash, Study of $x Co_{0.8}Ni_{0.2}Fe_2O_4$+(1–$x$) $Pb_{0.99625}La_{0.0025}Zr_{0.55}Ti_{0.45}O_3$ magnetoelectric composites, *J. Magn. Magn. Mater.* 407, 279 (2016)

II.94. J. H. Peng, M. Hojamberdiev, H. G. Li, D. L. Mao, Y. J. Zhao, P. Liu, J. P. Zhou, and G. Q. Zhu, Electrical, magnetic, and direct and converse magnetoelectric properties of (1–x)$Pb(Zr_{0.52}Ti_{0.48})O_3$–($x$)$CoFe_2O_4$ (PZT–CFO) magnetoelectric composites, *J. Magn. Magn. Mater.* 378, 298 (2015)

II.95. S. Jangra, S. Sanghi, A. Agarwal, M. Rangi, K. Kaswan, and S. Khasa, Improved structural, dielectric and magnetic properties of Ca^{2+} and Nb^{5+} co-substituted $BiFeO_3$ multiferroics, *J. Alloys Compd.* 722, 606 (2017)

II.96. A. S. Kumar, C. S. Chitra Lekha, S. Vivek, V. Saravanan, K. Nandakumar, and S. S. Nair, Multiferroic and magnetoelectric properties of $Ba_{0.85}Ca_{0.15}Zr_{0.1}Ti_{0.9}O_3$–$CoFe_2O_4$ core–shell nanocomposite, *J. Magn. Magn. Mater.* 418, 294 (2016)

II.97. N. S. Negi, A. Sharma, J. Shah, and R. K. Kotnala, Investigation on impedance response, magnetic and ferroelectric properties of $0.20(Co_{1-x}Zn_xFe_{2-y}Mn_yO_4)$–$0.80(Pb_{0.70}Ca_{0.30}TiO_3)$ magnetoelectric composites, *Mater. Chem. Phys.* 148(3), 1221 (2014)

II.98. M. Kumar, S. Shankar, O. Parkash, and O. P. Thakur, Dielectric and multiferroic properties of $0.75BiFeO_3$–$0.25BaTiO_3$ solid solution, *J. Mater. Sci. Mater. Electron.* 25(2), 888 (2014)

II.99. T. Ramesh, V. Rajendar, and S. R. Murthy, $CoFe_2O_4$–$BaTiO_3$ multiferroic composites: Role of ferrite and ferroelectric phases on the structural, magneto dielectric properties, *J. Mater. Sci. Mater. Electron.* 28(16), 11779 (2017)

II.100. Y. Liu, Y. Wu, D. Li, Y. Zhang, J. Zhang, and J. Yang, A study of structural, ferroelectric, ferromagnetic, dielectric properties of $NiFe_2O_4$–$BaTiO_3$ multiferroic composites, *J. Mater. Sci. Mater. Electron.* 24(6), 1900 (2013)

II.101. Y. Liu, Y. Wu, D. Li, Y. Zhang, J. Zhang, and J. Yang, A study of structural, ferroelectric, ferromagnetic, dielectric properties of $NiFe_2O_4$–$BaTiO_3$ multiferroic composites, *J. Mater. Sci. Mater. Electron.* 24(6), 1900 (2013)

II.102. L. K. Pradhan, R. Pandey, R. Kumar, and M. Kar, Lattice strain induced multiferroicity in PZT–CFO particulate composite, *J. Appl. Phys.* 123(7), 074101 (2018)

II.103. R. Sharma, P. Pahuja, and R. P. Tandon, Structural, dielectric, ferromagnetic, ferroelectric and ac conductivity studies of the $BaTiO_3$–$CoFe_{1.8}Zn_{0.2}O_4$ multiferroic particulate composites, *Ceram. Int.* 40(7), 9027 (2014)

II.104. X. Qi, J. Zhou, Z. Yue, Z. Gui, L. Li, and S. Buddhudu, A ferroelectric ferromagnetic composite material with significant permeability and permittivity, *Adv. Funct. Mater.* 14(9), 920 (2004)

II.105. A. S. Mahapatra, A. Mitra, A. Mallick, A. Shaw, and P. K. Chakrabarti, Structural, magnetic, dielectric and magneto-dielectric properties of $(BaTiO_3)_{0.70}(Li_{0.3}Zn_{0.4}Fe_{2.3}O_4)_{0.30}$, *Mater. Res. Bull.* 102, 226 (2018)

II.106. S. K. Mandal, S. Chakraborty, P. Dey, B. Saha, and T. K. Nath, Zn doped $NiFe_2O_4$–Pb $(Zr_{0.58}Ti_{0.42})O_3$ multiferroic nanocomposites: Magnetoelectric coupling, dielectric and electrical transport, *J. Alloys Compd.* 747, 834 (2018)

II.107. R. G. Ganapathi, R. B. Lakshmi, K. C. Arun, K. K. N. Chidambara, K. Samatha, M. K. Sreeramachandra, and P. D. Madhava, Ferroelectric and dielectric properties of $BaTi_{0.9}Zr_{0.1}O_3$ doped with $Li_{0.5}Fe_{2.5}O_4$ ceramics, *Physica B* 539, 44 (2018)

II.108. J. S. Bangruwa, B. K. Vashisth, N. Singh, N. Singh, and V. Verma, A systematic study of structural, magnetic and electric properties of perovskite-spinel composites prepared by sol-gel technique, *J. Alloys Compd.* 739, 319 (2018)

II.109. R. Pandey, L. K. Pradhan, and M. Kar, Structural, magnetic, and electrical properties of $(1–x)Bi_{0.85}La_{0.15}FeO_3$–$(x)CoFe_2O_4$ multiferroic composites, *J. Phys. Chem. Solids* 115, 42 (2018)

II.110. H. Mana-ay, J. Anthoniappen, C. S. Tu, R. Sarmiento-Jr, C.-S. Chen, P.-Y. Chen, and F. M. Ruiz, Improved microstructure and ferroelectric properties in B-site Ti^{4+}-substituted $(Bi_{0.86}Sm_{0.14})FeO_3$ polycrystalline ceramics, *Mater. Chem. Phys.* 225, 272 (2019)

II.111. S. Shankar, M. Kumar, A. K. Ghosh, O. P. Thakur, and M. Jayasimhadri, Anomalous ferroelectricity and strong magnetoelectric coupling in $CoFe_2O_4$-ferroelectric composites, *J. Alloys Compd.* 779, 918 (2019)

II.112. A. Ghani, S. Yang, S. S. Rajput, S. Ahmed, A. Murtaza, C. Zhou, Y. Zhang, X. Song, and X. Ren, Enhanced multiferroic properties of lead-free $(1-x)GaFeO_{3-x}Co_{0.5}Zn_{0.5}Fe_2O_4$ composities, *J. Appl. Phys.* 124(15), 154101 (2018)

II.113. R. Rani, J. K. Juneja, S. Singh, K. K. Raina, and C. Prakash, Dielectric, ferroelectric, magnetic and magnetoelectric properties of $0.1Ni_{0.8}Zn_{0.2}Fe_2O_4$–$0.9Pb_{1-3x/2}Sm_xZr_{0.65}Ti_{0.35}O_3$ magnetoelectric composites, *Ceram. Int.* 39(7), 7845 (2013)

II.114. H. F. Zhang, S. W. Or, and H. L. W. Chan, Dielectric and magnetic properties of fine grained ferromagnetic–ferroelectric composites, *Mater. Res. Innov.* 12(3), 142 (2008)

II.115. H. Y. Dai, Z. P. Chen, T. Li, C. M. Wang, Y. Li, and Y. S. Guo, Influence of samarium substitution on structural and multiferroic properties of bismuth ferrite ceramics, *Mater. Res. Innov.* 17(2), 62 (2013)

II.116. R. Xu, S. Hang, F. Wang, Q. Zhang, Z. Li, Z. Wang, R. Gao, W. Cai, and C. Fu, The study of microstructure, dielectric and multiferroic properties of $(1–x)Co_{0.8}Cu_{0.2}Fe_2O_4$–$(x)Ba_{0.6}Sr_{0.4}TiO_3$ composites, *J. Electron. Mater.* 48(1), 386 (2019)

II.117. V. N. Shut, V. M. Laletin, S. R. Syrtsov, V. L. Trublovsky, Yu. V. Medvedeva, K. I. Yanushkevich, M. V. Bushinskii, and T. V. Petlitskaya, Structure, ferroelectric, and magnetoelectric properties of bulk PZT–$NiFe_{1.9}Co_{0.02}O_{4-\delta}$ composites, *Phys. Solid State* 60(9), 1744 (2018)

II.118. A. S. Dzunuzovic, M. M. Vijatovic Petrovic, J. D. Bobic, N. I. Ilic, M. Ivanov, R. Grigalaitis, J. Banys, and B. D. Stojanovic, Magneto-electric properties of $xNi_{0.7}Zn_{0.3}Fe_2O_4$–$(1-x)BaTiO_3$ multiferroic composites, *Ceram. Int.* 44(1), 683 (2018)

II.119. M. K. Sharif, M. A. Khan, M. F. Warsi, M. Ramzan, and A. Hussain, Structural and ferroelectric properties of hafnium substituted $BiFeO_3$ multiferroics synthesized via auto combustion technique, *Ceram. Int.* 44(17), 20648 (2018)

II.120. X. Wang, Z. Wang, Q. Hu, C. Zhang, D. Wang, and L. Li, Room temperature multiferroic properties of Fe-doped nonstoichiometric $SrTiO_3$ ceramics at both A and B sites, *Solid State Commun.* 289, 22 (2019)

II.121. S. Atiq, M. Faizan, A. H. Khan, A. Mahmood, S. M. Ramay, and S. Naseem, Co-existence of magnetic and electric ferroic orders in La-substituted $BiFeO_3$, *Results Phys.* 12, 1269 (2019)

II.122. D. Ginting, S. C. Yu, T. L. Phan, N. V. Dang, T. D. Thanh, and V. D. Lam, Electron-spin-resonance spectra and ferroelectricity of $BaTi_{1-x}Fe_xO_3$, *J. Korean Phys. Soc.* 62(12), 2128 (2013)

II.123. A. Kumar, K. L. Yadav, S. Kumar, N. Kumar, A. Mishra, N. Kumar, U. Shankar, T. Mehrotra, G. Sharma, R. Kumar, and G. D. Adhikary, Magnetic, ferroelectric, and magnetodielectric properties of $BiFeO_3$ ceramic co-doped with Eu and Gd, *J. Phys. Chem. Solids* 124, 19 (2019)

II.124. L. G. Wang, W. J. Kong, X. X. Wang, J. X. Lei, and Y. Y. Liang, Room-temperature multiferroic properties of Ba^{2+} doped $0.7Bi_{0.5}Na_{0.5}TiO_3$–$0.3NiFe_2O_4$ ceramics, *Ceram. Int.* 45(1), 1135 (2019)

II.125. F. N. Sayed, B. P. Mandal, O. D. Jayakumar, A. Arya, R. M. Kadam, A. Dixit, R. Naik, and A. K. Tyagi, Rare examples of fluoride-based multiferroic materials in Mn-substituted $BaMgF_4$ systems: Experimental and theoretical studies, *Inorg. Chem.* 50(22), 11765 (2011)

II.126. A. Stroppa, P. Jain, P. Barone, M. Marsman, J. M. Perez-Mato, A. K. Cheetham, H. W. Kroto, and S. Picozzi, Electric control of magnetization and interplay between orbital ordering and ferroelectricity in a multiferroic metal–organic framework, *Angew. Chem. Int. Ed.* 50(26), 5847 (2011)

II.127. J. R. Sahu, A. Ghosh, A. Sundaresan, and C. N. R. Rao, Multiferroic properties of $ErMnO_3$, *Mater. Res. Bull.* 44(11), 2123 (2009)

II.128. L. J. Wang, S. M. Feng, J. L. Zhu, R. C. Yu, C. Q. Jin, W. Yu, X. H. Wang, and L. T. Li, Ferroelectricity of multiferroic hexagonal $TmMnO_3$ ceramics synthesized under high pressure, *Appl. Phys. Lett.* 91(17), 172502 (2007)

II.129. J. H. Choi, J. S. Kim, and C. I. Cheon, Effect of process condition on the ferroelectric properties in $BiFeO_3$–$(Bi,K)TiO_3$ ceramics, *J. Korean Phys. Soc.* 65(3), 382 (2014)

II.130. W. Yansen, K. J. Parwanta, D. Hadiyawarman, D. Kim, Y. Gwan, J. Kim, C. Liu, C. U. Jung, and B. W. Lee, Effects of bismuth donor doping on the phase structure and the magnetic and ferroelectric properties of Fe-doped BaTiO3, *J. Korean Phys. Soc.* 63(3), 306 (2013)

II.131. P. Jarupoom and P. Jaita, Enhanced magnetic performance of lead-free $(Bi_{0.5}Na_{0.5})TiO_3$–$CoFe_2O_4$ magnetoelectric ceramics, *Electron. Mater. Lett.* 11(5), 788 (2015)

II.132. T. Amjad, I. Sadiq, A. B. Javaid, S. Riaz, S. Naseem, and M. Nadeem, Investigation of structural, electrical, electrical polarization and dielectric properties of CTAB assisted Ni^{2+} substituted R-type nano-hexaferrites, *J. Alloys Compd.* 770, 1112 (2019)

II.133. C. W. Baek, N. K. Oh, G. Han, W. H. Yoon, J. W. Kim, J. J. Choi, B. D. Han, D. S. Park, K. D. Sung, J. H. Jung, D. Y. Jeong, J. J. Kim, and J. Ryu, Effect of $Ba(Cu_{1/3}Nb_{2/3})O_3$ content on multiferroic properties in $BiFeO_3$ ceramics, *Mater. Sci. Eng.* 177(6), 451 (2012)

II.134. Z. M. Tian, Y. S. Zhang, S. L. Yuan, M. S. Wu, C. H. Wang, Z. Z. Ma, S. X. Huo, and H. N. Duan, Enhanced multiferroic properties and tunable magnetic behavior in multiferroic $BiFeO_3$–$Bi_{0.5}Na_{0.5}TiO_3$ solid solutions, *Mater. Sci. Eng.* 177(1), 74 (2012)

II.135. C. S. Devi, M. B. Suresh, G. S. Kumar, and G. Prasad, Microstructural and high temperature dielectric, ferroelectric and complex impedance spectroscopic properties of $BiFeO_3$ modified NBT-BT lead free ferroelectric ceramics, *Mater. Sci. Eng.* 228, 38 (2018)

II.136. J. Singh, A. Agarwal, S. Sanghi, T. Bhasin, M. Yadav, U. Bhakar, and O. Singh, Effect of Ba and Ho co-doping on crystal structure, phase transformation, magnetic properties and dielectric properties of $BiFeO_3$, *Curr. Appl. Phys.* 19(3), 321 (2019)

II.137. J. S. Hwang, Y. J. Yoo, Y. P. Lee, J. H. Kang, K. H. Lee, B. W. Lee, and S. Y. Park, Reinforced magnetic properties of Ni-doped $BiFeO_3$ ceramic, *J. Korean Phys. Soc.* 69(3), 282 (2016)

II.138. D. L. Golić, A. Radojković, J. Ćirković, A. Dapčević, D. Pajić, N. Tasić, S. M. Savić, M. Počuča-Nešić, S. Marković, G. Branković, Z. M. Stanojević, and Z. Branković, Structural, ferroelectric and magnetic properties of $BiFeO_3$ synthesized by sonochemically assisted hydrothermal and hydro-evaporation chemical methods, *J. Eur. Ceram. Soc.* 36(7), 1623 (2016)

II.139. H. Paik, H.-C. Kim, K. No, Y.-I. Kim, D. P. Cann, and J. Hong, Structural and physical properties of room temperature stable multiferroic properties of single-phase $(Bi_{0.9}La_{0.1})FeO_3$–$Pb(Fe_{0.5}Nb_{0.5})O_3$ solid solution systems, *J. Appl. Phys.* 105, 07D919 (2009)

II.140. A. Kumar, P. Sharma, and D. Varshney, Structural and ferroic properties of La, Nd, and Dy doped $BiFeO_3$ ceramics, *J. Ceram.* 2015, 869071 (2015)

II.141. A. Kumar, P. Sharma, W. Yang, J. Shen, D. Varshney, and Q. Li, Effect of La and Ni substitution on structure, dielectric and ferroelectric properties of $BiFeO_3$ ceramics, *Ceram. Int.* 42(13), 14805 (2016)

II.142. R. D. Liu, L. H. He, L. Q. Yan, Z. C. Wang, Y. Sun, Y. T. Liu, D. F. Chen, S. Zhang, Y. G. Zhao, and F. W. Wang, Al-doping-induced magnetocapacitance in the multiferroic $AgCrS_2$, *Chin. Phys. B* 24(12), 127507 (2015)

II.143. A. Gautam and V. S. Rangra, Effect of Ba ions substitution on multiferroic properties of $BiFeO_3$ perovskite, *Cryst. Res. Technol.* 45(9), 953 (2010)

II.144. A. Beniwal, J. S. Bangruwa, B. Vasisth, S. P. Gairola, and V. Verma, Modification in structural, electrical and magnetic properties of Pr doped bismuth ferrites, *Inter. J. Engn. Res. Technol.* 5(03), 56 (2016)

II.145. Y. Ma and X. M. Chen, Enhanced multiferroic characteristics in $NaNbO_3$-modified $BiFeO_3$ ceramics, *J. Appl. Phys.* 105(5), 054107 (2009)

II.146. Z. Z. Ma, Z. M. Tian, J. Q. Li, C. H. Wang, S. X. Huo, H. N. Duan, and S. L. Yuan, Enhanced polarization and magnetization in multiferroic $(1–x)BiFeO_{3-x}SrTiO_3$ solid solution, *Solid State Sci.* 13(12), 2196 (2011)

II.147. A. K. Pradhan, K. Zhang, D. Hunter, J. B. Dadson, G. B. Loiutts, P. Bhattacharya, R. Katiyar, J. Zhang, D. J. Sellmyer, U. N. Roy, Y. Cui, and A. Burger, Magnetic and electrical properties of single-phase multiferroic $BiFeO_3$, *J. Appl. Phys.* 97(9), 093903 (2005)

II.148. J. Wu, S. Mao, Z. G. Ye, Z. Xie, and L. Zheng, Room-temperature ferromagnetic/ferroelectric $BiFeO_3$ synthesized by a self-catalyzed fast reaction process, *J. Mater. Chem.* 20(31), 6512 (2010)

II.149. M. M. Kumar, V. R. Palkar, K. Srinivas, and S. V. Suryanarayana, Ferroelectricity in a pure $BiFeO_3$ ceramic, *Appl. Phys. Lett.* 76(19), 2764 (2000)

II.150. Y. P. Wang, L. Zhou, M. F. Zhang, X. Y. Chen, J. M. Liu, and Z. G. Liu, Room-temperature saturated ferroelectric polarization in $BiFeO_3$ ceramics synthesized by rapid liquid phas, sintering, *Appl. Phys. Lett.* 84(10), 1731 (2004)

II.151. P. N. Francis, S. Dhanuskodi, M. S. Jayalakshmy, M. Muneeswaran, J. Philip, and N. V. Giridharan, Optical limiting and magnetoelectric coupling in multiferroic $BiFeO_3$ nanoparticles, *Mater. Chem. Phys.* 216, 93 (2018)

II.152. J. Xu, D. Xie, C. Yin, T. Feng, X. Zhang, G. Li, H. Zhao, Y. Zhao, S. Ma, T. L. Ren, Y. Guan, X. Gao, and Y. Zhao, Enhanced dielectric and multiferroic properties of single-phase Y and Zr co-doped $BiFeO_3$ ceramics, *J. Appl. Phys.* 114(15), 154103 (2013)

II.153. S. Zhang, W. Luo, L. Wang, D. Wang, and Y. Ma, Simultaneously improved magnetization and polarization in $BiFeO_3$ based multiferroic composites, *J. Appl. Phys.* 107(5), 054110 (2010)

II.154. S. Chandel, P. Thakur, S. S. Thakur, A. Sharma, J. H. Hsu, M. Tomar, V. Gupta, and A. Thakur, Investigation of excess and deficiency of iron in $BiFeO_3$, *Mater. Chem. Phys.* 204, 207 (2018)

II.155. Y. Li, J. Yu, J. Li, C. Zheng, Y. Wu, Y. Zhao, M. Wang, and Y. Wang, Influence of Dy-doping on ferroelectric and dielectric properties in $Bi_{1.05-x}Dy_xFeO_3$ ceramics, *J. Mater. Sci. Mater. Electron.* 22(4), 323 (2011)

II.156. J. Xu, G. Ye, M. Zeng, Y. Deng, X. Chang, J. Sun, and Q. Wang, Enhanced multiferroic properties of Nd and Co co-doped $BiFeO_3$ ceramics, *J. Mater. Sci. Mater. Electron.* 26(9), 6907 (2015)

II.157. Q. Yao, X. Xu, S. Peng, Y. Zhu, Z. Wang, Y. Ma, X. Wang, W. Mao, and X. Li, Structural, optical and multiferroic properties of Eu, Ba co-doped $BiFeO_3$, *J. Mater. Sci. Mater. Electron.* 28(1), 463 (2017)

II.158. A. S. Prima, I. B. Shameem Banu, and Z. Mohammed, Effect of novel (Gd, Cu) substitution on the electrical properties and magnetoelectric coupling of bismuth ferrite ceramics, *J. Mater. Sci. Mater. Electron.* 28(12), 8467 (2017)

II.159. M. Kumar, S. Shankar, O. P. Thakur, and A. K. Ghosh, Studies on magnetoelectric coupling and magnetic properties of $(1–x)BiFeO_{3-x}BaTiO_3$ solid solutions, *J. Mater. Sci. Mater. Electron.* 26(3), 1427 (2015)

II.160. M. Banerjee, A. Mukherjee, A. Banerjee, D. Das, and S. Basu, Enhancement of multiferroic properties and unusual magnetic phase transition in Eu doped bismuth ferrite nanoparticles, *New J. Chem.* 41(19), 10985 (2017)

II.161. S. K. Satpathy, S. Sen, and B. Behera, Dielectric, electrical and magnetic properties of La doped $BiFeO_3$–$PbZrO_3$ composites, *J. Mater. Sci. Mater. Electron.* 28(12), 9102 (2017)

II.162. R. R. Raut, P. H. Salame, J. T. Kolte, C. S. Ulhe, and P. Goplan, Giant dielectric response and magnetoelectric behavior of $95BiFeO_3$–$5BaTiO_3$ (95BFO–5BT) ceramics, *J. Mater. Sci. Mater. Electron.* 27(1), 730 (2016)

II.163. K. Sen, K. Singh, A. Gautam, and M. Singh, Dispersion studies of La substitution on dielectric and ferroelectric properties of multiferroic $BiFeO_3$ ceramic, *Ceram. Int.* 38(1), 243 (2012)

II.164. D. S. García-Zaleta, A. M. Torres-Huerta, M. A. Domínguez-Crespo, J. A. Matutes-Aquino, A. M. González, and M. E. Villafuerte-Castrejón, Solid solutions of La-doped $BiFeO_3$ obtained by the Pechini method with improvement in their properties, *Ceram. Int.* 40(7), 9225 (2014)

II.165. H. Y. Dai, J. Chen, T. Li, D. W. Liu, R. Z. Xue, H. W. Xiang, and Z. P. Chen, Effect of $BaTiO_3$ doping on the structural, electrical and magnetic properties of $BiFeO_3$ ceramics, *J. Mater. Sci. Mater. Electron.* 26(6), 3717 (2015)

II.166. I. B. Shameem Banu and S. D. Lakshmi, Simultaneous enhancement of room temperature multiferroic properties of $BiFeO_3$ by Nd doping at Bi site and Co doping at Fe site, *J. Mater. Sci. Mater. Electron.* 28(21), 16044 (2017)

II.167. W. Zheng, L. Zhang, Y. Lin, Z. Shi, F. Cao, G. Yuan, and J. Yu, Ferroic phase transitions and switching properties of modified $BiFeO_3$–$SrTiO_3$ multiferroic perovskites, *J. Mater. Sci. Mater. Electron.* 27(11), 12067 (2016)

II.168. T. Murtaza, J. Ali, M. S. Khan, and K. Asokan, Structural, electrical and magnetic properties of multiferroic $BiFeO_3$–$SrTiO_3$ composites, *J. Mater. Sci. Mater. Electron.* 29(3), 2110 (2018)

II.169. M. Sahni, N. Kumar, M. Kumar, and S. Singh, Effect of Sr substitution on structural, dielectric, magnetic and magnetoelectric properties of rapid liquid sintered $BiFe_{0.8}Ti_{0.2}O_3$ ceramics, *J. Mater. Sci. Mater. Electron.* 25(11), 4743 (2014)

II.170. R. Gupta, S. Verma, V. Singh, and K. K. Bamzai, Preparation, structural, electrical, and ferroelectric properties of lead niobate–lead zirconate–lead titanate ternary system, *J. Ceram.* 2015, 835150 (2015)

II.171. H. Y. Dai, L. T. Gu, X. Y. Xie, T. Li, Z. P. Chen, and Z. J. Li, The structure, defects, electrical and magnetic properties of $BiFe_{1-x}Zr_xO_3$ multiferroic ceramics, *J. Mater. Sci. Mater. Electron.* 29(3), 2275 (2018)

II.172. B. Dhanalakshmi, K. Pratap, B. P. Rao, and P. S. V. Subba Rao, Effects of Mn doping on structural, dielectric and multiferroic properties of $BiFeO_3$ nanoceramics, *J. Alloys Compd.* 676, 193 (2016)

II.173. R. Mazumder and A. Sen, Effect of Pb-doping on dielectric properties of $BiFeO_3$ ceramics, *J. Alloys Compd.* 475(1–2), 577 (2009)

II.174. G. L. Song, Y. C. Song, J. Su, X. H. Song, N. Zhang, T. X. Wang, and F. G. Chang, Crystal structure refinement, ferroelectric and ferromagnetic properties of Ho3+ modified $BiFeO_3$ multiferroic material, *J. Alloys Compd.* 696, 503 (2017)

II.175. P. Saxena, A. Kumar, P. Sharma, and D. Varshney, Improved dielectric and ferroelectric properties of dual-site substituted rhombohedral structured $BiFeO_3$ multiferroics, *J. Alloys Compd.* 682, 418 (2016)

II.176. H. Deng, M. Zhang, Z. Hu, Q. Xie, Q. Zhong, J. Wei, and H. Yan, Enhanced dielectric and ferroelectric properties of Ba and Ti co-doped $BiFeO_3$ multiferroic ceramics, *J. Alloys Compd.* 582, 273 (2014)

II.177. K. S. Kumar, P. Aswini, and C. Venkateswaran, Effect of Tb–Mn substitution on the magnetic and electrical properties of $BiFeO_3$ ceramics, *J. Magn. Magn. Mater.* 364, 60 (2014)

II.178. P. Sharma and V. Verma, Structural, magnetic and electrical properties of La and Mn co-substituted BFO samples prepared by the sol–gel technique, *J. Magn. Magn. Mater.* 374, 18 (2015)

II.179. W. S. Kim, Y. K. Jun, K. H. Kim, and S. H. Hong, Enhanced magnetization in Co and Ta-substituted $BiFeO_3$ ceramics, *J. Magn. Magn. Mater.* 321(19), 3262 (2009)

II.180. A. Anju, A. Agarwal, P. Aghamkar, and B. Lal, Structural and multiferroic properties of barium substituted bismuth ferrite nanocrystallites prepared by sol–gel method, *J. Magn. Magn. Mater.* 426, 800 (2017)

II.181. Y. A. Chaudhari, A. Singh, C. M. Mahajan, P. P. Jagtap, E. M. Abuassaj, R. Chatterjee, and S. T. Bendre, Multiferroic properties in Zn and Ni co-doped $BiFeO_3$ ceramics by solution combustion method (SCM), *J. Magn. Magn. Mater.* 347, 153 (2013)

II.182. M. Manikandan, K. S. Kumar, N. Aparnadevi, N. P. Shanker, and C. Venkateswaran, Multiferroicity in polar phase $LiNbO_3$ at room temperature, *J. Magn. Magn. Mater.* 391, 156 (2015)

II.183. Y. Chaudhari, C. M. Mahajan, A. Singh, P. Jagtap, R. Chatterjee, and S. Bendre, Multiferroic properties of nanocrystalline $BiFe_{1-x}Ni_xO_3$ ($x = 0.0$–0.15) perovskite ceramics, *J. Magn. Magn. Mater.* 395, 329 (2015)

II.184. M. M. El-Desoky, M. S. Ayoua, M. M. Mostafa, and M. A. Ahmed, Multiferroic properties of nanostructured barium doped bismuth ferrite, *J. Magn. Magn. Mater.* 404, 68 (2016)

II.185. A. S. Priya, I. B. S. Banu, and S. Anwar, Influence of Dy and Cu doping on the room temperature multiferroic properties of $BiFeO_3$, *J. Magn. Magn. Mater.* 401, 333 (2016)

II.186. S. T. Dadami, S. Matteppanavar, I. Shivaraja, S. Rayaprol, B. Angadi, and B. Sahoo, Investigation on structural, Mössbauer and ferroelectric properties of $(1-x)PbFe_{0.5}Nb_{0.5}O_3$–$(x)BiFeO_3$ solid solution, *J. Magn. Magn. Mater.* 418, 122 (2016)

II.187. A. G. Lone and R. N. Bhowmik, Study of room temperature ferromagnetic and ferroelectric properties in α-$Fe_{1.6}Ga_{0.4}O_3$ alloy, *J. Magn. Magn. Mater.* 379, 244 (2015)

II.188. V. Verma, A. Beniwal, A. Ohlan, and R. Tripathi, Structural, magnetic and ferroelectric properties of Pr doped multi-ferroics bismuth ferrites, *J. Magn. Magn. Mater.* 394, 385 (2015)

II.189. J. Pal, S. Kumar, L. Singh, M. Singh, and A. Singh, Detailed investigation on structural, dielectric, magnetic and magnetodielectric properties of $BiFeO_3$–$BaSrTiO_3$ solid solutions, *J. Magn. Magn. Mater.* 441, 339 (2017)

II.190. M. Banerjee, A. Mukherjee, A. Banerjee, D. Das, and S. Basu, Enhancement of multiferroic properties and unusual magnetic phase transition in Eu doped bismuth ferrite nanoparticles, *New J. Chem.* 41(19), 10985 (2017)

II.191. S. S. Yadava, A. Khare, P. Gautam, A. Kumar, and K. D. Mandal, Dielectric, ferroelectric and magnetic study of iron doped hexagonal $Ba_4YMn_3O_{11.5-\delta}$(BYMO) and its dependence on temperature as well as frequency, *New J. Chem.* 41(11), 4611 (2017)

II.192. H. Dai, F. Ye, Z. Chen, T. Li, and D. Liu, The effect of ion doping at different sites on the structure, defects and multiferroic properties of $BiFeO_3$ ceramics, *J. Alloys Compd.* 734, 60 (2018)

II.193. A. Anwar, M. A. Basith, and S. Choudhury, From bulk to nano: A comparative investigation of structural, ferroelectric and magnetic properties of Sm and Ti co-doped $BiFeO_3$ multiferroics, *Mater. Res. Bull.* 111, 93 (2019)

II.194. S. R. Wadgane, S. T. Alone, A. Karim, G. Vats, S. E. Shirsath, and R. H. Kadam, Magnetic field induced polarization and magnetoelectric effect in $Na_{0.5}Bi_{0.5}TiO_3$–$Co_{0.75}Zn_{0.25}Cr_{0.2}Fe_{1.8}O_4$ multiferroic composite, *J. Magn. Magn. Mater.* 471, 388 (2019)

II.195. X. Peng, Y. Pu, Y. Guo, Z. J. Dong, Y. Shi, and L. Zhang, Effect of Y_2O_3 dopant on dielectric, magnetic, magnetodielectric properties of $Bi_{0.95}La_{0.05}Fe_{0.95}Ti_{0.05}O_3$ ceramics, *J. Alloys Compd.* 773, 970 (2019)

II.196. M. Nadeem, W. Khan, S. Khan, S. Husain, and A. Ansari, Tailoring dielectric properties and multiferroic behavior of nanocrystalline $BiFeO_3$ via Ni doping, *J. Appl. Phys.* 124(16), 164105 (2018)

II.197. H. Zhao, H. Wang, Z. Cheng, Q. Fu, H. Tao, Z. Ma, T. Jia, H. Kimura, and H. Li, Electric and magnetic properties of Aurivillius-phase compounds: $Bi_5Ti_3XO_{15}$ (X = Cu, Mn, Ni, V), *Ceram. Int.* 44(11), 13226 (2018)

II.198. A. Amouri, N. Abdelmoula, and H. Khemakhem, Improved multiferroic properties in $(1-x)BiFeO_3$–$(x)BaTi_{0.95}(Yb_{0.5}Nb_{0.5})_{0.05}O_3$ system ($0 \leq x \leq 0.3$), *J. Magn. Magn. Mater.* 417, 302 (2016)

II.199. A. K. Yadav, P. Rajput, O. Alshammari, M. Khan, Anita, G. Kumar, S. Kumar, P. M. Shirage, S. Biring, and S. Sen, Structural distortion, ferroelectricity and ferromagnetism in $Pb(Ti_{1-x}Fe_x)O_3$, *J. Alloys Compd.* 701, 619 (2017)

II.200. S. Sahoo, P. K. Mahapatra, R. N. P. Choudhary, and P. Alagarsamy, Influence of compositional variation on structural, electrical and magnetic characteristics of $(Ba_{1-x}Gd)(Ti_{1-x}Fe_x)O_3$ $(0.2 \leq x \leq 0.5)$, *Mater. Res. Express* 5(1), 016101 (2018)

II.201. G. H. Jaffari, M. Aftab, A. Samad, F. Mumtaz, M. S. Awan, and S. I. Shah, Effects of dopant induced defects on structural, multiferroic and optical properties of $Bi_{1-x}Pb_xFeO_3$ $(0 \leq x \leq 0.3)$ ceramics, *Mater. Res. Express* 5(1), 016103 (2018)

II.202. A. Anwar, M. A. Basith, and S. Choudhury, From bulk to nano: A comparative investigation of structural, ferroelectric and magnetic properties of Sm and Ti co-doped $BiFeO_3$ multiferroics, *Mater. Res. Bull.* 111, 93 (2019)

II.203. P. Uniyal and K. L. Yadav, Study of dielectric, magnetic and ferroelectric properties in $Bi_{1-x}Gd_xFeO_3$, *Mater. Lett.* 62(17–18), 2858 (2008)

II.204. S. Sharma, A. Mishra, P. Saravanan, O. P. Pandey, and P. Sharma, Effect of Gd-substitution on the ferroelectric and magnetic properties of $BiFeO_3$ processed by high-energy ball milling, *J. Magn. Magn. Mater.* 418, 188 (2016)

II.205. C. Zhang, M. Shang, M. Liu, L. Ge, H. Yuan, and S. Feng, Multiferroicity in $SmFeO_3$ synthesized by hydrothermal method, *J. Alloys Compd.* 665, 152 (2016)

II.206. R. Muduli, R. Pattanayak, S. Raut, P. Sahu, V. Senthil, S. Rath, P. Kumar, S. Panigrahi, and R. K. Panda, Dielectric, ferroelectric and impedance spectroscopic studies in TiO_2-doped $AgNbO_3$ ceramic, *J. Alloys Compd.* 664, 715 (2016)

II.207. M. Manikandan, A. Muthukumaran, and C. Venkateswaran, Intrinsic magneto-dielectric effect in the diluted magnetic ferroelectric fluoride $BaMg_{1-x}Mn_xF_4$ $(0 \leq x \leq 0.07)$, *J. Magn. Magn. Mater.* 393, 40 (2015)

II.208. C. X. Chen, Y. K. Liu, and R. K. Zheng, Magnetic and ferroelectric properties of $SmBi_4Fe_{0.5}Co_{0.5}Ti_3O_{15}$ compounds prepared with different synthesis methods, *J. Mater. Sci. Mater. Electron.* 28(11), 7562 (2017)

II.209. J. D. Bobić, R. M. Katiliute, M. Ivanom, M. M. V. Petrović, N. I. Ilić, A. S. Džunuzović, J. Banys, and B. D. Stojanović, Dielectric, ferroelectric and magnetic properties of La doped $Bi_5Ti_3FeO_{15}$ ceramics, *J. Mater. Sci. Mater. Electron.* 27(3), 2448 (2016)

II.210. S. Liu, S. Yan, H. Luo, L. Yao, Z. Hu, S. Huang, and L. Deng, Enhanced magnetoelectric coupling in La-modified $Bi_5Co_{0.5}Fe_{0.5}Ti_3O_{15}$ multiferroic ceramics, *J. Mater. Sci.* 53(2), 1014 (2018)

II.211. S. Das, R. C. Sahoo, K. P. Bera, and T. K. Nath, Doping effect on ferromagnetism, ferroelectricity and dielectric constant in sol-gel derived $Bi_{1-x}Nd_xFe_{1-y}Co_yO_3$ nanoceramics, *J. Magn. Magn. Mater.* 451, 226 (2018)

II.212. H. Paik, H. Hwang, K. No, S. Kwon, and D. P. Cann, Room temperature multiferroic properties of single-phase $(Bi_{0.9}La_{0.1})FeO_3$-$Ba(Fe_{0.5}Nb_{0.5})O_3$ solid solution ceramics, *Appl. Phys. Lett.* 90(4), 042908 (2007)

II.213. X. Jia, J. Zhang, and J. Wang, Dielectric, ferroelectric and ferromagnetic properties of multiferroic $(1–x)Ba_{0.99}Ca_{0.01}Zr_{0.02}Ti_{0.98}O_{3-x}BiFeO_3$ ceramics, *Ferroelctrics Lett.* 44(4–6), 113 (2017)

II.214. M. A. Jalaja and S. Dutta, Switchable photovoltaic properties of multiferroic $KBiFe_2O_5$, *Mater. Res. Bull.* 88, 9 (2017)

II.215. S. Mohanty, A. Kumar, and R. N. P. Choudhary, Studies of structural, dielectric, electrical and ferroelectric characteristics of $BiFeO_3$ and $(Bi_{0.5}K_{0.5})(Fe_{0.5}Ta_{0.5})O_3$, *J. Mater. Sci. Mater. Electron.* 26(12), 9640 (2015)

II.216. M. M. Sutar, S. R. Jigajeni, A. N. Tarale, S. B. Kulkarni, and P. B. Joshi, Magnetoelectric and magnetodielectric effect in BST–LSMO ferromagnetic/ferroelectric composites, *J. Mater. Sci. Mater. Electron.* 25(9), 3771 (2014)

II.217. W. Cai, C. Fu, G. Chen, R. Gao, and X. Deng, Dielectric and ferroelectric properties of $xBaZr_{0.52}Ti_{0.48}O_3$–$(1–x)BiFeO_3$ solid solution ceramics, *J. Mater. Sci. Mater. Electron.* 26(1), 322 (2015)

II.218. K. Praveena and K. B. R. Varma, Ferroelectric and optical properties of $Ba_5Li_2Ti_2Nb_8O_{30}$ ceramics potential for memory applications, *J. Mater. Sci. Mater. Electron.* 25(7), 3103 (2014)

II.219. R. Castañeda, G. Rojas-George, J. Silva, M. E. Fuentes-Montero, J. A. Matutes-Aquino, A. Reyes-Rojas, and L. Fuentes, Effects of Ni doping on ferroelectric and ferromagnetic properties of $Bi_{0.75}Ba_{0.25}FeO_3$, *Ceram. Int.* 39(7), 8527 (2013)

II.220. K. L. Manjusha and K. L. Yadav, Enhanced dielectric, ferroelectric and magnetodielectric properties in three phase $0.45Bi_{0.9}La_{0.1}FeO_3$–$0.55Co_{0.5}Ni_{0.5}Fe_2O_4$–$BaTiO_3$ composite, *J. Mater. Sci. Mater. Electron.* 27(6), 6347 (2016)

II.221. Y. Guo, P. Xiao, L. Luo, N. Jiang, F. Lei, Q. Zheng, and D. Lin, Structure, ferroelectric and piezoelectric properties of $Bi_{0.5}(Na_{0.8}K_{0.2})_{0.5}TiO_3$ modified $BiFeO_3$–$BaTiO_3$ lead-free piezoelectric ceramics, *J. Mater. Sci. Mater. Electron.* 25(9), 3753 (2014)

II.222. S. Dash, R. Padhee, P. R. Das, and R. N. P. Choudhary, Enhancement of dielectric and electrical properties of $NaNbO_3$-modified $BiFeO_3$, *J. Mater. Sci. Mater. Electron.* 24(9), 3315 (2013)

II.223. S. Godara and B. Kumar, Effect of Ba–Nb co-doping on the structural, dielectric, magnetic and ferroelectric properties of $BiFeO_3$ Nanoparticles, *Ceram. Int.* 41(5), 6912 (2015)

II.224. T. Ramesh, V. Rajendar, and S. R. Murthy, $CoFe_2O_4$–$BaTiO_3$ multiferroic composites: Role of ferrite and ferroelectric phases on the structural, magneto dielectric properties, *J. Mater. Sci. Mater. Electron.* 28(16), 11779 (2017)

II.225. S. Ahmed and S. K. Barik, Preparation of novel $(Sb_{1/2}Na_{1/2})(Fe_{2/3}W_{1/3})O_3$ compound by solid state reaction technique and their multiferroic property, *J. Mater. Sci. Mater. Electron.* 27(10), 10294 (2016)

II.226. V. Anbarasu, M. Dhilip, K. Saravana Kumar, and K. Sivakumar, Effect of trivalent transition metal ion substitution in multifunctional properties of Dy_2O_3 system, *J. Mater. Sci. Mater. Electron.* 28(12), 8976 (2017)

II.227. S. Nath, S. K. Barik, and R. N. P. Choudhary, Dielectric relaxation and magnetic characteristics of $(La_{1/2}Li_{1/2})(Fe_{1/2}V_{1/2})O_3$ multiferroics, *J. Mater. Sci. Mater. Electron.* 26(10), 8199 (2015)

II.228. S. Nath, S. K. Barik, and R. N. P. Choudhary, Electrical and ferroelectric characteristics of $(LaLi)_{1/2}(Fe_{2/3}Mo_{1/3})O_3$, *J. Mater. Sci. Mater. Electron.* 27(8), 8717 (2016)

II.229. B. Want, M. D. Rather, and R. Samad, Dielectric, ferroelectric and magnetic behavior of $BaTiO_3$–$BaFe_{12}O_{19}$ composite, *J. Mater. Sci. Mater. Electron.* 27(6), 5860 (2016)

II.230. M. Wang, and G. Tan, Multiferroic properties of $Pb_2Fe_2O_5$ ceramics, *Mater. Res. Bull.* 46(3), 438 (2011)

II.231. V. G. Kostishyn, L. V. Panina, L. V. Kozitov, A. V. Timofeev, A. K. Zyuzin, and A. N. Kovalev, Synthesis of Hexagonal $BaFe_{12}O_{19}$ and $SrFe_{12}O_{19}$ Ferrite Ceramics with Multiferroic Properties, *Inorg. Mater.: Appl. Res.* 6(5), 461 (2015)

II.232. V. G. Kostishyn, L. V. Panina, A. V. Timofeev, L. V. Kozhitov, A. N. Kovalev, and A. K. Zyuzin, Dual ferroic properties of hexagonal ferrite ceramics $BaFe_{12}O_{19}$ and $SrFe_{12}O_{19}$, *J. Magn. Magn. Mater.* 400, 327 (2016)

II.233. Z. Guo, L. Pan, C. Bi, H. Qiu, X. Zhao, L. Yang, and M. Y. Rafique, Structural and multiferroic properties of Fe-doped $Ba_{0.5}Sr_{0.5}TiO_3$ solids, *J. Magn. Magn. Mater.* 325, 24 (2013)

II.234. O. Subohi, C. R. Bowen, M. M. Malik, and R. Kurchania, Dielectric spectroscopy and ferroelectric properties of magnesium modified bismuth titanate ceramics, *J. Alloys Compd.* 688, 27 (2016)

II.235. P. Gupta, R. Padhee, P. K. Mahapatra, R. N. P. Choudhary, and S. Das, Structural and electrical properties of Bi_3TiVO_9 ferroelectric ceramics, *J. Alloys Compd.* 731, 1171 (2018)

II.236. A. Lavado and M. G. Stachiotti, Fe^{3+}/Nb^{5+} co-doping effects on the properties of Aurivillius $Bi_4Ti_3O_{12}$ ceramics, *J. Alloys Compd.* 731, 914 (2018)

II.237. W. Cai, C. Fu, W. Hu, G. Chen, and X. Deng, Effects of microwave sintering power on microstructure, dielectric, ferroelectric and magnetic properties of bismuth ferrite ceramics, *J. Alloys Compd.* 554, 64 (2013)

II.238. T. Ahmad and I. H. Lone, Citrate precursor synthesis and multifunctional properties of $YCrO_3$ nanoparticles, *New J. Chem.* 40(4), 3216 (2016)

II.239. K. Praveena and K. B. R. Varma, Enhanced electric field tunable magnetic properties of lead-free $Na_{0.5}Bi_{0.5}TiO_3$–$MnFe_2O_4$ multiferroic composites, *J. Mater. Sci. Mater. Electron.* 25(12), 5403 (2014)

II.240. V. Anbarasu, A. Manigandan, T. Karthik, and K. Sivakumar, Inducing multiferroic behaviour in the diamagnetic Y2O3 system, *J. Mater. Sci. Mater. Electron.* 23(6), 1201 (2012)

II.241. S. K. Pradhan, S. N. Das, S. Bhuyan, C. Behera, and R. N. P. Choudhary, Structural and electrical properties of lead reduced lanthanum modified $BiFeO_3$–$PbTiO_3$ solid solution, *J. Mater. Sci. Mater. Electron.* 28(2), 1186 (2017)

II.242. K. Mukhopadhyay, A. S. Mahapatra, and P. K. Chakrabarti, Multiferroic behavior, enhanced magnetization and exchange bias effect of Zn substituted nanocrystalline $LaFeO_3$ ($La_{1-x}Zn_xFeO_3$, $x = 0.10$ and 0.30), *J. Magn. Magn. Mater.* 329, 133 (2013)

II.243. R. Das and K. Mandal, Magnetic, ferroelectric and magnetoelectric properties of Ba-doped $BiFeO_3$, *J. Magn. Magn. Mater.* 324(11), 1913 (2012)

II.244. A. Jain, A. K. Panwar, and A. K. Jha, Significant enhancement in structural, dielectric, piezoelectric and ferromagnetic properties of $Ba_{0.9}Sr_{0.1}Zr_{0.1}Ti_{0.9}O_3$–$CoFe_2O_4$ multiferroic composites, *Mater. Res. Bull.* 100, 367 (2018)

II.245. S. Jindal, S. Devi, K. M. Batoo, G. Kumar, and A. Vasishth, Impact of copper substitution on the structural, ferroelectric and magnetic properties of tungsten bronze ceramics, *Physica B* 537, 87 (2018)

II.246. P. Tirupathi and A. Chandra, Observation of bi-relaxor characteristic in multiferroic $0.70Bi_{0.90}Ca_{0.10}FeO_3$–$0.30PbTiO_3$ ceramics, *J. Phys. D Appl. Phys.* 46(37), 375304 (2013)

II.247. L. H. Yin, W. H. Song, X. L. Jiao, W. B. Wu, X. B. Zhu, Z. R. Yang, J. M. Dai, R. L. Zhang, and Y. P. Sun, Multiferroic and magnetoelectric properties of $Bi_{1-x}Ba_xFe_{1-x}Mn_xO_3$ system, *J. Phys. D Appl. Phys.* 42(20), 205402 (2009)

II.248. G. H. Jaffari, M. Aftab, A. Samad, F. Mumtaz, M. S. Awan, and S. I. Shah, Effects of dopant induced defects on structural, multiferroic and optical properties of $Bi_{1-x}Pb_xFeO_3$ ($0 \leq x \leq 0.3$) ceramics, *Matter. Res. Expr.* 5(1), 016103 (2018)

II.249. X. Q. Chen, F. J. Yang, W. Q. Cao, D. Y. Wang, and K. Chen, Room-temperature magnetoelectric coupling in $Bi_4(Ti_1Fe_2)O_{12-\delta}$ system, *J. Phys. D Appl. Phys.* 43(6), 065001 (2010)

II.250. X. Chen, C. Wei, J. Xiao, Y. Xue, X. Zeng, F. Yang, P. Li, and Y. He, Room temperature multiferroic properties and magnetocapacitance effect of modified ferroelectric $Bi_4Ti_3O_{12}$ ceramic, *J. Phys. D Appl. Phys.* 46(42), 425001 (2013)

II.251. S. K. Patri and R. N. P. Choudhary, Phase transition in $Bi_8Fe_6Ti_3O_{27}$ multiferroic ceramics, *Cent. Eur. J. Phys.* 6, 450 (2008)

II.252. S. Sahoo, P. K. Mahapatra, R. N. P. Choudhary, and P. Alagarsamy, Influence of compositional variation on structural, electrical and magnetic characteristics of $(Ba_{1-x}Gd)(Ti_{1-x}Fe_x)O_3$ ($0.2 \leq x \leq 0.5$), *Matter. Res. Expr.* 5(1), 016101 (2018)

II.253. N. Kumar, A. Shukla, and R. N. P. Choudhary, Structural, dielectric, electrical and magnetic characteristics of lead-free multiferroic: $Bi(Cd_{0.5}Ti_{0.5})O_3$–$BiFeO_3$ solid solution, *J. Alloys Compd.* 747, 895 (2018)

II.254. R. Samantaray, R. J. Clark, E. S. Choi, H. Zhou, and N. S. Dalal, $M_{3-x}(NH_4)_xCrO_8$ (M = Na, K, Rb, Cs): A new family of Cr^{5+} based magnetic ferroelectrics, *J. Am. Chem. Soc.* 133(11), 3792 (2011)

II.255. R. Samantaray, R. J. Clark, E. S. Choi, and N. S. Dalal, Elucidating the mechanism of multiferroicity in $(NH_4)_3Cr(O_2)_4$ and its tailoring by alkali metal substitution, *J. Am. Chem. Soc.* 134(38), 15953 (2012)

II.256. S. J. Kim, S. H. Han, H. G. Kim, A. Y. Kim, J. J. Kim, and C. J. Cohen, Multiferroic properties of Ti-doped $BiFeO_3$ ceramics, *J. Korean Phys. Soc.* 56(1(2)), 439 (2010)

II.257. N. H. Kim, E. J. Yoon, C. I. Cheon, and J. S. Kim, Multiferroic properties of a bismuth layer structured $Bi_{3.25}La_{0.75}Ti_3O_{12}$–$(La_{0.7}Sr_{0.3})MnO_3$ solid solution at low temperatures, *J. Korean Phys. Soc.* 56(1(2)), 393 (2010)

II.258. S. Liu, S. Yan, H. Luo, L. Yao, Z. Hu, S. Huang, and L. Deng, Enhanced magnetoelectric coupling in La-modified $Bi_5Co_{0.5}Fe_{0.5}Ti_3O_{15}$ multiferroic ceramics, *J. Mater. Sci.* 53(2), 1014 (2018)

II.259. Y. J. Wu, S. P. Gu, Y. Q. Lin, Z. J. Hong, X. Q. Liu, and X. M. Chen, Multiferroic ceramics in BaO–Y_2O_3–Fe_2O_3–Nb_2O_5 system, *Ceram. Int.* 36(8), 2415 (2010)

II.260. Y. Ma, X. M. Chen, Y. J. Wu, and Y. Q. Lin, Dielectric relaxation and enhanced multiferroic properties in $YMn_{0.8}Fe_{0.2}O_3$ ceramics prepared by in situ spark plasma sintering, *Ceram. Int.* 36(2), 727 (2010)

II.261. T. Karthik, A. Srinivas, V. Kamaraj, and V. Chandrasekeran, Influence of in-situ magnetic field pressing on the structural and multiferroic behaviour of $BiFeO_3$ ceramics, *Ceram. Int.* 38(2), 1093 (2012)

II.262. K. Sen, K. Singh, A. Gautam, and M. Singh, Dispersion studies of La substitution on dielectric and ferroelectric properties of multiferroic $BiFeO_3$ ceramic, *Ceram. Int.* 38(1), 243 (2012)

II.263. A. Prasatkhetragarn, P. Muangkonkad, P. Aommongkol, P. Jantaratana, N. Vittayakorn, and R. Yimnirun, Investigation on ferromagnetic and ferroelectric properties of (La, K)-doped $BiFeO_3$–$BaTiO_3$ solid solution, *Ceram. Int.* 39, S249 (2013)

II.264. H. Dai, Z. Chen, R. Xue, T. Li, J. Chen, and H. Xiang, Structural and electric properties of polycrystalline $Bi_{1-x}ErxFeO_3$ ceramics, *Ceram. Int.* 39(5), 5373 (2013)

II.265. V. Kumar, A. Gaur, N. Sharma, J. Shah, and R. K. Kotnala, High temperature dielectric and magnetic response of Ti and Pr doped $BiFeO_3$ ceramics, *Ceram. Int.* 39(7), 8113 (2013)

II.266. H. Dai, R. Xue, Z. Chen, T. Li, J. Chen, and H. Xiang, Effect of Eu, Ti co-doping on the structural and multiferroic properties of $BiFeO_3$ ceramics, *Ceram. Int.* 40(10), 15617 (2014)

II.267. H. Bouzidi, H. Chaker, M. Es-souni, C. Chaker, and H. Khemakhem, Structural, Raman, ferroelectric and magnetic studies of the $(1-x)$BF–xBCT multiferroic system, *J. Alloys Compd.* 772, 877 (2019)

II.268. X. Chen, J. Xiao, J. Yao, Z. Kang, F. Yang, and X. Zeng, Room temperature magnetoelectric coupling study in multiferroic $Bi_4NdTi_3Fe_{0.7}Ni_{0.3}O_{15}$ prepared by a multicalcination procedure, *Ceram. Int.* 40(5), 6815 (2014)

II.269. J. Wei, M. Zhang, H. Deng, S. Chu, M. Du, and H. Yan, Effect of Cr doping on ferroelectric and magnetic properties of $Bi_{0.8}Ba_{0.2}FeO_3$, *Ceram. Int.* 41(7), 8665 (2015)

II.270. G. Zerihun, S. Huang, G. Gong, and S. Yuan, Influence of Eu doping on the magnetoelectric and dielectric properties of $BiFeO_3$–$Bi_{0.5}Na_{0.5}TiO_3$ ceramics, *Ceram. Int.* 41(5), 6589 (2015)

II.271. J. Wei, Y. Liu, X. Bai, C. Li, Y. Liu, Z. Xu, P. Gemeiner, R. Haumont, I. C. Infante, and B. Dkhil, Crystal structure, leakage conduction mechanism evolution and enhanced multiferroic properties in Y-doped $BiFeO_3$ ceramics, *Ceram. Int.* 42(12), 13395 (2016)

II.272. M. Wu, W. Wang, X. Jiao, G. Wei, L. He, S. Han, Y. Liu, and D. Chen, Structural and multiferroic properties of Pr and Ti co-doped $BiFeO_3$ ceramics, *Ceram. Int.* 42(13), 14675 (2016)

II.273. A. Beniwal, J. S. Bangruwa, R. Walia, and V. Verma, A systematic study on multiferroics $Bi_{1-x}Ce_xFe_{1-y}MnyO_3$: Structural, magnetic and electrical properties, *Ceram. Int.* 42(8), 10373 (2016)

II.274. W. Mao, W. Chen, X. Wang, Y. Zhu, Y. Ma, H. Xue, L. Chu, J. Yang, X. Li, and W. Huang, Influence of Eu and Sr co-substitution on multiferroic properties of $BiFeO_3$, *Ceram. Int.* 42(11), 12838 (2016)

II.275. S. Ahmed and S. Kumar Barik, Enhanced electric and magnetic properties of $(BiLi)_{1/2}(Fe_{2/3}W_{1/3})O_3$ multiferroic as compared to $BiFeO_3$, *Ceram. Int.* 42(5), 5659 (2016)

II.276. A. S. Mahapatra, K. Mukhopadhyay, M. Ghosh, P. K. Mallick, T. Matsumoto, A. Taguchi, Y. Tanioku, K. Yoshimura, and P. K. Chakrabarti, Enhanced magnetoelectric property and Raman spectroscopy of nanocrystalline $Al_xGa_{1-x}FeO_3$ ($x = 0.05$, 0.10 and 0.20), *Ceram. Int.* 42(14), 15904 (2016)

II.277. Y. Gu, J. Zhao, W. Zhang, H. Zheng, L. Liu, and W. Chen, Structural transformation and multiferroic properties of Sm and Ti co-doped $BiFeO_3$ ceramics with Fe vacancies, *Ceram. Int.* 43(17), 14666 (2017)

II.278. P. Xiong, J. Yang, Y. F. Qin, W. J. Huang, X. W. Tang, L. H. Yin, W. H. Song, J. M. Dai, X. B. Zhu, and Y. P. Sun, Room temperature multiferroicity in Aurivillius compounds $Bi_6Fe_{2-x}Ni_xTi_3O_{18}$ ($0 \le x \le 1$), *Ceram. Int.* 43(5), 4405 (2017)

II.279. T. Wang, H. Deng, X. Meng, H. Cao, W. Zhou, P. Shen, Y. Zhang, P. Yang, and J. Chu, Tunable polarization and magnetization at room-temperature in narrow bandgap Aurivillius $Bi_6Fe_{2-x}Co_{x/2}Ni_{x/2}Ti_3O_{18}$, *Ceram. Int.* 43(12), 8792 (2017)

II.280. X. Zuo, M. Zhang, E. He, P. Zhang, J. Yang, X. Zhu, and J. Dai, Magnetic, dielectric, and magneto-dielectric properties of Aurivillius $Bi_7Fe_2CrTi_3O_{21}$ ceramic, *Ceram. Int.* 44(5), 5319 (2018)

II.281. J. D. Bobić, M. Ivanov, N. I. Ilić, A. S. Dzunuzović, M. M. V. Petrović, J. Banys, A. Ribic, Z. Despotovic, and B. D. Stojanovic, PZT-nickel ferrite and PZT-cobalt ferrite comparative study: Structural, dielectric, ferroelectric and magnetic properties of composite ceramics, *Ceram. Int.* 44(6), 6551 (2018)

II.282. S. Chandel, P. Thakur, S. S. Thakur, V. Kanwar, M. Tomar, V. Gupta, and A. Thakur, Effect of non-magnetic Al^{3+} doping on structural, optical, electrical, dielectric and magnetic properties of $BiFeO_3$ ceramics, *Ceram. Int.* 44(5), 4711 (2018)

II.283. N. Kumar, A. Shukla, N. Kumar, R. N. P. Choudhary, and A. Kumar, Structural, electrical, and multiferroic characteristics of lead-free multiferroic: $Bi(Co_{0.5}Ti_{0.5})O_3$–$BiFeO_3$ solid solution, *RSC Advances* 8(64), 36939 (2018)

II.284. W. Hu, Y. Chen, H. Yuan, G. Li, Y. Qiao, Y. Qin, and S. Feng, Structure, magnetic, and ferroelectric properties of $Bi_{1-x}Gd_xFeO_3$ nanoparticles, *J. Phys. Chem. C* 115(18), 8869 (2011)

II.285. A. Chaudhuri and K. Mandal, Study of structural, ferromagnetic and ferroelectric properties of nanostructured barium doped bismuth ferrite, *J. Magn. Magn. Mater.* 353, 57 (2014)

II.286. S. V. Vijayasundaram, G. Suresh, R. A. Mondal, and R. Kanagadurai, Substitution-driven enhanced magnetic and ferroelectric properties of $BiFeO_3$ nanoparticles, *J. Alloys Compd.* 658, 726 (2016)

II.287. W. Mao, Q. Yao, Y. Fan, Y. Wang, X. Wang, Y. Pu, and X. Li, Combined experimental and theoretical investigation on modulation of multiferroic properties in $BiFeO_3$ ceramics induced by Dy and transition metals co-doping, *J. Alloys Compd.* 784, 117 (2019)

II.288. H. Bai, J. Li, Y. Wu, Y. Hong, K. Shi, Q. Meng, Z. Zhou, D. Jia, R. Guo, and A. S. Bhalla, Structural, dielectric, ferroelectric, and ferromagnetic properties of multiferroic ceramics $(1-x)Ba(Zr_{0.2}Ti_{0.8})O_{3-x}Ba_{0.7}Ca_{0.3}FeTaO_5$, *Ferroelectrics* 534(1), 164 (2018)

II.289. S. Dash, R. N. P. Choudhary, and M. N. Goswami, Modification of ferroelectric and resistive properties of $(Bi_{0.5}Na_{0.5})(Nb_{0.5}Fe_{0.5})O_3$–PVDF composite, *J. Polym. Res.* 22(4), 54 (2015)

II.290. U. Naresh, R. J. Kumar, and K. C. B. Naidu, Optical, magnetic and ferroelectric properties of $Ba_{0.2}Cu_{0.8-x}La_xFe_2O_4$ (x = 0.2–0.6) nanoparticles, *Ceram. Int.* 45(6), 7515 (2019)

II.291. M. Muneeswaran, S. H. Lee, D. H. Kim, B. S. Jung, S. H. Chang, J. W. Jang, B. C. Choi, J. H. Jeong, N. V. Giridharan, and C. Venkateswaran, Structural, vibrational, and enhanced magneto-electric coupling in Ho-substituted $BiFeO_3$, *J. Alloys Compd.* 750, 276 (2018)

II.292. F. Xue, Y. Tian, L. Tang, P. Guo, Z. Luo, and W. Li, Rietveld refinement and multiferroic properties of Gd andTi co-doped $BiFeO_3$, *Ferroelectr. Lett. Sect.* 45(1–3), 30 (2018)

II.293. X. Yuan, L. Shi, J. Zhao, S. Zhou, J. Guo, S. Pan, X. Miao, L. Wu, Tuning ferroelectric, dielectric, and magnetic properties of $BiFeO_3$ Ceramics by Ca and Pb Co-doping, *phys. stat. sol. (b)* 256(3), 1800499 (2019)

II.294. M. Hemeda, A. Tawfik, D. E. El Refaey, A. H. El-Sayed, and S. Mohamed, Electric and magnetic properties of $[(NCZF)_{1-x}(Na(ac.ac))_x]$ nanocomposite, *J. Miner. Mater. Charact. Eng.* 7, 559 (2017)

II.295. T. Kanai, S. Ohkoshi, A. Nakajima, T. Watanabe, and K. Hashimoto, A ferroelectric ferromagnet composed of $(PLZT)_x(BiFeO_3)_{1-x}$ solid solution, *Adv. Mater.* 13(7), 487 (2001)

II.296. J. Li, X. K. Lan, X. Q. Song, W. Z. Lu, X. H. Wang, F. Shi, and W. Lei, Crystal structures, dielectric properties and ferroelectricity in stuffed tridymite-type $BaAl_{2-2x}(Zn_{0.5}Si_{0.5})_{2x}O_4$ solid solutions, *Dalton Trans.* 48(11), 3625 (2019)

II.297. V. Singh, S. Sharma, R. K. Dwivedi, M. Kumar, R. K. Kotnala, N. C. Mehra, and R. P. Tandon, Structural, dielectric, ferroelectric and magnetic properties of $Bi_{0.80}A_{0.20}FeO_3$ (A = Pr, Y) multiferroics, *J. Supercond. Nov. Magn.* 26(3), 657 (2013)

II.298. M. Kumar, K. L. Yadav, and G. D. Varma, Large magnetization and weak polarization in sol–gel derived $BiFeO_3$ ceramics, *Mater. Lett.* 62(8–9), 1159 (2008)

II.299. M. Kumar and K. L. Yadav, Study of room temperature magnetoelectric coupling in Ti substitutedbismuth ferrite system, *J. Appl. Phys.* 100(7), 074111 (2006)

II.300. T. Acharyaa and R. N. P. Choudhary, Inducing ferroelectricity and magneto-electric effect in the iron titanate ilmenite by modifying with bismuth and lead titanate, *J. Alloys Compd.* 788, 495 (2019)

II.301. Z. Li, W. Qi, J. Cao, Y. Li, G. Viola, C. Jia, and H. Yan, Multiferroic properties of single phase Bi_3NbTiO_9 based textured ceramics, *J. Alloys Comp.* 788, 701 (2019)

II.302. L. Zia, G. H. Jaffari, N. A. Awan, J. U. Rahman, and S. Lee, Electrical response of mixed phase $(1-x)BiFeO_{3-x}PbTiO_3$ solid solution: Role of tetragonal phase and tetragonality, *J. Alloys Compd.* 786, 98 (2019)

II.303. W. Maoa, Q. Yaob, Y. Fanb, Y. Wangb, X. Wanga, Y. Pua, and X. Li, Combined experimental and theoretical investigation on modulation of multiferroic properties in $BiFeO_3$ ceramics induced by Dy and transition metals co-doping, *J. Alloys Compd.* 784, 117 (2019)

References for Part III

III.1. T. Okubo, R. Kawajiri, T. Mitani, T. Shimoda, A mixed-valence coordination polymer featuring two-dimensional ferroelectric order: $\{[Cu^{I}_4Cu^{II}(Et_2dtc)_2Cl_3][Cu^{II}(Et_2dtc)_2]_2(FeCl_4)\}_n$($Et_2dtc^-$ = diethyldithiocarbamate), *J. Am. Chem. Soc.* 127(50), 17598 (2005)

III.2. S. Ohkoshi, H. Tokoro, T. Matsuda, H. Takahashi, H. Irie, and K. Hashimoto, Coexistence of ferroelectricity and ferromagnetism in a rubidium manganese hexacyanoferrate, *Angew. Chem. Int. Ed.* 46(18), 3238 (2007)

III.3. P. Bhatt, S. S. Meena, M. D. Mukadam, B. P. Mandal, A. K. Chauhan, and S. M. Yusuf, Synthesis of CoFe Prussian blue analogue/polyvinylidene fluoride nanocomposite material with improved thermal stability and ferroelectric properties, *New J. Chem.* 42(6), 4567 (2018)

III.4. K. I. Shivakumar, K. Swathi, T. C. Das Goudappagouda, A. Kumar, R. D. Makde, K. Vanka, K. S. Narayan, S. S. Babu, and G. J. Sanjayan, Mixed-stack charge transfer crystals of pillar[5]quinone and tetrathiafulvalene exhibiting ferroelectric features, *Chemistry* 23(51), 12630 (2017)

III.5. R. H. Hu, Y. Sui, J. W. Wen, Z. G. Luo, and L. J. Zhong, A new type of organic ferroelectric N-dehydroabietyl-4-bromobenzamide, *Asian J. Chem.* 27(7), 2627 (2015)

III.6. C. Y. Pan, S. Hu, D. G. Li, P. Ouyang, F. H. Zhao, and Y. Y. Zheng, The first ferroelectric templated borate: $[Ni(en)_2pip][B_5O_6(OH)_4]_2$, *Dalton Trans.* 39(25), 5772 (2010)

III.7. X. Z. Li, Z. R. Qu, and R. G. Xiong, A new chiral schiff base with ferroelectric property, *Chin. J. Chem.* 26(11), 1959 (2008)

III.8. F. Du, H. Zhang, C. Tian, and S. Du, Synthesis and structure of two acentric heterometallic inorganic–organic hybrid frameworks with both nonlinear optical and ferroelectric properties, *Cryst. Growth Des.* 13(4), 1736 (2013)

III.9. W. Zhang, H. Y. Ye, H. L. Cai, J. Z. Ge, R. G. Xiong, and S. D. Huang, Discovery of new ferroelectrics: $[H_2dbco]_2{\cdot}[Cl_3]{\cdot}[CuCl_3(H_2O)_2]{\cdot}H_2O$ (dbco = 1, 4-diazabicyclo[2.2.2]octane), *J. Am. Chem. Soc.* 132(21), 7300 (2010)

III.10. J. Wang, J. Q. Tao, X. J. Xu, and C. Y. Tan, Synthesis, crystal structure, and properties of a cadmium(II) complex with the flexible ligand (1_H-[2, 2_]biimidazoly-1-yl)-acetic acid, *Z. Anorg. Allg. Chem.* 638(9), 1261 (2012)

III.11. Y. M. Xie, J. H. Liu, X. Y. Wu, Z. G. Zhao, Q. S. Zhang, F. Wang, S. C. Chen, and C. Z. Lu, New ferroelectric and nonlinear optical porous coordination polymer constructed from a rare $(CuBr)_\infty$ castellated chain, *Cryst. Growth Des.* 8(11), 3914 (2008)

III.12. D. S. Liu, Y. Sui, W. T. Chen, and P. Feng, Two new nonlinear optical and ferroelectric Zn(II) compounds based on nicotinic acid and tetrazole derivative ligands, *Cryst. Growth Des.* 15(8), 4020 (2015)

III.13. L. Song, S. W. Du, J. D. Lin, H. Zhou, and T. Li, A 3D metal–organic framework with rare 3-fold interpenetrating dia-g nets based on silver(I) and novel tetradentate imidazolate ligand: Synthesis, structure, and possible ferroelectric property, *Cryst. Growth Des.* 7(11), 2268 (2007)

III.14. O. Sengupta, and P. S. Mukherjee, Mixed azide and 5-(Pyrimidyl)tetrazole bridged Co(II)/Mn(II) polymers: Synthesis, crystal structures, ferroelectric and magnetic behavior, *Inorg. Chem.* 49(18), 8583 (2010)

III.15. W. W. Zhou, J. T. Chen, G. Xu, M. S. Wang, J. P. Zou, X. F. Long, G. J. Wang, G. C. Guo, and J. S. Huang, Nonlinear optical and ferroelectric properties of a 3-D Cd(II) triazolate complex with a novel (63)2(610·85) topology, *Chem. Commun. (Camb.)* (24), 2762 (2008)

III.16. H. X. Zhao, G. L. Zhuang, S. T. Wu, L. S. Long, H. Y. Guo, Z. G. Ye, R. B. Huang, and L. S. Zheng, Experimental and theoretical demonstration of ferroelectric anisotropy in a one-dimensional copper(II)-based coordination polymer, *Chem. Commun. (Camb.)* (13), 1644 (2009)

III.17. Q. Ye, Y. Z. Tang, X. S. Wang, and R. G. Xiong, Strong enhancement of second-harmonic generation (SHG) response through multi-chiral centers and metal-coordination, *Dalton Trans.* (9), 1570 (2005)

III.18. G. X. Wang, G. F. Han, Q. Ye, R. G. Xiong, T. Akutagawa, T. Nakamura, P. W. H. Chan, and S. D. Huang, Dielectric anisotropy of a homochiral rare-earth metal complex, *Dalton Trans.* 19, 2527 (2008)

III.19. S. T. Zheng and G. Y. Yang, The first polyoxometalate-templated four-fold interpenetrated coordination polymer with new topology and ferroelectricity, *Dalton Trans.* 39(3), 700 (2010)

III.20. H. B. Duan, H. R. Zhao, X. M. Ren, H. Zhou, Z. F. Tian, and W. Q. Jin, Inorganic–organic hybrid compounds based on face-sharing octahedral $[PbI_3]_\infty$ chains: Self-assemblies, crystal structures, and ferroelectric, photoluminescence properties, *Dalton Trans.* 40(8), 1672 (2011)

III.21. S. P. Zhao and X. M. Ren, Toward design of multiple-property inorganic–organic hybrid compounds based on face-sharing octahedral iodoplumbate chains, *Dalton Trans.* 40(33), 8261 (2011)

III.22. H. R. Zhao, D. P. Li, X. M. Ren, Y. Song, and W. Q. Jin, Larger spontaneous polarization ferroelectric inorganic–organic hybrids: $[PbI_3]_\infty$ chains directed organic cations aggregation to Kagomé-shaped tubular architecture, *J. Am. Chem. Soc.* 132(1), 18 (2010)

III.23. T. Hang, D. W. Fu, Q. Ye, H. Y. Ye, R. G. Xiong, and S. D. Huang, Tanklike metal–organic framework filled with perchloric acid and its dielectric–ferroelectric properties, *Cryst. Growth Des.* 9(5), 2054 (2009)

III.24. Q. Ye, T. Hang, D. W. Fu, G. H. Xu, and R. G. Xiong, Typical ferroelectric olefin-copper(I) organometallic oligmer with flexible organic ligand, *Cryst. Growth Des.* 8(10), 3501 (2008)

III.25. T. Hang, D. W. Fu, Q. Ye, and R. G. Xiong, Two novel noncentrosymmetric zinc coordination compounds with second harmonic generation response, and potential piezoelectric and ferroelectric properties, *Cryst. Growth Des.* 9(5), 2026 (2009)

III.26. M. Mon, J. Ferrando-Soria, M. Verdaguer, C. Train, C. Paillard, B. Dkhil, C. Versace, R. Bruno, D. Armentano, and E. Pardo, Postsynthetic approach for the rational design of chiral ferroelectric metal–organic frameworks, *J. Am. Chem. Soc.* 139(24), 8098 (2017)

III.27. P. C. Guo, Z. Chu, X. M. Ren, W. H. Ning, and W. Jin, Comparative study of structures, thermal stabilities and dielectric properties for a ferroelectric MOF $[Sr(m\text{-}BDC)(DMF)]_\infty$ with its solvent-free framework, *Dalton Trans.* 42(18), 6603 (2013)

III.28. W. K. Han, L. F. Qin, C. Y. Pang, C. K. Cheng, W. Zhu, Z. H. Li, Z. Li, X. Ren, and Z. G. Gu, Polymorphism of a chiral iron(II) complex: spin-crossover and ferroelectric properties, *Dalton Trans.* 46(25), 8004 (2017)

III.29. D. P. Li, T. W. Wang, C. H. Li, D. S. Liu, Y. Z. Li, and X. Z. You, Single-ion magnets based on mononuclear lanthanide complexes with chiral Schiff base ligands $[Ln(FTA)_3L]$ (Ln = Sm, Eu, Gd, Tb and Dy), *Chem. Commun. (Camb.)* 46(17), 2929 (2010)

III.30. W. Zhang, R. G. Xiong, and S. D. Huang, 3D framework containing Cu_4Br_4 cubane as connecting node with strong ferroelectricity, *J. Am. Chem. Soc.* 130(32), 10468 (2008)

III.31. Y. Q. Zheng, W. Xu, H. L. Zhu, J. L. Lin, L. Zhao, and Y. R. Dong, New pyridine-2, 4, 6-tricarboxylato coordination polymers: Synthesis, crystal structures and properties, *CrystEngComm* 13(7), 2699 (2011)

III.32. J. D. Lin, X. F. Long, P. Lin, and S. W. Du, A series of cation-templated, polycarboxylate-based Cd(II) or Cd(II)/Li(I) frameworks with second-order nonlinear optical and ferroelectric properties, *Cryst. Growth Des.* 10(1), 146 (2010)

III.33. Q. Ye, Y. M. Song, G. X. Wang, K. Chen, D. W. Fu, P. W. H. Chan, J. S. Zhu, S. D. Huang, and R. G. Xiong, Ferroelectric metal–organic framework with a high dielectric constant, *J. Am. Chem. Soc.* 128(20), 6554 (2006)

III.34. X. Q. Liang, J. T. Jia, T. Wu, D. P. Li, L. Liu, G. S. Tsolmon, and G. S. Zhu, A spontaneously resoluted zinc–organic framework with nonlinear optical and ferroelectric properties generated from tetrazolate-ethyl ester ligand, *CrystEngCom* 12(11), 3499 (2010)

III.35. Z. Su, J. Fan, T. Okamura, W. Y. Sun, and N. Ueyama, Ligand-directed and ph-controlled assembly of chiral 3d–3d heterometallic metal–organic frameworks, *Cryst. Growth Des.* 10(8), 3515 (2010)

III.36. L. Yu, X. N. Hua, X. J. Jiang, L. Qin, X. Z. Yan, L. H. Luo, and L. Han, Histidine-controlled homochiral and ferroelectric metal–organic frameworks, *Cryst. Growth Des.* 15(2), 687 (2015)

III.37. Q. Ye, Y. M. Song, D. W. Fu, G. X. Wang, R. G. Xiong, P. W. H. Chan, and S. D. Huang, Deuteration effect of ferroelectricity and permittivity on homochiral zinc coordination compound, *Cryst. Growth Des.* 7(9), 1568 (2007)

III.38. D. W. Fu, W. Zhang, and R. G. Xiong, Isotope effect on SHG response and ferroelectric properties of a homochiral zinc coordination compound containing tetrazole ligand, *Cryst. Growth Des.* 8(9), 3461 (2008)

III.39. H. R. Wen, Y. Z. Tang, C. M. Liu, J. L. Chen, and C. L. Yu, One-dimensional homochiral cyano-bridged heterometallic chain coordination polymers with metamagnetic or ferroelectric properties, *Inorg. Chem.* 48(21), 10177 (2009)

III.40. L. Li, J. Ma, C. Song, T. Chen, Z. Sun, S. Wang, J. Luo, and M. Hong, A 3D polar nanotubular coordination polymer with dynamic structural transformation and ferroelectric and nonlinear-optical properties, *Inorg. Chem.* 51(4), 2438 (2012)

III.41. X. L. Li, C. L. Chen, L. F. Han, C. M. Liu, Y. Song, X. G. Yang, and S. M. Fang, First one-dimensional homochiral stairway-like Cu(II) chains: Crystal structures, circular dichroism (CD) spectra, ferroelectricity and antiferromagnetic properties, *Dalton Trans.* 42(14), 5036 (2013)

III.42. X. L. Li, Z. Zhang, X. L. Zhang, J. L. Kang, A. L. Wang, L. Zhou, and S. Fang, A pair of dinuclear Re(I) enantiomers: synthesis, crystal structures, chiroptical and ferroelectric properties, *Dalton Trans.* 44(9), 4180 (2015)

III.43. G. X. Wang, G. F. Han, Q. Ye, R. G. Xiong, T. Akutagawa, T. Nakamura, P. W. H. Chan, and S. D. Huang, Dielectric anisotropy of a homochiral rare-earth metal complex, *Dalton Trans.* (19), 2527 (2008)

III.44. L. L. Liang, S. B. Ren, J. Zhang, Y. Z. Li, H. B. Du, and X. Z. You, Two unprecedented NLO-active coordination polymers constructed by a semi-rigid tetrahedral linker, *Dalton Trans.* 39(33), 7723 (2010)

III.45. C. F. Wang, Z. G. Gu, X. M. Lu, J. L. Zuo, and X. Z. You, Ferroelectric heterobimetallic clusters with ferromagnetic interactions, *Inorg. Chem.* 47(18), 7957 (2008)

III.46. Q. Ye, D. W. Fu, H. Tian, R. G. Xiong, P. W. H. Chan, and S. D. Huang, Multiferroic homochiral metal–organic framework, *Inorg. Chem.* 47(3), 772 (2008)

III.47. L. Li, J. Ma, C. Song, T. Chen, Z. Sun, S. Wang, J. Luo, and M. Hong, A 3D polar nanotubular coordination polymer with dynamic structural transformation and ferroelectric and nonlinear-optical properties, *Inorg. Chem.* 51(4), 2438 (2012)

III.48. D. Asthana, A. Kumar, A. Pathak, P. K. Sukul, S. Malik, R. Chatterjee, S. Patnaik, K. Rissanen, and P. Mukhopadhyay, An all-organic steroid–D–p-A modular design drives ferroelectricity in supramolecular solids and nano-architectures at RT, *Chem. Commun. (Camb.)* 47(31), 8928 (2011)

III.49. Y. T. Wang, G. M. Tang, C. He, S. C. Yan, Q. C. Hao, L. Chen, X. F. Long, T. D. Li, and S. W. Ng, Nonlinear optical and ferroelectric materials based on 1-benzyl-2-phenyl-1H-benzimidazole salts, *CrystEngComm* 13(21), 6365 (2011)

III.50. H. R. Chen, and W. W. Zhang, A novel two-dimensional CdII coordination polymer: poly[aqua[m4-2-(carboxylatobenzoyl)benzonato]-cadmium(II)], *Acta Crystallogr. C* 70(11), 1079 (2014)

III.51. M. L. Feng, P. X. Li, K. Z. Du, and X. Y. Huang, $[Ni(en)_3][InSbS_4]$: A one-dimensional polymeric indium thioantimonate with a polar structure, *Eur. J. Inorg. Chem.* 2011(26), 3881 (2011)

III.52. Z. Guo, R. Cao, X. Wang, H. Li, W. Yuan, G. Wang, H. Wu, and J. Li, A multifunctional 3D ferroelectric and NLO-active porous metal-organic framework, *J. Am. Chem. Soc.* 131(20), 6894 (2009)

III.53. X. Duan, Q. Meng, Y. Su, Y. Li, C. Duan, X. Ren, and C. Lu, Multifunctional polythreading coordination polymers: Spontaneous resolution, nonlinear-optic, and ferroelectric properties, *Chemistry* 17(36), 9936 (2011)

III.54. H. Zhao, Q. Ye, Z. R. Qu, D. W. Fu, R. G. Xiong, S. D. Huang, and P. W. H. Chan, Huge deuterated effect on permittivity in a metal–organic framework, *Chemistry* 14(4), 1164 (2008)

III.55. Z. R. Qu, H. Zhao, Y. P. Wang, X. S. Wang, Q. Ye, Y. H. Li, R. G. Xiong, B. F. Abrahams, Z. G. Liu, Z. L. Xue, and X. Z. You, Synthesis of novel chiral and acentric coordination polymers by the reaction of zinc or cadmium salts with racemic 3-pyridyl-3-aminopropionic acid, *Chemistry* 10(1), 53 (2004)

III.56. H. Zhao, Y. H. Li, X. S. Wang, Z. R. Qu, L. Z. Wang, R. G. Xiong, B. F. Abrahams, and Z. Xue, Noncentrosymmetric organic solids with very strong harmonic generation response, *Chemistry* 10(10), 2386 (2004)

III.57. Z. R. Qu, Q. Ye, H. Zhao, D. W. Fu, H. Y. Ye, R. G. Xiong, T. Akutagawa, and T. Nakamura, Homochiral laminar europium metal–organic framework with unprecedented giant dielectric anisotropy, *Chemistry* 14(11), 3452 (2008)

III.58. S. Bhattacharya, S. Pal, and S. Natarajan, Switchable room-temperature ferroelectric behavior, selective sorption and solvent-exchange studies of $[H_3O][Co_2(dat)(sdba)_2]\cdot H_2sdba\cdot 5H_2O$, *ChemPlusChem* 81(8), 733 (2016)

III.59. Y. H. Tan, Y. M. Yu, J. B. Xiong, J. X. Gao, Q. Xu, C. W. Fu, Y. Z. Tang, and H. R. Wen, Synthesis, structure and ferroelectric–dielectric properties of an acentric 2D framework with imidazole-containing tripodal ligands, *Polyhedron* 70, 47 (2014)

III.60. H. R. Wen, T. T. Qi, S. J. Liu, C. M. Liu, Y. Z. Tang, and J. L. Chen, Syntheses and structures of chiral tri- and tetranuclear Cd(II) clusters with luminescent and ferroelectric properties, *Polyhedron* 85, 894 (2015)

III.61. X. P. Zhang, X. W. Qi, D. S. Zhang, L. H. Zhu, X. H. Wang, Z. F. Shi, and Q. Lin, Distinct optoelectronic properties of four-coordinate and five-coordinate Zn(II) complexes with chiral polypyridine ligands, *Polyhedron* 126, 111 (2017)

III.62. Y. Z. Tang, Y. M. Yu, Y. H. Tan, J. S. Wu, J. B. Xiong, and H. R. Wen, Two acentric (6, 3) topological 2-D frameworks with imidazole-containing tripodal ligand and their ferroelectric properties, *Dalton Trans.* 42(28), 10106 (2013)

III.63. L. Z. Chen and J. Sun, Reversible ferroelectric phase transition of 1, 4-diazabicyclo [2, 2, 2]octane N,N′-dioxide di(perchlorate), *Inorg. Chem. Commun.* 76, 67 (2017)

III.64. Y. T. Yang, Y. X. Che, and J. M. Zheng, A novel chiral helical coordination complex with ferroelectric and weak ferromagnetic properties, *Inorg. Chem. Commun.* 17, 49 (2012)

III.65. Y. H. Zhou, J. Li, T. Wu, X. P. Zhao, Q. L. Xu, X. L. Li, M. B. Yu, L. L. Wang, P. Sun, and Y. X. Zheng, Photoluminescent and ferroelectric properties of a chiral rhenium(I) complex based on the chiral (−)−4, 5-pinene-2, 2′-bipyridine ligand, *Inorg. Chem. Commun.* 29, 18 (2013)

III.66. X. Tan, Y. X. Che, and J. M. Zheng, Two chiral complexes constructed from mixed L-histidine and L-alanine/thiocyanate ligands: Synthesis, structure, ferromagnetic and ferroelectric properties, *Inorg. Chem. Commun.* 22, 10 (2012)

III.67. Y. Wang, F. H. Zhao, A. H. Shi, Y. X. Che, and J. M. Zheng, Magnetic and ferroelectric properties of two Co(II) complexes based on flexible bis(imidazole) ligands, *Inorg. Chem. Commun.* 20, 23 (2012)

III.68. Y. Wang, Y. X. Che, and J. M. Zheng, A 3D ferroelectric Co(II) polymer showing (3,5)-connected hms topology with 2-fold interpenetration, *Inorg. Chem. Commun.* 21, 69 (2012)

III.69. F. H. Zhao, S. H. Liang, S. Jing, Y. Wang, Y. X. Che, and J. M. Zheng, Magnetic and ferroelectric properties of a chiral cyano-bridged Pr(III)-Cr(III) complex, *Inorg. Chem. Commun.* 21, 109 (2012)

III.70. Y. Zhao, L. Luo, C. Liu, M. Chen, and W. Y. Sun, Helical silver(I) coordination polymer with oxazoline-containing ligand: Structure, non-linear and ferroelectric property, *Inorg. Chem. Commun.* 14(7), 1145 (2011)

III.71. Y. T. Wang, G. M. Tang, Y. Q. Wei, T. X. Qin, T. D. Li, J. B. Ling, and X. F. Long, One new nonlinear optical and ferroelectric one-dimensional chain constructed by an unsymmetric bridging ligand, *Inorg. Chem. Commun.* 12(11), 1164 (2009)

III.72. F. Du, M. Zhao, X. Long, and S. Du, A new acentric heterometallic inorganic–organic hybrid framework with an unusual $\{Cd_3Na_4\}_n$ array: NLO and ferroelectric properties, *Inorg. Chem. Commun.* 38, 39 (2013)

III.73. Z. Su, G.C. Lv, J. Fan, G.X. Liu, and W.Y. Sun, Homochiral ferroelectric three-dimensional cadmium(II) frameworks from racemic camphoric acid and 3, 5-di(imidazol-1-yl)benzoic acid, *Inorg. Chem. Commun.* 38, 39 (2013)

III.74. H. W. Kuai, J. J. Xia, and H. Y. Sang, Syntheses, characterization and properties of manganese, cobalt and copper complexes from chelate N-donor ligands, *Inorg. Chem. Commun.* 72, 73 (2016)

III.75. X. L. Li, M. Hu, Y. J. Zhang, X. L. Zhang, F. C. Li, A. L. Wang, J. P. Du, and H. P. Xiao, Synthesis, crystal structure, chiroptical and ferroelectric properties of a multifunctional chiral silver(I) complex based on the chiral bis-bidentate bridging ligand, *Inorg. Chim. Acta* 444, 221 (2016)

III.76. G. X. Liu, W. Guo, S. Nishihara, and X. M. Ren, A chiral copper(II) inverse-9-metallacrown-3 complex: Synthesis, crystal structure, ferroelectric and magnetic properties, *Inorg. Chim. Acta* 368(1), 165 (2011)

III.77. W. W. Zhou, W. Zhao, B. Wei, F. W. Wang, Y. H. Chen, W. Y. Fang, and X. Zhao, A new 1D Cd(II) pyridinate polymer: Structure, second-harmonic generation response, dielectric and potential ferroelectric properties, *Inorg. Chim. Acta* 386, 17 (2012)

III.78. L. Z. Chen, D. D. Huang, J. Z. Ge, and F. M. Wang, A novel Ag(I) coordination polymers based on 2-(pyridin-4-yl)-1H-imidazole-4, 5-dicarboxylic acid: Syntheses, structures, ferroelectric, dielectric and optical properties, *Inorg. Chim. Acta* 406, 95 (2013)

III.79. X. F. Wang, G. X. Liu, and H. Zhou, Syntheses, structures and physical properties of two zinc(II) coordination polymers with 1, 3, 5-tris(imidazol-1-ylmethyl)-2, 4, 6-trimethylbenzene and 1, 3, 5-benzenetricarboxylate, *Inorg. Chim. Acta* 406, 223 (2013)

III.80. W. Xu, W. Liu, F. Y. Yao, and Y. Q. Zheng, Synthesis, crystal structure and properties of the novel chiral 3D coordination polymer with S-carboxymethyl-l-cysteine, *Inorg. Chim. Acta* 365(1), 297 (2011)

III.81. W. J. Ji, Q. G. Zhai, S. N. Li, Y. C. Jiang, and M. C. Hu, The first ionothermal synthesis of a 3D ferroelectric metal–organic framework with colossal dielectric constant, *Chem. Commun. (Camb.)* 47(13), 3834 (2011)

III.82. H. Zhao, Z. R. Qu, Q. Ye, B. F. Abrahams, Y. P. Wang, Z. G. Liu, Z. Xue, R. G. Xiong, and X. Z. You, Ferroelectric copper quinine complexes, *Chem. Mater.* 15(22), 4166 (2003)

III.83. F. H. Zhao, Y. X. Che, J. M. Zheng, F. Grandjean, and G. J. Long, Two acentric mononuclear molecular complexes with unusual magnetic and ferroelectric properties, *Inorg. Chem.* 51(8), 4862 (2012)

III.84. T. Hang, D. W. Fu, Q. Ye, H. Y. Ye, R. G. Xiong, and S. D. Huang, Tanklike metal–organic framework filled with perchloric acid and its dielectric–ferroelectric properties, *Cryst. Growth Des.* 9(5), 2054 (2009)

III.85. H. R. Wen, Y. Z. Tang, C. M. Liu, J. L. Chen, and C. L. Yu, One-dimensional homochiral cyano-bridged heterometallic chain coordination polymers with metamagnetic or ferroelectric properties, *Inorg. Chem.* 48(21), 10177 (2009)

III.86. Y. T. Wang, G. M. Tang, Y. Q. Wei, T. X. Qin, T. D. Li, C. He, J. B. Ling, X. F. Long, and S. W. Ng, Two new nonlinear optical and ferroelectric three-dimensional metal–organic frameworks with an sqp-net, *Cryst. Growth Des.* 10(1), 25 (2010)

III.87. Y. H. Li, Z. R. Qu, H. Zhao, Q. Ye, L. X. Xing, X. S. Wang, R. G. Xiong, and X. Z. You, A novel TGS-like inorganic–organic hybrid and a preliminary investigation of its possible ferroelectric behavior, *Inorg. Chem.* 43(13), 3768 (2004)

III.88. Y. Z. Tang, M. Zhou, J. Huang, Y. H. Tan, J. S. Wu, and H. R. Wen, In situ synthesis and ferroelectric, shg response, and luminescent properties of a novel 3D acentric zinc coordination polymer, *Inorg. Chem.* 52(4), 1679 (2013)

III.89. Z. G. Gu, X. H. Zhou, Y. B. Jin, R. G. Xiong, J. L. Zuo, and X. Z. You, Crystal structures and magnetic and ferroelectric properties of chiral layered metal–organic frameworks with dicyanamide as the bridging ligand, *Inorg. Chem.* 46(14), 5462 (2007)

III.90. T. K. Pal, R. Katoch, A. Garg, and P. K. Bharadwaj, Metal–organic frameworks built from a linear rigid dicarboxylate and different colinkers: Trap of the Keto form of ethylacetoacetate, luminescence and ferroelectric studies, *Cryst. Growth Des.* 15(9), 4526 (2015)

III.91. A. K. Gupta, D. De, R. Katoch, A. Garg, and P. K. Bharadwaj, Synthesis of a NbO type homochiral Cu(II) metal–organic framework: Ferroelectric behavior and heterogeneous catalysis of three-component coupling and pechmann reactions, *Inorg. Chem.* 56(8), 4697 (2017)

III.92. M. Manivannan, S. A. M. Britto Dhas, and M. Jose, Ferroelectric behavior of organic terahertz radiating DAST crystal, *J. Inorg. Organomet. Polym.* 27(6), 1870 (2017)

III.93. J. L. Qi, S. L. Ni, W. Xu, J. Y. Qian, and Y. Q. Zheng, The first two examples of (R)-2-chloromandelato coordination polymers: Synthesis, structure, magnetic and ferroelectric properties, *J. Inorg. Organomet. Polym.* 24(3), 600 (2014)

III.94. C. Hou, Q. Liu, Y. Lu, T. Okamura, P. Wang, M. Chen, and W. Y. Sun, Metal-organic frameworks with N-(4-pyridylmethyl)iminodiacetate ligand: Synthesis, structure and sorption properties, *Microporous Mesoporous Mater.* 152, 96 (2012)

III.95. D. P. Li, C. H. Li, J. Wang, L. C. Kang, T. Wu, Y. Z. Li, and X. Z. You, Synthesis and physical properties of two chiral terpyridyl europium(III) complexes with distinct crystal polarity, *Eur. J. Inorg. Chem.* 2009(32), 4844 (2009)

III.96. Y. R. Xie, H. Zhao, X. S. Wang, Z. R. Qu, R. G. Xiong, X. Xue, Z. Xue, and X. Z. You, 2D chiral uranyl(VI) coordination polymers with second-harmonic generation response and ferroelectric properties, *Eur. J. Inorg. Chem.* 2003(20), 3712 (2003)

III.97. M. L. Feng, P. X. Li, K. Z. Du, and X. Y. Huang, $[Ni(en)_3][InSbS_4]$: A one-dimensional polymeric indium thioantimonate with a polar structure, *Eur. J. Inorg. Chem.* 2011(26), 3881 (2011)

III.98. A. A. Bahgat, S. M. Sayyah, and H. M. Abd-Elsalam, Study of ferroelectricity in polyaniline, *Int. J. Polym. Mater.* 52(6), 499 (2003)

III.99. H. Zhao, Z. R. Qu, H. Y. Ye, and R. G. Xiong, In situ hydrothermal synthesis of tetrazole coordination polymers with interesting physical properties, *Chem. Soc. Rev.* 37(1), 84 (2008)

III.100. J. D. Lin, C. Rong, R. X. Lv, Z. J. Wang, X. F. Long, G. C. Guo, and C. Y. Pan, A 3D metal-organic framework with a pcu net constructed from lead(II) and thiophene-2, 5-dicarboxylic acid: Synthesis, structure and ferroelectric property, *J. Solid State Chem.* 257, 34 (2018)

III.101. L. H. Cao, Y. L. Wei, C. Ji, M. L. Ma, S. Q. Zang, and T. C. W. Mak, A multifunctional 3D chiral porous ferroelectric metal–organic framework for sensing small organic molecules and dye uptake, *Chem. Asian J.* 9(11), 3094 (2014)

III.102. S. R. Sushrutha, S. Mohana, S. Pal, and S. Natarajan, Solvent-dependent delamination, restacking, and ferroelectric behavior in a new charge-separated layered compound: $[NH_4][Ag_3(C_9H_5NO_4S)_2(C_{13}H_{14}N_2)_2]\cdot 8H_2O$, *Chem. Asian J.* 12(1), 101 (2017)

III.103. G. X. Liu, X. F. Wang, and H. Zhou, Versatile frameworks constructed from divalent metals with 4, 4′-methylenedibenzoic acid and imidazole derivative ligands: Syntheses, crystal structures and physical properties, *J. Solid State Chem.* 199, 305 (2013)

III.104. D. S. Liu, W. T. Chen, G. M. Ye, J. Zhang, and Y. Sui, Synthesis and characterization of a multifunctional inorganic–organic hybrid mixed-valence copper(I/II) coordination polymer: $\{[CuCN][Cu(isonic)_2]\}_n$, *J. Solid State Chem.* 256, 14 (2017)

III.105. Y. N. Ren, W. Xu, L. X. Zhou, and Y. Q. Zheng, Efficient tetracycline adsorption and photocatalytic degradation of rhodamine B by uranyl coordination polymer, *J. Solid State Chem.* 251, 105 (2017)

III.106. X. X. Li, L. Cheng, and G. Y. Yang, Open frameworks based on mono-lanthanide-substituted polyoxometaloaluminate building units: Syntheses, structures and properties, *J. Solid State Chem.* 203, 193 (2013)

III.107. H. W. Kuai, X. C. Cheng, D. H. Li, T. Hu, and X. H. Zhu, Syntheses, characterization and properties of silver, copper and palladium complexes from bis(oxazoline)-containing ligands, *J. Solid State Chem.* 228, 65 (2015)

III.108. J. Zhang, M. Zhao, W. Xie, J. Jin, F. Xie, X. Song, S. Zhang, J. Wu, and Y. Tian, A series of novel cadmium(II) coordination polymers with photoluminescence and ferroelectric properties based on zwitterionic ligands, *New J. Chem.* 41(17), 9152 (2017)

III.109. S. R. Sushrutha, S. Mohana, S. Pal, and S. Natarajan, Solvent-dependent delamination, restacking, and ferroelectric behavior in a new charge-separated layered compound: $[NH_4][Ag_3(C_9H_5NO_4S_2(C_{13}H_{14}N_2)_2]\cdot 8H_2O$, *Chem. Asian J.* 12(1), 101 (2017)

III.110. A. K. Srivastava, B. Praveenkumar, I. K. Mahawar, P. Divya, S. Shalini, and R. Boomishankar, Anion driven $[Cu^{II}L_2]_n$ frameworks: Crystal structures, guest-encapsulation, dielectric, and possible ferroelectric properties, *Chem. Mater.* 26(12), 3811 (2014)

III.111. G. X. Liu, W. Guo, S. Nishihara, and X. M. Ren, A chiral copper(II) inverse-9-metallacrown-3 complex: Synthesis, crystal structure, ferroelectric and magnetic properties, *Inorg. Chim. Acta* 368(1), 165 (2011)

III.112. L. Z. Chen, D. D. Huang, J. Z. Ge, and F. M. Wang, A novel Ag(I) coordination polymers based on 2-(pyridin-4-yl)-1H-imidazole-4, 5-dicarboxylic acid: Syntheses, structures, ferroelectric, dielectric and optical properties, *Inorg. Chim. Acta* 406, 95 (2013)

III.113. X. F. Wang, G. X. Liu, and H. Zhou, Syntheses, structures and physical properties of two zinc(II) coordination polymers with 1, 3, 5-tris(imidazol-1-ylmethyl)-2, 4, 6-trimethylbenzene and 1, 3, 5-benzenetricarboxylate, *Inorg. Chim. Acta* 406, 223 (2013)

III.114. W. Xu, W. Liu, F. Y. Yao, and Y. Q. Zheng, Synthesis, crystal structure and properties of the novel chiral 3D coordination polymer with S-carboxymethyl-l-cysteine, *Inorg. Chim. Acta* 365(1), 297 (2011)

III.115. X. K. Yu and Y. Q. Zheng, Syntheses, structures, dielectric and ferroelectric properties of a chiral coordination compound with m-nitro-benzoic acid, *J. Coord. Chem.* 66(12), 2208 (2013)

III.116. W. G. Zhu, Y. Q. Zheng, L. X. Zhou, and H. L. Zhu, Structural diversity for three Zn(II) coordination polymers from 4-nitrobenzene-1, 2-dicarboxylate and bispyridyl ligand, *J. Coord. Chem.* 69(2), 270 (2016)

III.117. J. L. Qi, S. L. Ni, W. Xu, and Y. Q. Zhang, Three Cu(II) (R)-2-chloromandelato complexes generated from dipyridyl-type ligands with different spacer lengths: syntheses, crystal structures, and ferroelectric properties, *J. Coord. Chem.* 67(13), 2287 (2014)

III.118. C. J. Lin, J. L. Qi, Y. Q. Zheng, and J. L. Lin, Two new Cu(II) m-hydroxybenzoato complexes with chloro- and carboxylato-bridged dinuclear [Cu(μ_2–Cl)(μ_2–COO)Cu] cores, *J. Coord. Chem.* 66(21), 3877 (2013)

III.119. W. Xu, H. S. Chang, W. Liu, and Y. Q. Zheng, Synthesis, crystal structure, and properties of a new lanthanide tartrate coordination polymer, *Russ. J. Coord. Chem.* 40(4), 251 (2014)

III.120. L. Chen, G. Han, H. Ye, and R. Xiong, A new chiral quinoxaline derivative with ferroelectric property, *Chin. J. Chem.* 28(10), 1799 (2010)

III.121. Z. Su, M. S. Chen, J. Fan, M. Chen, S. S. Chen, L. Luo, and W. Y. Sun, Spontaneous resolution of two homochiral ferroelectric cadmium (II) frameworks and an achiral framework from a one-pot reaction involving achiral rigid ligands, *CrystEngComm* 12(7), 2040 (2010)

III.122. J. L. Qi, S. L. Ni, Y. Q. Zheng, and W. Xu, Syntheses, structural characterizations and ferroelectric properties of new Ce(III) coordination polymers via isomeric tartaric acid ligands, *Solid State Sci.* 28, 61 (2014)

III.123. J. Zhang, M. Zhao, W. Xie, J. Jin, F. Xie, X. Song, S. Zhang, J. Wu, and Y. Tian, A series of novel cadmium(II) coordination polymers with photoluminescence and ferroelectric properties based on zwitterionic ligands, *New J. Chem.* 41(17), 9152 (2017)

III.124. Y. Q. Zheng, H. L. Zhu, X. X. Guo, and J. Y. Liu, Synthesis, crystal structures and properties of three glutarato and adipato bridged manganese(II) coordination polymers under ambient conditions, *Solid State Sci.* 18, 42 (2013)

III.125. Z. R. Qu, Z. F. Chen, J. Zhang, R. G. Xiong, B. F. Abrahams, and Z. L. Xue, The first highly stable homochiral Olefin–Copper(I) 2D coordination polymer grid based on quinine as a building block, *Organometallics* 22(14), 2814 (2003)

III.126. D. P. Li, C. H. Li, J. Wang, L. C. Kang, T. Wu, Y. Z. Li, and X. Z. You, Synthesis and physical properties of two chiral terpyridyl europium(III) complexes with distinct crystal polarity, *Eur. J. Inorg. Chem.* 2009(32), 4844 (2009)

III.127. Y. R. Xie, H. Zhao, X. S. Wang, Z. R. Qu, R. G. Xiong, X. Xue, Z. Xue, and X. Z. You, 2D chiral uranyl(VI) coordination polymers with second-harmonic generation response and ferroelectric properties, *Eur. J. Inorg. Chem.* 2003(20), 3712 (2003)

III.128. M. L. Feng, P. X. Li, K. Z. Du, and X. Y. Huang, $[Ni(en)_3][InSbS_4]$: A one-dimensional polymeric indium thioantimonate with a polar structure, *Eur. J. Inorg. Chem.* 2011(26), 3881 (2011)

III.129. W. Xu, H. S. Chang, W. Liu, and Y. Q. Zheng, Synthesis, crystal structure, and properties of a new lanthanide tartrate coordination polymer, *Russ. J. Coord. Chem.* 40(4), 251 (2014)

III.130. H. Yu, M. Liu, X. Gao, and Z. Liu, Construction and crystal structure of a pair of tetranuclear Zn(II) chiral clusters that exhibit ferroelectric behavior under a higher frequency electric field at room temperature, *Polyhedron* 137, 217 (2017)

III.131. C. F. Wang, J. X. Gao, C. Li, C. S. Yang, J. B. Xiong, and Y. Z. Tang, A novel co-crystallization molecular ferroelectric induced by the ordering of sulphate anions and hydrogen atoms, *Inorg. Chem. Front.* 5(10), 2413 (2018)

III.132. Y. T. Wang, G. M. Tang, W. Z. Wan, Y. Wu, T. C. Tian, J. H. Wang, C. He, X. F. Long, J. J. Wang, and S. W. Ng, New homochiral ferroelectric supramolecular networks of complexes constructed by chiral S-naproxen ligand, *CrystEngComm* 14(10), 3802 (2012)

III.133. M. Ahmad, R. Katoch, A. Garg, and P. K. Bharadwaj, A novel 3D 10-fold interpenetrated homochiralcoordination polymer: Large spontaneouspolarization, dielectric loss and emission studies, *CrystEngComm* 16(22), 4766 (2014)

III.134. M. Liu, H. Yu, and Z. Liu, A pair of homochiral trinuclear Zn(II) clusters exhibiting unusual ferroelectric behaviour at high-temperature, *CrystEngComm* 21(14), 2355 (2019)

III.135. S. Moharana, M. K. Mishra, B. Behera, and R. N. Mahaling, Enhanced dielectric properties of polyethylene glycol (PEG) modified $BaTiO_3$ (BT)-poly(vinylidene fluoride) (PVDF) composites, *Polym. Sci. A* 59(3), 405 (2017)